

**To Mom and Dad
for their love and support.**

Copyright


by

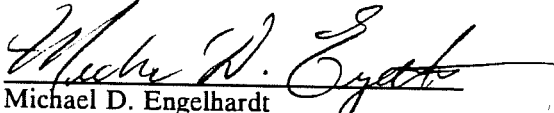
James Matthew Light

1993

**TENSILE FATIGUE TESTS OF PIPE BUTT WELDS
AND ANALYSIS OF PROPOSED STRESS
SHADOWING GROOVES**

APPROVED:


Karl H. Frank


Michael D. Engelhardt

**To Mom and Dad
for their love and support.**

Copyright

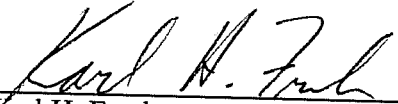
by

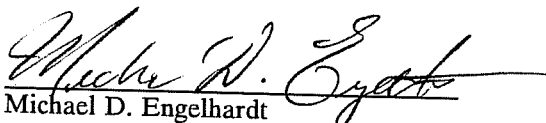
James Matthew Light

1993

**TENSILE FATIGUE TESTS OF PIPE BUTT WELDS
AND ANALYSIS OF PROPOSED STRESS
SHADOWING GROOVES**

APPROVED:


Karl H. Frank


Michael D. Engelhardt

**TENSILE FATIGUE TESTS OF PIPE BUTT WELDS
AND ANALYSIS OF PROPOSED STRESS
SHADOWING GROOVES**

by

JAMES MATTHEW LIGHT, B.S.

THESIS

Presented to the Faculty of the Graduate School of

The University of Texas at Austin

in Partial Fulfillment

of the Requirements

for the Degree of

MASTER OF SCIENCE IN ENGINEERING

THE UNIVERSITY OF TEXAS AT AUSTIN

May 1993

ACKNOWLEDGMENTS

Funding for this project was provided by Shell Pipeline Corporation. The author would like to express thanks to Shell for making this research project possible and to Mr. Frans Kopp for his sincere interest and helpful input throughout the course of the project.

The author would like thank Professor Karl Frank for his support and guidance throughout the course of the testing, analysis, and thesis writing portions of this project. Professor Frank's high personal standards and personable and professional attitude served as sources of inspiration to the author throughout the project. Thanks also to Dr. Michael Engelhardt for his thoughtful comments on this thesis.

Sincere thanks are expressed to the author's four undergraduate assistants, Tom Harrison, Karl McArthur, Kyle Kolsti, and Jon Abel, whose constant attention to the details of test specimen preparation freed the author to concentrate on things both very important and very trivial. A rigorous testing schedule was maintained over 15 months of fatigue testing which would not have been possible without the help of Tom, Karl, Kyle, and Jon. The author could not have wished for more competent or reliable assistants.

Special thanks are extended to Blake Stassney whose technical support was invaluable in keeping the test frame and the hydraulic system in working order. Special thanks also to Wayne Fontenot whose superb skills as a machinist saved countless weeks of downtime during a major overhaul of the hydraulic ram. Thanks also to the "Ram Busters" Blake, Wayne Fontenot, Wayne Little, Pat Ball, and Ray Madonna who always found the time, often on short notice, to help replace seals in an overgrown hydraulic ram.

For keeping the author in touch with the non-academic parts of a seemingly academic life, thanks are extended to Tom Pechillo, Bruce English, Rich Denio, Jeff Borger, Stacy Bartoletti, and the others who shared the belief that golf and suds are more important on the weekends than school and books.

Thanks to Carole Reese for always being a friendly source of information to a confused graduate student, to April Jenkins for always knowing who to call to solve bureaucratic problems, to Laurie Golding for dealing with many "I need it yesterday" requests, to Jean Gehrke for always taking care of film with a smile, to Sharon Cunningham for her support and technical advice during thesis writing, and to Ryan Green for his tireless efforts at the impossible job of keeping the Ferguson Lab computers in working order.

Finally, thanks to Mom and Dad Light and Barb and Don Light for their continuous and unquestioning love, support, and guidance throughout.

James M. Light

January 3, 1993

TABLE OF CONTENTS

List of Tables	xiii
List of Figures	xiv
Chapter 1 Introduction	
1.1 Background	1
1.2 Scope	4
1.3 Objectives	4
Chapter 2 Background Information	
2.1 Overview	6
2.2 Weld Fatigue in General	6
2.3 Fracture Mechanics and Fatigue	8
2.4 Increased Fatigue Life by Decreasing Stress Intensity Factor	10
2.5 Increased Fatigue Life by Decreasing Initial Crack Size	13
2.6 Increased Fatigue Life by Increasing Crack Initiation Life	15
2.7 Pipe Welds	17
2.8 Test Specimen Welds	18
Chapter 3 Experimental Procedure	
3.1 Overview	20
3.2 Parameters Investigated	20
3.3 Test Specimen	
3.3.1 Specimen Fabrication	21

3.3.2	Material and Section Properties	22
3.3.3	End Fixtures	23
3.3.4	Measurements Made Prior to Welding	24
3.3.5	Welding Procedures	24
3.3.6	Weld Inspection	25
3.3.7	Strain Gages	29
3.3.8	Measurements Made Prior to Testing	30
3.4	Testing Apparatus	
3.4.1	Test Frame	31
3.4.2	Loading System and Safety Features	32
3.4.5	Data Acquisition System	33
3.5	Testing Procedure	
3.5.1	Overview	33
3.5.2	Static Loading Cycles	33
3.5.3	Fatigue Loading	35
3.5.4	Fatigue Crack Detection and Failure Definition	35
3.5.5	Post Fatigue Analysis	36
Chapter 4	Results of Fatigue Tests	
4.1	Overview	37
4.2	Presentation of Fatigue Test Results	
4.2.1	Observed Failure Patterns	37
4.2.2	Test Data	43

4.3	Discussion of Fatigue Test Results	
4.3.1	Observed Failure Patterns	43
4.3.2	Discussion of Weld Failures	
4.3.2.1	Overview	48
4.3.2.2	5G GTAW Root Welds	48
4.3.2.3	2G GTAW Root Welds	49
4.3.2.4	2G SMAW Root Welds	50
4.3.2.5	5G Pulsed Tig Root Specimens	50
4.4	Analysis of Fatigue Test Data	
4.4.1	Overview	51
4.4.2	S-N Curve for 5G GTAW Root Welds	52
4.4.3	S-N Curve for 2G GTAW Root Welds	54
4.4.4	S-N Curve for 2G SMAW Root Welds	56
4.5	Factors Influencing Fatigue Strength	
4.5.1	Overview	56
4.5.2	Influence of Welding Position on Fatigue Behavior	58
4.5.3	Influence of Weld Root Process on Fatigue Behavior	61
4.5.4	Influence of Inside Pipe Offset on Fatigue Behavior	63
4.6	Summary of Results	66
Chapter 5	Proposed Stress Shadowing Grooves	
5.1	Overview	68
5.2	Critical Parameters	70
5.3	Finite Element Model	70

5.4	Results of Finite Element Analyses	
5.4.1	Overview	74
5.4.2	Inside Pipe Offset	74
5.4.3	Groove Depth	76
5.4.4	Groove Location	76
5.4.5	Groove Radius	77
5.4.6	Pipe Wall Thickness Mismatch	78
5.5	Discussion of Results	80
Chapter 6 SPATE Scans and Dynamic Strain Gage Readings for Specimen 7S		
6.1	Overview	85
6.2	SPATE Scans	
6.2.1	Testing Equipment	85
6.2.2	Testing Procedure	86
6.2.3	Results	87
6.3	Dynamic Strain Gage Readings	
6.3.1	Testing Equipment	92
6.3.2	Testing Procedure	92
6.3.3	Results	93
6.4	Summary and Conclusions	96
Chapter 7 Summary and Conclusions		
7.1	Summary	97
7.2	Conclusions	
7.2.1	Fatigue Tests	98

7.2.2	Analysis of Fatigue Test Results	98
7.2.3	Proposed Stress Shadowing Grooves	99

Appendix A Detailed Specimen Failure Descriptions

A1	Overview	101
A2	5G GTAW Root Specimens	
A2.1	Specimen 1	102
A2.2	Specimen 2	102
A2.3	Specimen 3	103
A2.4	Specimen 4	103
A2.5	Specimen 5	104
A2.6	Specimen 6	105
A2.7	Specimen 7	105
A2.8	Specimen 7A (Retest of Specimen 7)	106
A2.9	Specimen 8	106
A2.10	Specimen 9	107
A2.11	Specimen 10	108
A2.12	Specimen 11	108
A2.13	Specimen 12	109
A2.14	Specimen 13	109
A2.15	Specimen 14	110
A2.16	Specimen 15	110
A2.17	Specimen 16	111

A3	2G GTAW Root Specimens	
A3.1	Specimen 17	112
A3.2	Specimen 18	112
A3.3	Specimen 19	113
A3.4	Specimen 20	113
A3.5	Specimen 21	114
A3.6	Specimen 21A (Retest of Specimen 21)	114
A3.7	Specimen 22	115
A3.8	Specimen 3S	115
A3.9	Specimen 6S	116
A4	2G SMAW Root Specimens	
A4.1	Specimen 1S	117
A4.2	Specimen 1SA (Retest of Specimen 1S)	117
A4.3	Specimen 2S	118
A4.4	Specimen 2SA (Retest of Specimen 2S)	118
A4.5	Specimen 4S	119
A4.6	Specimen 5S	119
A4.7	Specimen 7S	120
A5	Pulsed Tig Root Specimens	
A5.1	Specimen PT1	121
A5.2	Specimen PT1A (Retest of Specimen PT1)	121
	Bibliography	123
	Vita	126

LIST OF TABLES

Table 3-1	Mechanical Properties of Pipe Steel	22
Table 3-2	Chemical Properties of Pipe Steel	23
Table 3-3	Welding Procedure for 5G GTAW Root Welds	26
Table 3-4	Welding Procedure for 2G GTAW Root Welds	27
Table 3-5	Welding Procedure for 2G SMAW Root Welds	28
Table 3-6	Test Stress Ranges and Load Ranges	34
Table 4-1	Fatigue Test Results for 5G GTAW Root Specimens	44
Table 4-2	Fatigue Test Results for 2G GTAW Root Specimens	45
Table 4-3	Fatigue Test Results for 2G SMAW Root Specimens	46
Table 4-4	Fatigue Test Results for Pulsed-Tig Root Specimens	47
Table 4-5	Parameter "A" for 5G GTAW Root Specimens	60
Table 4-6	Parameter "A" for 2G GTAW Root Specimens	61
Table 4-7	Parameter "A" for 2G SMAW Root Specimens	62
Table 4-8	Average Values of Parameter "A"	63
Table 6-1	Static and Dynamic Strain Gage Readings for 10 ksi Stress Range	94
Table 6-2	Static and Dynamic Strain Gage Readings for 42 ksi Stress Range	95

LIST OF FIGURES

Figure 1-1	Cross Section Through Typical Butt Weld	1
Figure 2-1	Weld Toe Angle and Radius	11
Figure 2-2	Misalignment Due to Changes in Wall Thickness	12
Figure 2-3	Axial Misalignment	12
Figure 2-4	Angular Misalignment	12
Figure 3-1	Inside Pipe Offset	21
Figure 3-2	Test Specimen	21
Figure 3-3	Original End Fixture Design	23
Figure 3-4	Modified End Fixture Design	23
Figure 3-5	Strain Gage Layout Typical Specimen	29
Figure 3-6	Strain Gage Layout Specimens 1 - 4	29
Figure 3-7	Strain Gage Layout Specimens 17 & 7S	29
Figure 3-8	Pipe Weld Geometric Parameters	30
Figure 3-9	Test Frame	31
Figure 3-10	Top Split Shim Plate Detail	31
Figure 3-11	Bottom Split Shim Plate Detail	31
Figure 4-1	Weld Root Crack	37

Figure 4-2	Weld Toe Crack	38
Figure 4-3	Fatigue Crack from Between Weld Passes	39
Figure 4-4	Root Crack Cross Section	40
Figure 4-5	Root Crack Fracture Surface	40
Figure 4-6	Toe Crack Cross Section	41
Figure 4-7	Toe Crack Fracture Surface	41
Figure 4-8	Cross Section of Fatigue Crack Initiating Between Weld Passes	42
Figure 4-9	Fracture Surface of Fatigue Crack Initiating Between Weld Passes	42
Figure 4-10	S-N Plot for 5G GTAW Root Welds	53
Figure 4-11	S-N Plot for 2G GTAW Root Welds	55
Figure 4-12	S-N Plot for 2G SMAW Root Welds	57
Figure 4-13	Comparison of S-N Plots	59
Figure 4-14	Inside Offset vs. Parameter "A"	64
Figure 4-15	Histogram of Inside Offset Ranks	65
Figure 5-1	Weld Section Modelled Using Finite Elements	69
Figure 5-2	Weld Geometry Defined	70
Figure 5-3	Finite Element Model	71
Figure 5-4	Layout of Elements in Middle Region of Finite Element Model	72
Figure 5-5	Stress Concentration Factor vs. Inside Pipe Offset	75
Figure 5-6	Stress Concentration Factor vs. Groove Depth	77
Figure 5-7	Stress Concentration Factor vs. Groove Location	78
Figure 5-8	Stress Concentration Factor vs. Groove Radius	79

Figure 5-9	Stress Concentration Factor vs. Pipe Wall Thickness	80
Figure 5-10	Axial Stress Distribution Without Stress Shadowing Grooves	82
Figure 5-11	Axial Stress Distribution With Stress Shadowing Grooves	83
Figure 6-1	Strain Gage Layout Specimen 7S	86
Figure 6-2	SPATE Scan Area 1	87
Figure 6-3	SPATE Scan Area 2	87
Figure 6-4	SPATE Scan Areas	88
Figure 6-5	SPATE Scan of Area 1	89
Figure 6-6	SPATE Scan of Area 2	90
Figure 6-7	Area Common to SPATE Scans 1 and 2	91
Figure 6-8	Profile of Area Common to SPATE Scan Areas 1 and 2	91

CHAPTER 1

INTRODUCTION

1.1 Background

The susceptibility of welded joints to fatigue problems has been known for many decades. Fatigue problems associated with welded structures first surfaced in the steel bridge industry in the 1930's, likely due to the fact that bridges were the first welded structures exposed to fatigue loading. Several catastrophic failures and near failures due to weld fatigue cracks prompted the need for research into the factors causing fatigue cracks to initiate at welds and into the development of design methods for weld fatigue. Chapter 2 of this thesis presents an overview of weld fatigue research completed to date. The information presented in Chapter 2 is generally applicable to many types of welded joints but focuses on transverse butt welds which were the subject of study for this project.

One of the more important discoveries in weld fatigue was made by Wilson¹⁹ in his pioneering tests of transverse butt welds in the early 1940's. Wilson identified that fatigue cracks initiated at welds simply due to stress concentrations at the abrupt change in geometry at the weld toe. The weld toe and other parts of a typical butt weld which will be referred to extensively in this thesis are labelled in the weld cross section illustrated in Figure 1-1. It was found that

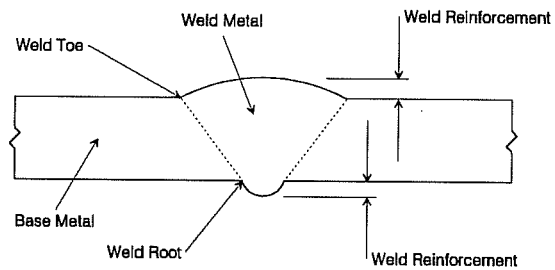


Figure 1-1 Cross Section Through Typical Butt Weld

the fatigue life of the butt weld joint could be increased to that of the parent plate by grinding or machining the weld metal flush with the base metal. This important discovery suggested that the weld metal did not behave differently in fatigue than the base metal, but rather that the fatigue problems associated with welds were due to the geometric presence of the weld reinforcement. Many fatigue problems, particularly in the steel bridge industry, have been prevented simply by controlling the geometry of weld details and by specifying that butt welds be ground flush with the base metal.

This project focused on the fatigue behavior of transverse butt welds in pipe sections. Although fatigue problems at butt welds in flat plates or I-shaped sections can be easily controlled by grinding, pipe welds present an interesting problem in that the weld reinforcement on the inside of the pipe is inaccessible after welding. Grinding to remove sources of stress concentration is not an option to improve fatigue life.

For welds in flat plates, it has been shown^{6,7} that misalignment of plates at transverse butt welds leads to increased stress concentrations at the weld toes and thus decreased fatigue life. Offset in flat plates can generally be controlled by rigorous pre-weld fit-up procedures, but offsets in pipe butt welds are often due to unavoidable changes in pipe wall thickness and out-of-roundness in the pipe section. Offsets due to the geometry of the pipe section are thus unavoidable in pipe butt welds.

Stress concentrations due to the inaccessible inside weld reinforcement, aggravated by unavoidable offsets due to the geometry of the pipe sections, mean that butt welds in pipe will invariably fail from fatigue cracks initiating at the edge of the weld root pass. Methods of improving the fatigue strength of pipe butt welds thus must focus on methods of reducing the magnitude of this unavoidable source of stress concentration.

The pipe welds tested in this project used a Gas Tungsten Arc Welding (GTAW) root pass in place of the more commonly used Shielded Metal Arc Welding (SMAW) process. It was thought that the GTAW process would allow the welder more control over the shape of the inside weld reinforcement and that smoother transitions between weld metal and base metal at the weld root could be achieved. It was the intention that the improved weld root geometry would result in improved fatigue life.

The test specimens used in this series of pipe butt weld fatigue tests are described in detail in Chapter 3. Also included in Chapter 3 are specific details of the welding procedures used and the fatigue testing apparatus. Chapter 4 details the results of the fatigue tests and shows comparisons between observed fatigue lives of the GTAW root welds and similar SMAW root welds.

Realizing that the fatigue life of the pipe butt weld is controlled by unavoidable stress concentrations at the weld root, a method of using stress shadowing grooves to reduce the magnitude of stress concentration at the weld root was proposed. These grooves would be machined on the inner surface of the pipe before welding and it is the intention that the grooves would cause the stresses to "flow around" the changes in geometry at the weld root rather than concentrating in the root area. Chapter 5 presents the results of a series of preliminary finite element analyses into the feasibility of the proposed stress shadowing grooves.

As the test series progressed, more of the test specimens seemed to be failing in the pipe-to-end fixture welds than in the interior pipe-to-pipe welds. In order to assure that irregularities in the applied stress were not present in the specimen during fatigue loading, a SPATE (Stress Pattern Analysis by Thermal Emission) was used to study the stress distribution at a pipe-to-end fixture weld. Chapter 6 presents background information on the SPATE

equipment, the theory upon which the SPATE operation is based, and results of the SPATE scans of the weld area.

Results of both the experimental and analytical portions of this project are summarized in the conclusions in Chapter 7.

1.2 Scope

Thirty-five pipe butt weld specimens were tested in cyclic tensile fatigue, each specimen having six welds spaced along its length. Welds were tested having GTAW and SMAW root passes and the effect of weld root process on fatigue life was investigated. The GTAW root specimens were fabricated both in the American Welding Society (AWS) 2G and AWS 5G positions and the effect of root welding position on fatigue life also was investigated. Results of the fatigue tests are presented in Chapter 4 and are summarized in Chapter 7.

A method of using machined grooves to improve the fatigue life of pipe butt welds by shadowing the stress concentration at the weld root was proposed. A preliminary finite element analysis was completed into the feasibility of the proposed stress shadowing grooves. Results of the finite element analyses are presented in Chapter 5 and are summarized in Chapter 7.

1.3 Objectives

This project was sponsored by the pipeline division of a major oil company. The sponsor needed to use pipe butt welds in an application where fatigue loading would be present and fatigue failure costly to repair. The GTAW root procedure was designed by the sponsor in an effort to improve the fatigue life of the welds and the sponsor contracted with the university to perform fatigue testing of the welds. The goals of the sponsor were to identify the

effect of weld root process and position on fatigue life, to identify factors which could be controlled during fabrication which might improve in-service fatigue life, and to develop fatigue design curves to be used for the GTAW root welds.

The goals of the university were first to fulfill the needs of the project's sponsor, but also to examine pipe butt weld fatigue from an academic point of view. The goals of the investigators were to correlate the results of this series of fatigue tests with previous research, to identify the factors controlling weld fatigue life, and finally to investigate methods of improving the fatigue life of pipe butt welds.

CHAPTER 2

BACKGROUND INFORMATION

2.1 Overview

This chapter presents a general overview of weld fatigue including the results of previous investigations and correlations of trends in these data with the principles of fracture mechanics. The ideas and information presented are generally applicable to many types of welded joints but will focus on transverse butt welds in particular. The primary goals of this chapter are to put into context the factors contributing to the weld failures observed in this test series and to present enough background information so that the reader can appreciate the peculiarities of butt welds in pipe and evaluate the possible benefits of the proposed stress shadowing grooves.

2.2 Weld Fatigue in General

The fatigue behavior of welds is a very complicated issue in the sense that many factors contribute to the formation and growth of a weld fatigue crack. Factors known to influence weld fatigue behavior include⁷, in no particular order:

- applied stress magnitude and distribution
- the effects of weld joint macro-geometry on the magnitude and distribution of stresses within the weld, including the effects of weld reinforcement and misalignments of the base plates

- the effects of weld micro-geometry on the magnitude and distribution of stresses at the weld toes and at flaws within the weld metal
- post-weld machining, grinding, or heat treatment
- the extreme states of residual stress in the weld metal and base metal introduced by the welding process
- the slight differences in material properties of the weld metal, the base metal, and the heat affected zone
- the effects of different sized and shaped weld flaws

An analytical model of weld fatigue including all of these factors is simply not practical or possible. Fortunately, all of these factors are taken into account by completing experimental fatigue tests on welds which are representative of in-service conditions. Typically results of these tests are presented in the form of log-log plots of applied stress range versus number of cycles to failure (S-N plots). A structure can reasonably be designed for a given fatigue life by extrapolating the fatigue test results to expected in service stress ranges and frequencies. Over the past several decades fatigue tests have been completed for most common weld details and design specifications^{1,2,3} have been developed based on the results of these tests.

Through careful control of test variables in fatigue tests, correlations between fatigue performance and a number of parameters have been developed. This information combined with developments in the science of fracture mechanics goes a long way toward explaining why welds fail in certain locations. Perhaps more importantly, however, fracture mechanics provides a method for evaluating the fatigue life of new or different weld details and gives a basis for developing and evaluating methods of improving the fatigue performance of commonly used

weld details. The following sections present a quick overview of the fracture mechanics of fatigue and brief summaries of selected research into parameters which have been found to affect the fatigue performance of welded joints.

2.3 Fracture Mechanics and Fatigue

Following the principles of fracture mechanics, fatigue life is divided into separate periods of crack initiation and crack propagation. Crack initiation life is defined as the number of stress cycles necessary for a sharp, well defined fatigue crack to form. Methods of calculating crack initiation life involve several complicated material behavior assumptions, thus they are rarely used and often are difficult to verify experimentally. Conveniently, crack initiation life is often found to be negligible in weld fatigue due to the presence of unavoidable crack-like weld flaws from which fatigue cracks readily propagate¹². Neglecting crack initiation life for welds generally results in fatigue life estimates which are conservative but not overly conservative.

Crack propagation life refers to the number of stress cycles required for a crack to grow from a finite initial size to a finite final size. Crack growth rate calculations are fairly straightforward and have been verified experimentally. Crack growth rate is generally expressed by a power law in the following form⁵:

$$\frac{da}{dN} = C * (\Delta K)^n \quad (2-1)$$

Where: da/dN = Crack growth rate
 (Change in crack length per stress cycle)
 C = A material constant

ΔK = Change in stress intensity factor

n = A material constant, generally 2 to 4

The stress intensity factor, K , is a measure of the severity of the state of stress in the vicinity of the crack tip. The stress intensity factor or change in stress intensity factor are often expressed in the following form⁵:

$$K = \beta * \sigma \sqrt{\pi a} \quad \text{or} \quad \Delta K = \beta * \Delta \sigma \sqrt{\pi a} \quad (2-2)$$

Where: K = Stress intensity factor

ΔK = Change in stress intensity factor

β = A constant or a function of the geometry of the cracked body

σ = Remote stress on the cracked body

$\Delta \sigma$ = Change in remote stress on the cracked body

a = Crack size

Rearranging Equation 2-1, the number of stress cycles, N_p , required for a crack to propagate from an initial size, a_i , to a final size, a_f , when subjected to a cyclic change in stress intensity, ΔK , is expressed by Equation 2-3⁵:

$$N_p = \int_{a_i}^{a_f} \frac{1}{C * (\Delta K)^n} da \quad (2-3)$$

By carefully isolating particular parameters in fatigue tests of actual welds, correlations have been found between several parameters and improvements in weld fatigue life. These parameters can be grouped into three categories and their effect on fatigue life can be explained by the principles of fracture mechanics as expressed in Equations 2-1, 2-2, and 2-3.

The following sections present factors found to increase the fatigue life of welds by either decreasing the stress intensity factor, decreasing the initial crack size, or increasing the crack initiation life.

2.4 Increased Fatigue Life by Decreasing Stress Intensity Factor

From Equation 2-3, it is apparent that fatigue crack propagation life, N_p , can be increased by a decrease in the cyclic range of the stress intensity factor, ΔK . Since ΔK is raised to typically the third power in the denominator of Equation 2-3, even small changes in ΔK result in large increases in the crack propagation life, N_p . Examining Equation 2-2, the change in stress intensity factor, ΔK , is decreased by decreasing the geometric factor, β , for any given cyclic remote stress, $\Delta\sigma$. Since the factor β relates remote stresses to local stress at the crack, β is proportional to a local stress concentration factor for the weld. It has been found through numerous fatigue tests that decreasing the local stress concentration in an area where a fatigue crack is likely to form results in a dramatic increase in fatigue life⁷.

Probably the first correlation between fatigue life of butt welds and the effects of stress concentrations was noted by Wilson^{19,20} in several series of fatigue tests completed during the early 1940's. Wilson noted that for welds tested in the "as welded" condition with the reinforcement intact, fatigue life was longer for specimens having a smaller weld reinforcement height and a smoother concave transition between weld metal and base metal at the weld toe. Wilson did not attempt to quantitatively define any correlation between stress concentration and fatigue life, but later analytical work correlated his observations with reduced magnitudes of stress concentration at the weld toe¹⁰. Perhaps most importantly, Wilson found that the fatigue strength of a butt welded joint could be increased virtually to that of the parent plate by either

machining or grinding the weld reinforcement flush with the base metal. This discovery had important implications in that the fatigue strength of the weld metal itself was approximately equal to that of the base metal and that the factors causing weld fatigue strength to be less than that of the base plate were due to the geometric presence of the weld reinforcement.

Later experimental work by Newman and Gurney⁷ in tests of butt welds found quantitative correlations between fatigue life and the weld toe angle as defined in Figure 2-1.

The fatigue life was observed to increase as the weld toe angle increased. This relationship was confirmed by Sanders¹⁷ and separately by Yamaguchi⁷ in tests of specimens machined from solid stock to simulate butt weld reinforcement geometry. Simulated welds were tested

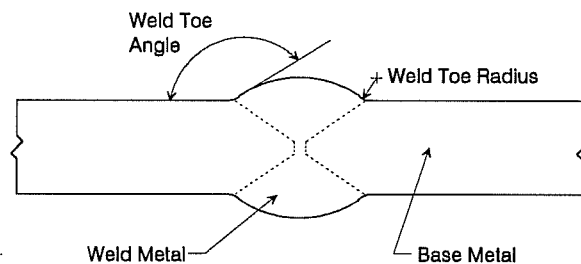


Figure 2-1 Weld Toe Angle and Radius

in order to remove the complicating factors of welding heat input and weld flaws from the study. Sanders also found correlation between fatigue life and the toe radius as defined Figure 2-1. It was found that fatigue life increased with increasing toe radius.

The stress concentrating effects of both weld toe angle and weld toe radius were verified analytically by Lawrence¹⁰ using finite element methods. It was found that stress concentration at the weld toe decreased with increasing toe radius and with increasing toe angle.

In addition to stress concentrations at the weld toes due to the presence of weld reinforcement, stress concentrations due to changes in plate thickness at the weld, as shown in Figure 2-2, or due to either axial or angular offset between plates, as shown in Figures 2-3 and

2-4, have been shown to reduce the fatigue life of welds⁷. Gunn and McLester⁶ found that fatigue life decreased with increasing axial offset for aluminum transverse butt welds. Similar results have been observed for butt welds in steel⁷. It was noted by Gunn and McLester that under axial load, the offset causes bending stresses which when added to the axial stress results in decreased fatigue life. Similar results showing decreased fatigue life with increasing offset were documented by Iida and Yazaki⁸ in bending fatigue tests of pipe butt welds having a uniform mismatch. The uniform mismatch was created by machining pipe sections to achieve differences in inside and outside diameter across the weld while keeping wall thicknesses the same.

An interesting set of tests was completed by Scholte and Buisman¹⁸ in which pipe specimens were fabricated with several welds spaced along the length and different defects in each weld. An axial fatigue load was applied to the specimen and it was intended to use the tests to compare the severity of different types of root flaws subjected to the same loading pattern. It was found that the first welds to fail were welds at transitions between pipe wall thicknesses and at welds having a significant amount

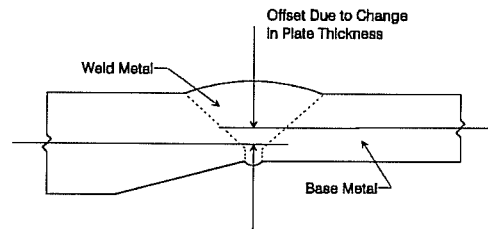


Figure 2-2 Misalignment Due to Changes in Wall Thickness

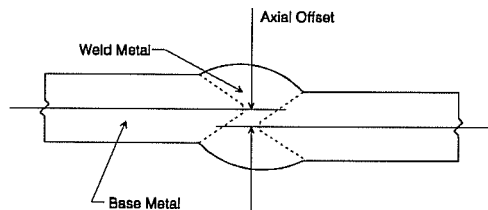


Figure 2-3 Axial Misalignment

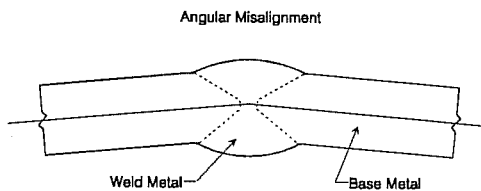


Figure 2-4 Angular Misalignment

of offset. This suggests that the additional bending stresses due to misalignment or changes in plate thickness can have a significant influence on fatigue life.

In summary, results of many experimental fatigue tests and analytical studies have identified sources of stress concentration which negatively influence fatigue life. In many instances, the stress concentration has been quite severe and the reduction in fatigue life quite significant. This behavior agrees well with expected behavior as expressed in Equation 2-3 which predicts that crack propagation life should decrease significantly with increasing stress in the vicinity of the crack tip.

2.5 Increased Fatigue Life by Decreasing Initial Crack Size

Studying Equation 2-2 and realizing that final crack size, a_f , is dependent only upon what is judged to be failure in the cracked body, it is apparent that fatigue crack propagation life, N_p , can be increased by decreasing the initial crack size, a_i . In general, the initial flaws from which weld fatigue cracks initiate are actual weld flaws and decreasing the initial flaw size means decreasing weld flaw sizes.

Closely associated with the idea of reducing the size of weld flaws to increase fatigue life is the principle of fitness-for-purpose design. According to this design philosophy, comparisons are made among different possible modes of fatigue failure to identify the controlling mode. Initial flaw sizes or allowable stress ranges for the non-controlling failure modes are relaxed to produce approximately equal fatigue lives from each failure mode. For example, if the stress concentration at the weld toe is known to control fatigue life, the principles of fracture mechanics can be used to calculate the maximum allowable size for a porosity flaw such that the fatigue life for failure from the porosity flaw would be approximately

the same as that for the weld toe failure. In order to increase fatigue life by decreasing initial flaw size, an evaluation must be made regarding which initial flaw will control fatigue life and thus which initial flaw size must be reduced.

It has generally been found that for butt welds tested with the reinforcement intact, the weld failure will initiate at the weld toe even when significant weld flaws exist within the weld^{7,12,16}. It is only when the stress concentrations at the weld toes are removed by grinding or machining that fatigue cracks initiating from weld flaws become the controlling mode of failure. These weld flaws can generally be divided into categories of planar and non-planar flaws. Planar flaws include cracks, lack of penetration/fusion, and undercut. Non-planar or three dimensional flaws include porosity and slag inclusions.

The non-planar defects generally do not have a tremendous effect on the fatigue life of a welded joint⁴. It has been found that for welds controlled by failures from these flaws that a significant portion of the fatigue life is spent in crack initiation and thus the overall fatigue life is quite long. Porosity especially is generally considered innocuous unless present in extreme amounts. The fatigue life of welds having small amounts of porosity has been found to reach nearly that of the base metal⁴. Slag inclusions are somewhat more severe, likely due to their non-uniform shape and the resulting non-uniform stress concentration about the surface of the slag inclusion. Tests have shown correlation between reduced fatigue life and increased size of slag inclusion⁴.

Planar weld defects are somewhat more severe in that fatigue cracks more readily initiate from these flaws. Newman and Dawes¹⁵ in fatigue tests of transverse butt welds containing internal lack of penetration flaws found that the fatigue life of welds was severely diminished from that of the base metal by the presence of lack of penetration defects. It was

noted that the fatigue life decreased with increasing length of defect, which is in agreement with Equation 2-3. It is important to note that in this test series it was necessary to grind smooth contours at the weld toes in order to force the failure to initiate from the weld defect.

Similar tests were completed by Lawrence and Munse¹¹ on transverse butt welds containing internal lack of penetration flaws. In these tests measurements were made of crack propagation throughout the fatigue life of the weld. It was noted that crack propagation lives calculated using the power law relationship agreed well with actual behavior when using measured initial flaw sizes in the calculations. Fracture mechanics principles have been widely used to calculate remaining fatigue lives of welds found to have planar defects. Excellent agreement has generally been found between experimental fatigue life and calculated crack propagation life based on a known initial flaw size, a known applied stress, and an elastic stress intensity solution⁵.

In summary, the power law relationship for crack growth has been verified experimentally for many different initial flaw configurations. Thus the principles of fracture mechanics can generally be used to show that fatigue life increases with decreased initial flaw size. It is important to note, however, that a fitness-for-purpose approach must be used to identify the controlling failure mode and thus the initial flaw which must be reduced in order to increase crack propagation life.

2.6 Increased Fatigue Life by Increasing Crack Initiation Life

In fracture mechanics, fatigue life is defined as the sum of crack initiation life and crack propagation life. The two previous sections have detailed methods of increasing fatigue

life by increasing crack propagation life. Methods have also been studied which increase overall fatigue life by increasing crack initiation life.

Using an analytical approach to estimate the crack initiation portion of fatigue life, Lawrence⁹ found that crack initiation was a function of weld geometry and of material properties of the base metal and weld metal. In particular, Lawrence found that crack initiation life was increased by increasing the radius of the notch at the weld toe. It was also found that crack initiation life as a fraction of total fatigue life was more important for higher strength steels and aluminum than for the more ductile structural steels. In his analysis, Lawrence assumed that no significant weld flaws were present in the area of fatigue crack initiation. Unfortunately, this is not generally the case.

Maddox¹² notes that minute crack-like weld flaws are generally found near the toes of welds and that fatigue cracks readily propagate from these flaws. He further states that these flaws appear to be unavoidable in steel welds made using normal arc welding procedures. The unavoidable presence of these flaws supports the common practice of neglecting the portion of fatigue life devoted to crack initiation for welds in structural steels tested in the "as welded" condition.

The fact that the minute crack-like flaws at the weld toe are unavoidable suggests that the only effective method of increasing the portion of fatigue life spent on crack initiation would be to remove the flaws. It has been found that removing some material at the weld toe, either by grinding^{7,13} or by eroding with a water jet¹³, resulted in increased crack initiation life and thus increased overall fatigue life.

It has also been shown that fatigue life can be improved when the weld toes are TIG dressed by using a TIG torch to remelt the material in the area of the weld toe. Improvements

in fatigue life are likely due to a combination of reduced size and frequency of minute flaws at the weld toes which increases initiation life and improved geometry at the weld toe which increases propagation life.

2.7 Pipe Welds

Up to this point no specific mention has been made of butt welds joining pipe sections. Most of the research on transverse butt welds has been for welds joining flat plates. The results of most of this research are directly applicable to butt welds in pipe, but important differences do exist.

As mentioned in Section 2.4, the most important influence on the fatigue strength of a butt welded joint tested in the "as welded" condition is the magnitude of the stress concentration at the weld toe. For welds in flat plates or I-shaped sections, this stress concentration can be removed and fatigue life increased simply by grinding the weld reinforcement flush with the base metal. Also, it is common practice for welds in flat plates to weld from one side, back-gouge the root pass from the other side, and fill the gouge with weld metal. This procedure removes any weld flaws which might have resulted from welding the root pass without any backing. It is common practice to weld from two sides and to grind all weld reinforcement flush in such fatigue critical weld details as girder splices in steel bridges. For welds in pipe, however, the inside weld reinforcement is inaccessible after welding and back-gouging to remove the root pass or grinding the weld root reinforcement to reduce the stress concentration are not available options for improving fatigue life.

For welds between flat plates, the amount of angular or axial misalignment in flat plates can generally be controlled through rigorous pre-weld fit-up procedures. For welds

between pipe sections, however, the misalignment at the weld is due to slight misalignments during pre-weld fit-up, but also is due to changes in wall thickness and any out of roundness which might exist between two pipe sections. Since slight changes in pipe wall thickness and slight degrees of out-of-roundness are unavoidable in pipe sections, the misalignments and associated stress concentrations are also unavoidable.

The unavoidable stress concentrations at the edge of the pipe weld root pass, aggravated by weld flaws from a root pass welded without backing and by unavoidable misalignments due to pipe section geometry, mean that the butt weld in pipe will invariably fail from a fatigue crack initiating at the edge of the weld root pass if reasonable care is taken to reduce sources of stress concentration at the outside weld reinforcement and at weld flaws.

2.8 Test Specimen Welds

The goal of this project was to refine a welding procedure for pipe welds to be used in an offshore application where fatigue life of the weld controlled the service life of the pipe. A GTAW process was chosen for the weld root pass over the more commonly used SMAW process since it was thought that fatigue life would be improved due to a combination of several factors. First, it was thought that the profile of the weld root pass could be controlled more easily when using the GTAW process than when using a SMAW process. Smoother transitions between weld metal and base metal at the edge of the root pass result in reduced stress concentrations and thus increased crack propagation life. Secondly, since the welder has more control over the deposition of weld metal in the GTAW process than in the SMAW process, it was thought that the size and frequency of weld root pass flaws could be decreased. Decreased initial flaw sizes result in increased crack propagation life. Thirdly, it was thought

that the lower heat input from the GTAW root process might decrease the incidence of minute weld flaws at the edge of the root pass reinforcement. Reducing the size or frequency of these flaws introduces a significant crack initiation life and results in increased overall fatigue life. Lastly, the pipe steel chosen for this application was known to have been fabricated to better than average tolerances for roundness and uniformity of wall thickness. More uniform pipe section geometry reduces stress concentrations due to misalignment at the weld and thus increases overall fatigue life.

CHAPTER 3

EXPERIMENTAL PROCEDURE

3.1 Overview

This chapter describes the test specimen and testing procedure used in this series of pipe butt weld fatigue tests. The parameters investigated during the fatigue tests and subsequent post-fatigue analysis of the failed welds are noted in Section 3.2. Section 3.3 details the geometry of the test specimens, test specimen fabrication, and measurements recorded prior to testing. The testing apparatus is described in Section 3.4, including descriptions of the methods used to apply and control specimen loading. Section 3.5 details the loading sequence used in testing the specimens, including all measurements recorded during initial static loading cycles and subsequent fatigue loading.

3.2 Parameters Investigated

The primary parameters investigated in this project were the effects of root pass welding process and welding position on the fatigue strength of pipe butt welds. Welds were tested having both Gas Tungsten Arc Welding (GTAW) root passes and Shielded Metal Arc Welding (SMAW) root passes. It was desired to determine the extent, if any, of the improvement in fatigue life by using a GTAW weld root pass in place of the more commonly used SMAW weld root pass. Root passes were welded in both the AWS 2G position with the pipe sections vertical and stationary and in the AWS 5G position with the pipe sections horizontal and stationary. It was desired to find the effect, if any, of welding position on the fatigue life of the welded joint.

Throughout the test series, sufficient data was recorded for each specimen to allow for post-fatigue analysis into the factors leading to the initiation and propagation of weld fatigue cracks. Based on the results of previous research as detailed in Chapter 2, it was known that the overall geometry of the weld joint and the shape of the weld reinforcement would have a significant influence on fatigue life. No attempt was made to study weld reinforcement shape, but overall joint geometry was characterized by the magnitude of the inside pipe offset and the effect of inside pipe offset on fatigue life was investigated in this test series. Inside pipe offset is defined in Figure 3-1.

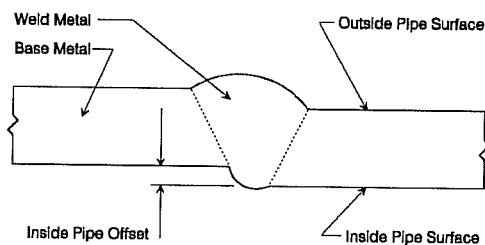


Figure 3-1 Inside Pipe Offset

3.3 Test Specimen

3.3.1 Specimen Fabrication. The test specimen used in this testing program is shown schematically in Figure 3-2. Each specimen was fabricated from five short lengths of pipe and two machined end fixtures and thus had six welds spaced along its length. Since it was the goal of the sponsor to develop fatigue design curves representing actual in-service performance, the

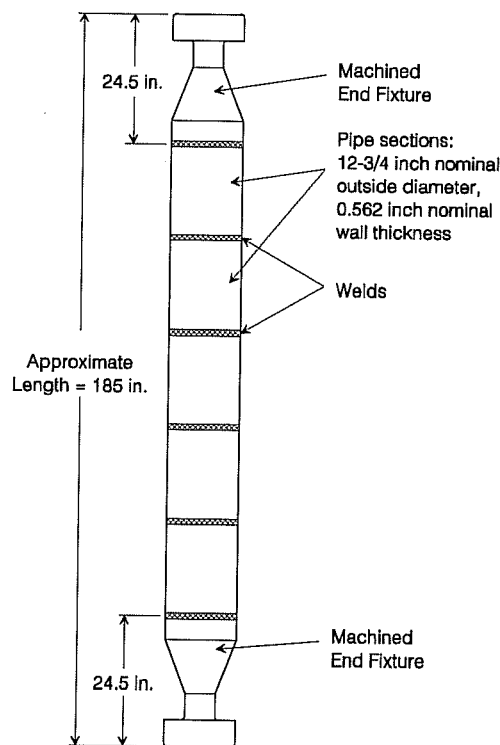


Figure 3-2 Test Specimen

specimens were fabricated by a commercial fabricator to simulate expected in-service welding conditions. Although this project investigates the effects of weld joint geometry on fatigue performance, no effort was made during fabrication of test specimens to introduce geometric irregularities into the weld joints.

3.3.2 Material and Section Properties. The pipe sections used in the fabrication of test specimens series were 12.75 inch nominal outside diameter by 0.562 inch nominal wall thickness seamless round pipe. The pipe steel was American Petroleum Institute (API) Grade X52 having mechanical properties and chemical composition as summarized in Tables 3-1 and 3-2. The pipe steel supplied was from 14 different heats and the values shown in Tables 3-1 and 3-2 reflect the average, minimum, and maximum values for each parameter based on mill reports for each of the 14 heats.

Table 3-1 Mechanical Properties of Pipe Steel

Mechanical Properties of Pipe Steel				
Property	Minimum Specified Value	Average Value	Minimum Value	Maximum Value
Yield Strength (ksi)	52	58.1	54.8	60.8
Tensile Strength (ksi)	66	75.3	73.0	78.4
Percent Elongation 2 inch gage length	27	46.0	43.5	49.0
Impact Value (ft-lb) Temperature: 32 F Direction: Transverse Specimen: 2V 10x10	40 (ea. test) 50 (avg. of three tests)	299.2	289.4	305.6

Table 3-2 Chemical Composition of Pipe Steel

Chemical Composition of Pipe Steel (All values are percent)							
Element	C	Si	Mn	P	S	Cu	Ni
Average	0.105	0.265	1.189	0.0081	0.0014	<0.01	0.014
Minimum	0.09	0.24	1.16	0.006	0.001	<0.01	0.01
Maximum	0.12	0.29	1.21	0.010	0.002	0.01	0.03
Element	Cr	Mo	Al	Ti	V	Nb	Ca
Average	0.021	<0.01	0.0324	<0.001	0.0037	0.002	0.0047
Minimum	0.02	<0.01	0.028	<0.001	0.003	<0.001	0.0033
Maximum	0.03	<0.01	0.039	0.001	0.005	0.002	0.0057

3.3.3 End Fixtures. Machined specimen end fixtures were required to accommodate the load transfer between the test frame and the specimen. Two slightly different end fixtures designs were used during the course of the testing program. A cross section through the original end fixture is illustrated in Figure 3-3. Two early specimens, specifically Specimens 3 and 7, failed away from the weld in the end

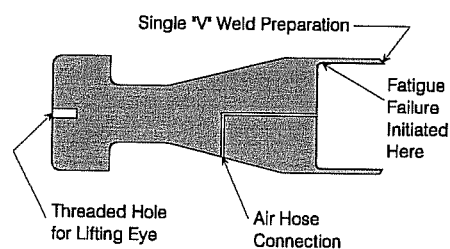


Figure 3-3 Original End Fixture Design

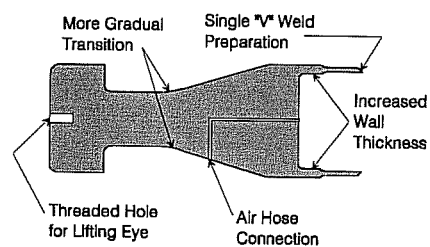


Figure 3-4 Modified End Fixture Design

fixture. To prevent such a failure during subsequent tests, the design of the end fixtures was modified slightly as illustrated in Figure 3-4.

3.3.4 Measurements Made Prior to Welding. Before welding pipe sections and end fixtures together, measurements were taken by the fabricator of the pipe wall thickness at four points roughly 90 degrees apart on each end of the pipe segments to be welded. These measurements were taken both using calipers and an ultrasonic thickness measurement device. Wall thickness measurements were recorded on the surface of the pipe as well as on a log sheet.

3.3.5 Welding Procedures. Welds tested for this project used a single "V" edge preparation with no backing bar. Welding was done using three different welding procedures. The first test series, Specimens 1 through 16, were fabricated using the welding procedure listed in Table 3-3. These welds had a manual GTAW root pass followed by two manual GTAW fill passes. Subsequent fill and cap weld passes used an automatic Submerged Arc Welding (SAW) process. The GTAW root and first fill passes were completed in the AWS 5G position with the pipe sections horizontal and stationary. The automatic SAW fill and cap passes were completed in the AWS 1G position with the welding equipment stationary and the pipe sections horizontal and rotated during welding.

The second test series, Specimens 17 through 22 and 1S through 7S, were welded in the AWS 2G position with the pipe sections vertical and stationary. Two different welding procedures were used in the fabrication of these test specimens, as listed in Tables 3-4 and 3-5. Specimens 17 through 22 were fabricated exclusively using welds having a manual GTAW root

pass and manual SMAW fill passes as listed in the procedure in Table 3-4. Specimens 1S and 2S were fabricated exclusively using welds having a manual SMAW root pass and manual SMAW fill passes according to the procedure listed in Table 3-5. Specimens 2S through 7S were fabricated using a combination of welding procedures. For the end welds between the pipe and end fixture on these specimens, the manual GTAW root pass was used, followed by manual SMAW fill passes. For the interior pipe to pipe welds, manual SMAW root and fill passes were used.

All welding was completed by qualified welders of McDermott, Incorporated, in Morgan City, Louisiana.

3.3.6 Weld Inspection. All welds on the test specimens were fully inspected using standard radiographic inspection techniques. The location and numbering of radiographic film plates was marked on the surface of the test specimen so that correlations could be made between the locations of fatigue cracks and the appearance of weld flaws during radiographic inspection.

Welds were rejected if radiographic inspection showed the presence of any significant flaws in the root pass. Significant flaws were any flaw that was linear in shape, including cracks, incomplete fusion in the root, and undercut at edge of the root pass. When a significant weld root flaw was found during radiographic inspection, the entire weld was cut out and replaced.

Table 3-3 Welding Procedure for 5G GTAW Root Welds

Welding Procedure for 5G GTAW Root Welds	
Process:	GTAW (Manual) Root and 2 fill passes SAW (Automatic) Fill and cap passes
Base Material:	API X52 Pipe 12-3/4 inch outside diameter, 0.562 inch wall thickness
Filler Metal:	GTAW ER70S-2 3/32 inch diameter SAW EM12K F72 1/8 inch diameter
Position:	GTAW 5G Pipe sections horizontal and stationary SAW 1G Pipe sections horizontal and rolled during welding
Joint design:	60 degree single "V" groove Root gap = 5/32 inch + 0 inch - 1/16 inch Root face = 1/32 inch + 0 inch - 1/32 inch
Electrical:	GTAW DC electrode negative SAW DC electrode positive
Backing:	Open root, no backing
Preheat:	Warm to 200 degrees Farenheit to remove condensation moisture
Interpass temperature:	Approximately 550 degrees Farenheit
Post weld heat treatment:	None
Cleaning:	Power grind and/or brush as required

Table 3-5 Welding Procedure for 2G SMAW Root Welds

Welding Procedure for 2G SMAW Root Welds	
Process:	SMAW (Manual)
Base Material:	API X52 Pipe 12-3/4 inch outside diameter, 0.562 inch wall thickness
Filler Metal:	SMAW E-7018 (Atom Arc) 1/8 inch and 5/32 inch diameter
Position:	2-G Pipe sections vertical and stationary
Joint design:	60 degree single "V" groove Root gap = 5/32 inch + 0 inch - 1/16 inch Root face = 1/32 inch + 0 inch - 1/32 inch
Electrical:	DC Electrode Positive
Backing:	Open root, no backing
Preheat:	Warm to 200 degrees Farenheit to remove condensation moisture
Interpass temperature:	Approximately 550 degrees Farenheit
Post weld heat treatment:	None
Cleaning:	Power grind and/or brush as required

3.3.7 Strain Gages. Strain gages were used on each test specimen to obtain the magnitude and distribution of axial stress in the pipe at each weld. Strain gage data were used by the project's sponsor to estimate bending moments in pipe sections, but these data were not extensively analyzed for this thesis. These data are not presented in this thesis but have been archived for possible future analysis.

A minimum of 24 electrical resistance strain gages were applied to each specimen, four gages located 90 degrees apart at each of the six welds. The strain gages used had a gage length of 6 millimeters and were located on the outside pipe surface 2 inches from the center of each weld, as shown in Figure 3-5. Additional strain gages were applied to some of the specimens. Specimens 1 through 4 had thirty-two strain gages arranged as shown in Figure 3-6.

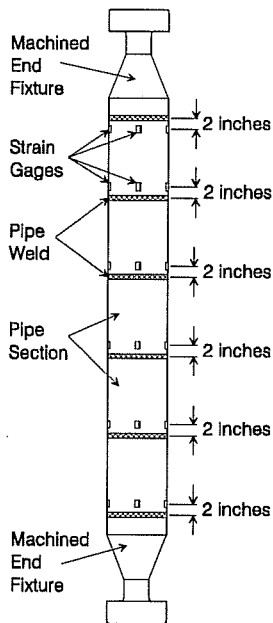


Figure 3-5
Strain Gage Layout
Typical Specimen

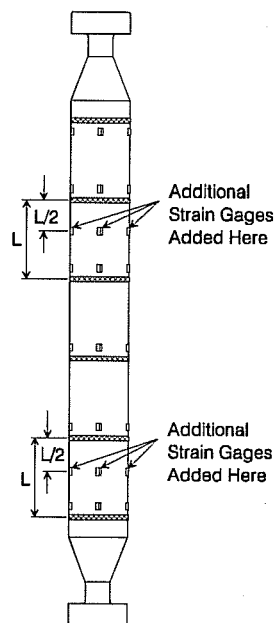


Figure 3-6
Strain Gage Layout
Specimens 1 - 4

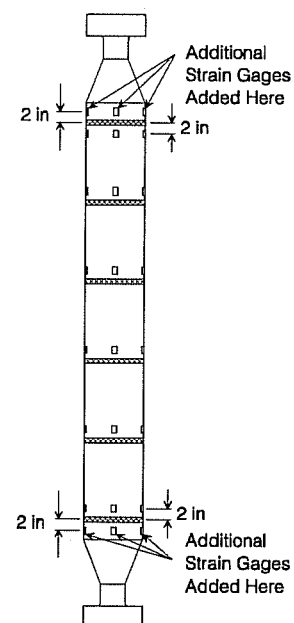


Figure 3-7
Strain Gage Layout
Specimens 17 & 7S

A slightly different arrangement of 32 strain gages was used on specimens 17 and 7S, as illustrated in Figure 3-7.

3.3.8 Measurements Made Prior to Testing. Several pieces of data were recorded for each test specimen before it was placed in the testing frame. The pipe wall thicknesses and locations of radiographic inspection film plates as marked on the pipe surface by the fabricator were recorded with respect to the strain gage locations. Measurements were made of the misalignment on the outside of the pipe sections at each strain gage location near a weld. These measurements were taken using a machined gage block and a digital depth micrometer. In Figure 3-8, the measurement recorded was the "outside pipe offset." The "inside pipe offset" was calculated from the measured outside offset and measured pipe wall thicknesses using the following equation in which "top" and "bottom" refer to the position on the specimen in its vertical testing position and "inside" and "outside" refer to the inside and outside of the pipe section:

$$Offset_{inside} = Offset_{outside} + Thickness_{top\ wall} - Thickness_{bottom\ wall} \quad (3-1)$$

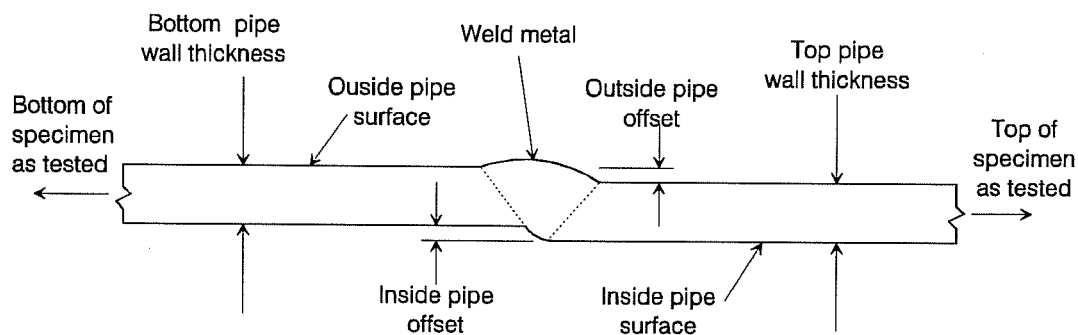


Figure 3-8 Pipe Weld Geometric Parameters

3.4 Testing Apparatus

3.4.1 Test Frame. Pipe specimens were tested vertically in the test frame shown schematically in Figure 3-9. This same testing frame has been used successfully in the past for fatigue tests on bridge stay cables.

Loads were applied to the pipe specimen by the large center-hole hydraulic cylinder at the top of the testing frame. Loads were monitored by the output from four 1000 kip load

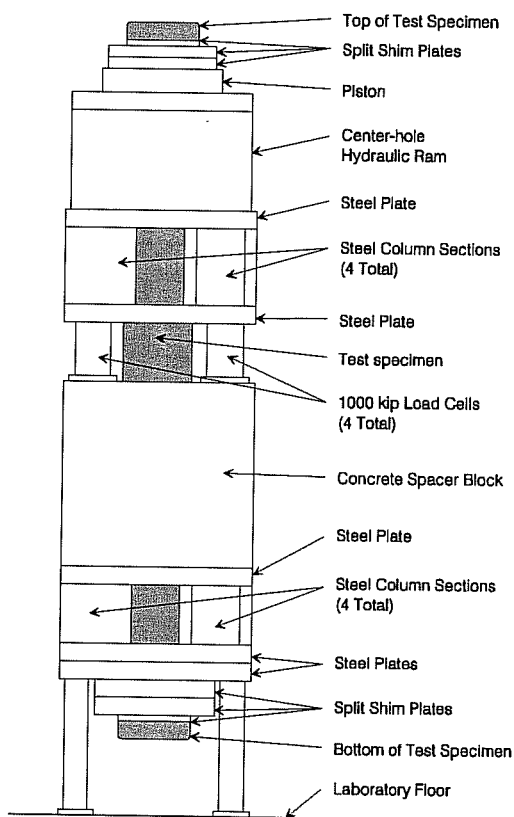


Figure 3-9 Test Frame

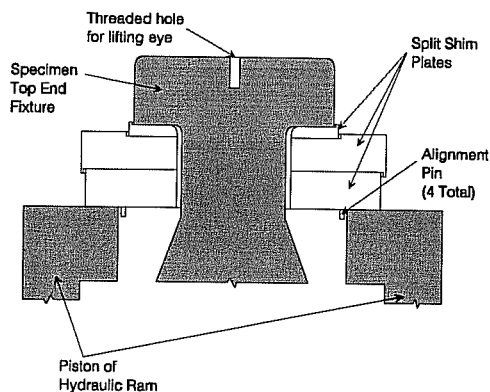


Figure 3-10 Top Split Shim Plate Detail

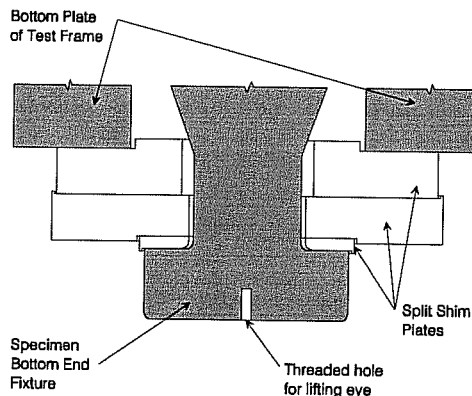


Figure 3-11 Bottom Split Shim Plate Detail

cells located just above mid-height of the test frame. Three sets of split shim plates were used at the top and bottom of the testing frame to transfer loads between the test frame and the test specimen. Figure 3-10 shows a section through the piston of the hydraulic cylinder, shim plates, and test specimen at the top of the testing frame illustrating the arrangement of split shim plates. Similarly, Figure 3-11 shows a section through the bottom of the testing frame, bottom shim plates, and test specimen illustrating the arrangement of shim plates at the bottom of the testing frame.

3.4.2 Loading System and Safety Features. Loads applied to the test specimens were controlled using a closed loop hydraulic system. Hydraulic pressure was supplied by two hydraulic pumps operating in parallel. Maximum oil flow from these pumps was 70 gallons per minute at 3000 psi. The hydraulic pump unit included safety shut-downs for high oil temperature, low oil level, and for clogged hydraulic oil filters.

The flow of oil to the loading and unloading sides of the piston was controlled by two servo valves operating in parallel. A Pegasus electronic unit was used to control the servo valves and thus the loads being applied to the specimen. The Pegasus unit included a signal generator and adjustable amplifiers to control the mean or "static" load and the load range or "span" during fatigue loading. An MTS Digital Data Display unit was used to monitor the loads applied to the specimen. The Pegasus unit included safety features to shut down the hydraulic pumps if the programmed load signal and the feedback signal from the load cells differed by more than a few percent or if the peak load exceeded a pre-set value.

3.4.5 Data Acquisition System. Strain gage readings as well as the readings from a linear potentiometer and the load cells were recorded using a Hewlett-Packard channel scanner controlled by a personal computer. Data acquisition software was the program HPDAS2 which was developed at Ferguson Laboratory and has been used successfully in the past. Strain gages were connected to the data acquisition system using a three-wire connection to compensate for temperature differentials and the associated changes in resistance of the strain gage wires during a test or among tests completed on different days. The linear potentiometer was attached to the piston of the hydraulic ram to measure overall elongation of the test specimen.

3.5 Testing Procedure

3.5.1 Overview. After all strain gages were applied to the specimen and the necessary measurements were obtained, the specimen was lowered into the test frame using an electric chain hoist mounted at the peak of the laboratory roof. Once lowered into position, split shim plates were installed at the top and bottom of the testing frame.

The loads applied to all specimens in this testing program were cyclic tensile loads. The minimum tensile load was either 100 kips or 200 kips and the maximum tensile load was determined as the sum of the minimum test load and the nominal pipe area, 21.88 in², times the desired stress range. The test loads and stress ranges are summarized in Table 3-6 on a specimen by specimen basis.

3.5.2 Static Loading Cycles. Each specimen was cycled statically through the test load range four times prior to the start of fatigue loading. Strain gage readings were taken at various load levels during each static load cycle. Generally readings were taken at 100 kip load

Table 3-6 Test Stress Ranges and Load Ranges

Test Stress Ranges and Load Ranges								
Specimen Number	Test Stress Range (ksi)	Min Load (kips)	Max Load (kips)		Specimen Number	Test Stress Range (ksi)	Min Load (kips)	Max Load (kips)
1	42	100	1,019		18	30	200	856.4
2	30	100	756.4		19	42	100	1,019
3	42	100	1,019		20	42	100	1,019
4	30	200	856.4		21	12	100	362.6
5	30	200	856.4		21A	12	100	362.6
6	30	200	856.4		22	12	100	362.6
7	30	200	856.4		1S	20	200	637.6
7A	30	200	856.4		1SA	20	200	637.6
8	30	200	856.4		2S	20	200	637.6
9	42	100	1,019		2SA	20	200	637.6
10	42	100	1,019		3S	20	200	637.6
11	30	200	856.4		4S	30	200	856.4
12	20	200	637.6		5S	30	200	856.4
13	30	200	856.4		6S	42	100	1,019
14	20	200	637.6		7S	42	100	1,019
15	15	200	528.2		PT1	20	200	637.6
16	20	200	637.6		PT1A	20	200	637.6
17	30	200	856.4					

intervals for the 20, 30, and 42 ksi stress range tests and at 50 kip load intervals for the 12 and 15 ksi stress range tests. It was the assumption during this test program that by the fourth static load cycle the specimen was fully seated into the test frame and that the strains measured during the fourth static load cycle were representative of the stresses in the specimen during subsequent dynamic fatigue loading. This assumption was later verified and is explained further in Chapter 6.

3.5.3 Fatigue Loading. After completing four static load cycles and obtaining all necessary strain gage data, a cyclic fatigue loading pattern was begun. No strain gage readings were taken during the dynamic loading portion of the test, with the exception of specimen 7S as described in Chapter 6. During the dynamic loading portion of the test, periodic checks of the test system were made to verify that the programmed loads were being maintained and that the hydraulic system was functioning properly.

3.5.4 Fatigue Crack Detection and Failure Definition. Since both ends of the test specimen were sealed by the end fixtures, it was possible to detect the first through-wall fatigue crack by monitoring the air pressure inside the specimen. At the start of fatigue loading, each specimen was pressurized with air to 5 psig through a flexible hose attached to the bottom end fixture at the locations shown in Figures 3-3 and 3-4. An electronic pressure switch was used to monitor the air pressure throughout the fatigue test. If the specimen internal air pressure dropped below 3 psig, the switch would shut down the hydraulic pumps. This system worked very well both for detecting the first through wall fatigue crack and for stopping the test prior to a potentially dangerous brittle fracture of the specimen.

Specimen failure was defined as the number stress cycles required for the first through-wall fatigue crack to form and the specimen internal air pressure to leak from 5 psig to 3 psig at which point the testing apparatus would shut down automatically.

3.5.5 Post Fatigue Analysis. After the presence of a through-wall fatigue crack was verified by the specimen failing to maintain internal air pressure, the test specimen was removed from the testing frame and the location of the fatigue crack noted with respect to the strain gage locations. Test specimens were then shipped back to the fabricator for post-fatigue radiographic inspection of the welds. Sections of weld were removed at all through-wall and non-through-wall fatigue cracks detected during post-fatigue radiographic inspection. These sections were sent to an independent failure analysis laboratory where each cracked section was broken open and examined for evidence of weld flaws which might have contributed to crack initiation. Photographs were taken of the fracture surface and weld cross sectional profile at each failure location. Results of the post-fatigue analysis of the failed welds are summarized in Chapter 4 and Appendix A.

CHAPTER 4

RESULTS OF FATIGUE TESTS

4.1 Overview

This chapter presents the results of fatigue tests performed on pipe butt welds specimens as described in the experimental procedures in Chapter 3. Fatigue test results are presented in Section 4.2, discussed in Section 4.3, and analyzed in Sections 4.4 and 4.5. The presentation of fatigue tests includes extensive reference to Appendix A which details the results of post-fatigue analysis of the failed welds. The discussion of test results primarily focuses on determining which specimens were representative of expected in-service conditions and thus which specimens to include in the analysis of test data. The analysis of test data section presents S-N plots for each welding procedure and details the observed influence of root pass welding process and position on fatigue life.

4.2 Presentation of Fatigue Test Results

4.2.1 Observed Failure Patterns. Four distinct failure modes were observed in the specimens tested. The most commonly observed failure was a weld root crack, as illustrated in Figure 4-1. Root cracks initiated on the inside of the pipe at the edge of the weld root pass reinforcement and propagated through the weld metal. Figure 4-4 shows a cross section through

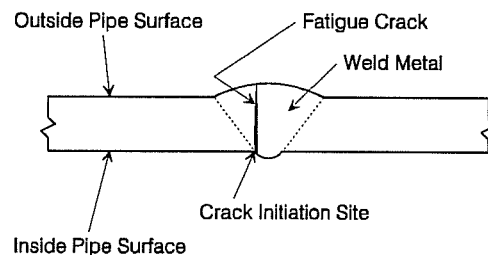


Figure 4-1 Weld Root Crack

the weld at a typical root crack. The crack initiated at the edge of the weld root pass at the bottom of the photo. Figure 4-5 shows the fracture surface for the crack shown in Figure 4-4. The darker area in the photograph is the fatigue crack fracture surface. The cross section shown in Figure 4-4 was removed at the split in the sample shown in Figure 4-5

Post fatigue analysis of several of the specimens with root cracks showed very small weld flaws at the edge of the root pass in the location of crack initiation. Typically these flaws were either a slight lack of fusion or a slight undercut in the root pass. Included in Appendix A are more specific details of each specimen failure, including notation of the failure pattern observed in each test specimen and any weld flaws which might have contributed to crack initiation.

Specimens 10 and 6S failed from weld toe cracks, as illustrated in Figure 4-2. The fatigue cracks initiated at the edge of the weld reinforcement on the outside of the pipe and propagated through the base metal toward the inside of the pipe. Figures 4-6 and 4-7 show the weld cross section and fracture surface, respectively, for the toe failure in Specimen 10. In Figure 4-6, it is apparent that the weld reinforcement height was large at the failure location. Also, there was a relatively sharp angle between the weld metal and base metal at the failure location. In Figure 4-7, the fracture surface is the darker area in the photograph. The cross section shown in Figure 4-6 was removed from the cut in the center of the specimen shown in Figure 4-7.

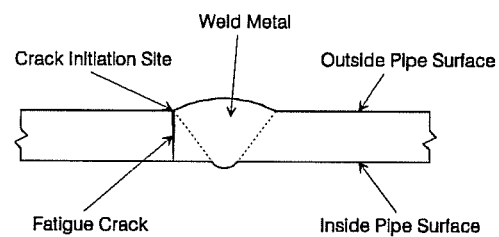


Figure 4-2 Weld Toe Crack

Test Specimens 3 and 7 failed away from the welds in the machined specimen end fixtures at the location shown in Figure 3-3. The end fixture design was modified slightly as described in Section 3.3.3 and was successful in preventing end fixture failures in the later test specimens.

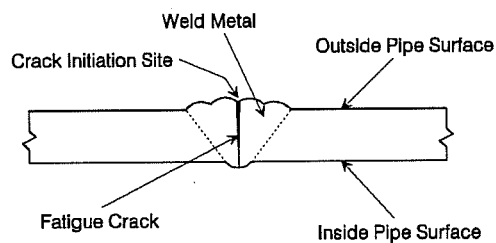


Figure 4-3 Fatigue Crack from Between Weld Passes

Specimen 17 failed from a fatigue crack initiating in a valley between two weld passes on the outside surface of the pipe, as illustrated in Figure 4-3. This crack propagated through the weld metal toward the inside surface of the pipe. Figures 4-8 and 4-9 show the weld cross sectional profile and fracture surface, respectively, at the failure location for Specimen 17. In Figure 4-9, two distinct areas of crack growth appear as darker areas in the photograph. The cross section shown in Figure 4-8 was removed from between the two cracks, at the split in the specimen shown in Figure 4-9. The outside weld reinforcement was ground flat on subsequent specimens to prevent this mode of failure.

Failure of a test specimen was defined as the propagation of the first crack through the entire pipe wall thickness. Post fatigue radiographic inspection of several specimens revealed fatigue cracks which did not propagate through the entire wall thickness. These non-through-wall fatigue cracks are listed in the detailed failure descriptions in Appendix A.

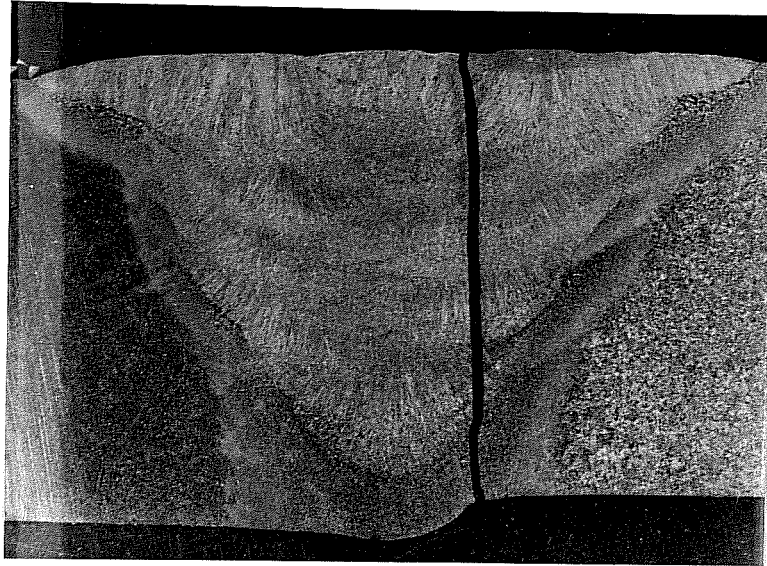


Figure 4-4 Root Crack Cross Section

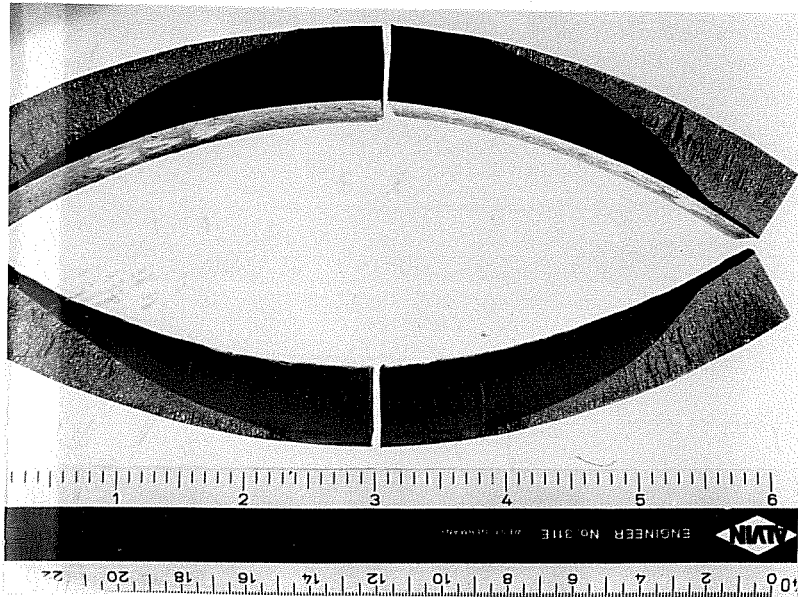


Figure 4-5 Root Crack Fracture Surface

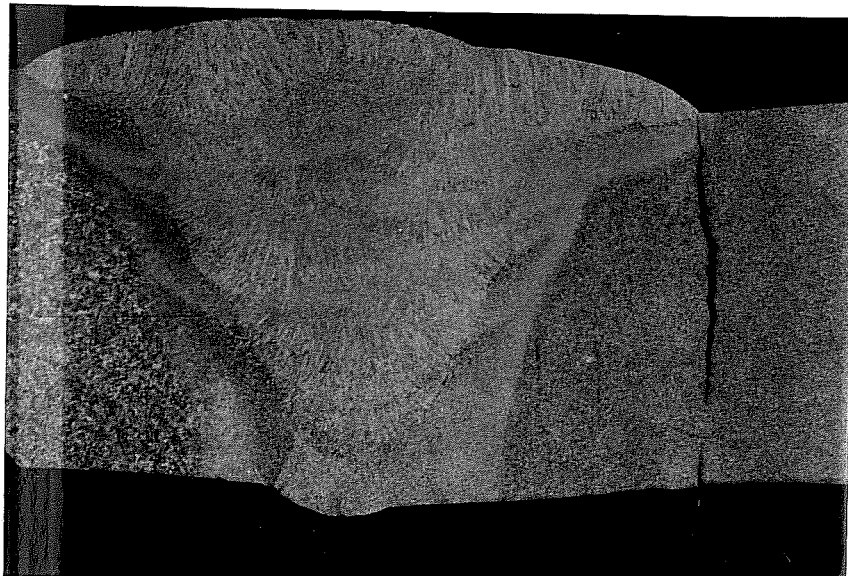


Figure 4-6 Toe Crack Cross Section

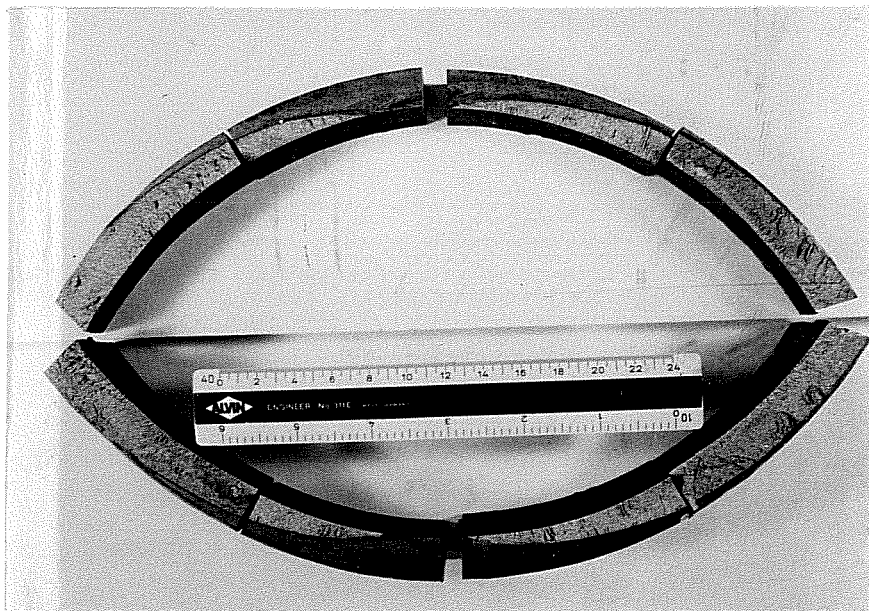


Figure 4-7 Toe Crack Fracture Surface



Figure 4-8 Cross Section of Fatigue Crack
Initiating Between Weld Passes

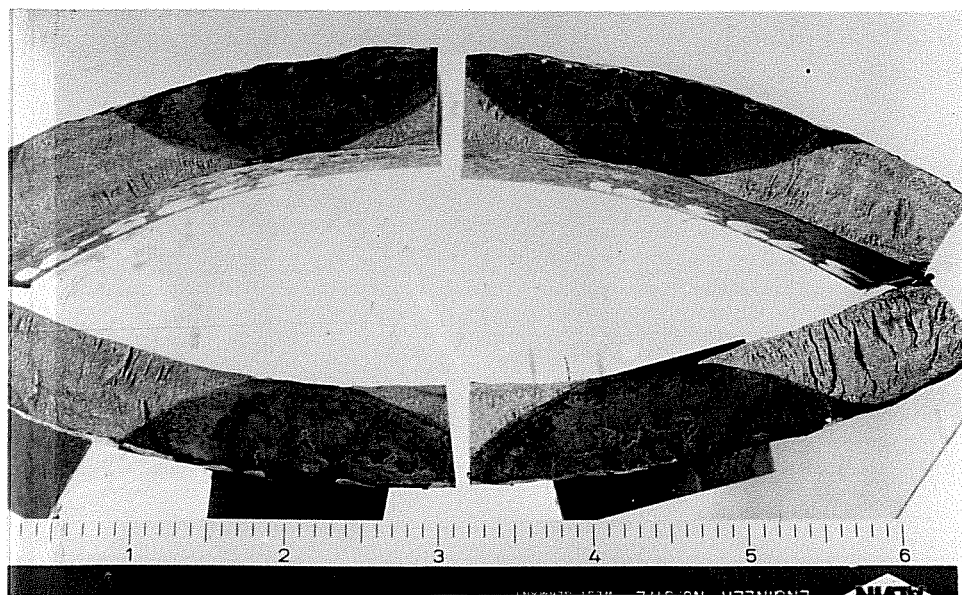


Figure 4-9 Fracture Surface of Fatigue Crack
Initiating Between Weld Passes

4.2.2 Test Data. Table 4-1 lists fatigue test results for the 5G GTAW root specimens. Included in the table are the nominal test stress range, the number of stress cycles to failure, and the failure mode for each specimen. The table also includes for each specimen a reference to a section in Appendix A which contains a more detailed description of the specimen failure. The last column on Table 4-1 indicates whether the data for a particular specimen was included in the analysis of test data as described in Section 4.4. More detailed information regarding why individual specimens were or were not included in this analysis is included in the discussion of weld failures in Section 4.3.2.

Tables 4.2, 4.3, and 4.4 list results of fatigue tests for the 2G GTAW, 2G SMAW, and Pulsed Tig root specimens, respectively. The organization of these tables is the same as that for Table 4.1 and the 5G GTAW specimens.

Specimen numbers ending in "A" indicate that the specimen was a continuation of a previous test. Specimen 7, for example, originally failed in the specimen end fixture away from the weld. The end fixture was replaced and testing continued as Specimen 7A until the first weld failure.

4.3 Discussion of Fatigue Test Results

4.3.1 Observed Failure Patterns. The most prevalent mode of failure in this test series was the weld root crack. The analysis of test data will focus on root failures exclusively since this failure mode is the most difficult to control and since this study was primarily aimed at the effects on fatigue life of root pass welding process and position.

Weld toe failures are caused by stress concentrations at the weld toe due to the presence of weld reinforcement on the outside of the pipe. As detailed in Chapter 2, the

Table 4-1 Fatigue Test Results for 5G GTAW Root Specimens

Summary of Fatigue Test Results for 5G GTAW Root Specimens					
Specimen Number	Nominal Stress Range	Cycles to Failure	Failure Mode	Appendix A Section	Include in S-N Curve?
1	42	38,113	Root Crack	A2.1	No
2	30	138,793	Root Crack	A2.2	No
3	42	24,391	End Fixture	A2.3	No
4	30	78,011	Root Crack	A2.4	No
5	30	133,629	Root Crack	A2.5	Yes
6	30	174,789	Root Crack	A2.6	Yes
7	30	96,708	End Fixture	A2.7	No
7A	30	197,372	Root Crack	A2.8	Yes
8	30	64,906	Root Crack	A2.9	No
9	42	69,839	Root Crack	A2.10	Yes
10	42	52,602	Toe Crack	A2.11	No
11	30	213,411	Root Crack	A2.12	Yes
12	20	707,673	Root Crack	A2.13	Yes
13	30	226,548	Root Crack	A2.14	Yes
14	20	616,112	Root Crack	A2.15	Yes
15	15	2,326,481	Root Crack	A2.16	Yes
16	20	924,337	Root Crack	A2.17	Yes

magnitude of the stress concentration at the weld toe increases as the angular transition between weld metal and base metal at the weld toe becomes more abrupt⁷. Machining or grinding the weld reinforcement flush with the base metal removes the stress concentration at

Table 4-2 Fatigue Test Results for 2G GTAW Root Specimens

Summary of Fatigue Test Results for 2G GTAW Root Specimens					
Specimen Number	Nominal Stress Range	Cycles to Failure	Failure Mode	Appendix A Section	Include in S-N Curve?
17	30	329,728	Between Weld Passes	A3.1	No
18	30	217,770	Root Crack	A3.2	Yes
19	42	78,818	Root Crack	A3.3	Yes
20	42	79,126	Root Crack	A3.4	Yes
21	12	7,583,900	Root Crack	A3.5	Yes
21A	12	8,131,410	Root Crack	A3.6	Yes
22	12	13,286,940	Root Crack	A3.7	Yes
3S	20	591,385	Root Crack	A3.8	Yes
6S	42	73,463	Toe Crack	A3.9	No

the weld toe and prevents toe crack failures.

Cracks initiating in valleys between weld passes on the outside of the pipe, as in the Specimen 17 failure, grow from stress concentrations at the valleys. Machining or grinding the weld metal below the level of the valleys between weld passes removes these stress concentrations and prevents this failure mode.

End fixture failures in Specimens 3 and 7 were the result of poor surface finishing during machining. The cracks originated at sharp surface grooves left during machining. A slight end fixture design change and more stringent requirements for surface finishing were effective in preventing end fixture failures in the later test specimens.

Table 4-3 Fatigue Test Results for 2G SMAW Root Specimens

Summary of Fatigue Test Results for 2G SMAW Root Specimens					
Specimen Number	Nominal Stress Range	Cycles to Failure	Failure Mode	Appendix A Section	Include in S-N Curve?
1S	20	415,455	Root Crack	A4.1	Yes
1SA	20	640,057	Root Crack	A4.2	Yes
2S	20	678,261	Root Crack	A4.3	Yes
2SA	20	877,832	Root Crack	A4.4	Yes
4S	30	118,311	Root Crack	A4.5	Yes
5S	30	120,975	Root Crack	A4.6	Yes
7S	42	48,613	Root Crack	A4.7	Yes

In general, failure modes with cracks initiating on the outside surface of the pipe represent an upper bound to the fatigue strength a weld considered to be controlled by weld root failure. The non-root cracks in this test series, however, all originated in welds left in the "as welded" condition. Fatigue strength for these welds could have been improved simply by grinding the weld reinforcement on the outside of the pipe. For the purpose of this project, it was desired to find the maximum practically obtainable fatigue strength of the butt welded pipe joint. Since grinding on the outside of the pipe was not considered impractical, weld root cracks were chosen as the controlling failure mode for this test series.

Weld root cracks grow from stress concentrations at the edge of the weld root pass due to the presence of weld reinforcement on the inside of the pipe. If this reinforcement could be ground flush with the base metal, stress concentrations would be eliminated and the fatigue

Table 4-4 Fatigue Test Results for Pulsed-Tig Root Specimens

Summary of Fatigue Test Results for Pulsed-Tig Root Specimens					
Specimen Number	Nominal Stress Range	Cycles to Failure	Failure Mode	Appendix A Section	Include in S-N Curve?
PT1	20	556,901	Root Crack	A5.1	No
PT1A	20	611,396	Root Crack	A5.2	No

strength would increase virtually to that of the base metal^{7,19}. The inside of the pipe is inaccessible after welding, however, and grinding or machining the weld reinforcement is not practical.

The stress concentrations at the weld root are aggravated by any offset between pipe sections at the weld^{6,7}. Offset due to poor pre-weld fitting of the pipes can be controlled by using more rigorous fit-up procedures, but misalignments also arise from the geometry of the pipe itself. The pipe sections are not perfectly round and wall thicknesses vary slightly around any given section. Offset at the weld due to the geometry of the pipe section cannot be easily eliminated.

The unavoidable stress concentrations due to the presence of inside weld reinforcement, aggravated by unavoidable pipe offsets at the weld, mean that the butt welded joint in pipe will invariably fail from a root crack if care is taken to remove or reduce sources of stress concentration on the outside surface of the pipe. The analysis of fatigue test results in Section 4.4 is intended to represent pipe butt welds having fatigue strength controlled by weld root crack failure.

4.3.2 Discussion of Weld Failures

4.3.2.1 Overview. The following sections briefly describe each specimen failure and outline any factors which might make the failure or the weld not representative of expected in-service conditions. Welds deemed not representative of expected in-service conditions were not included in the analysis of fatigue test results as presented in Section 4.4.

4.3.2.2 5G GTAW Root Welds. Specimens 1 and 2 were fabricated using intentionally large pipe offsets of roughly 1/16 inch. Fatigue failures in these two specimens occurred at points of large pipe offset and fatigue lives were much shorter than expected. These specimens were instrumental in defining pipe offset as a critical fatigue parameter to be controlled in specimen fabrication. The geometry of Specimens 1 and 2 were deemed not representative of expected in-service conditions and these specimens were not included in the analysis of test results.

Specimens 3 and 7 failed in the specimen end fixtures away from the weld. In general, end fixture failure should represent an upper bound to weld fatigue strength. In this case, however, the failure was due to stress concentrations at a surface groove created during machining of the end fixture. These failures were not considered representative of the fatigue strength of the welded joint as a whole and results were not included in the analysis of test results. The failed end fixture on Specimen 7 was replaced and fatigue testing continued as Specimen 7A. Results of Specimen 7A were included in the analysis of test data.

Specimen 4 had an abnormally short fatigue life when compared with the rest of the test specimen population. It is assumed that since this specimen was fabricated early in the testing sequence, the overall geometry of the specimen was not controlled as closely as in later

specimens. In particular, some of the early machined end fixtures were delivered with an improperly large root face on the single V weld preparation. This was corrected by manual grinding of the weld preparation, likely resulting in a steeper weld preparation angle and a highly variable root gap. Also, a small amount of cold lap of weld metal was evident at the failure location. Considering both questionable weld preparation geometry and weld flaws, this specimen was determined not to be representative of expected in-service conditions and was not included in the analysis of test results.

Post-fatigue analysis of Specimen 8 revealed a serious lack of fusion defect at the failure location. This defect should have been detected during pre-fatigue radiographic inspection of the weld. The fatigue life of this specimen was abnormally short, was not considered representative of in-service conditions, and thus was not included in the analysis of test results. Since this serious weld flaw escaped detection during test specimen fabrication, it is possible that a similar flaw might escape detection under in-service conditions. It is assumed that for actual weld design the regression fit to the test data as presented in Section 4.4 will be statistically adjusted to a design curve having a specified margin of safety and that possible in-service weld flaws will be accounted for by this margin of safety.

Specimen 10 failed from a weld toe crack. Since toe cracks can be easily prevented by grinding of the outside weld reinforcement, results from Specimen 10 were not included in the analysis of test results.

Specimens 5, 6, 7A, 9, and 11 through 16 failed from root cracks and were considered to have weld geometry representative of expected in-service conditions. Analysis of fatigue test results for the 5G GTAW root welds included data from these test specimens only. Results from all specimens are shown on the S-N plots in Section 4.4.2, however, for reference.

4.3.2.3 2G GTAW Root Welds. Test Specimens 17 through 22 and 1S through 7S were welded in the AWS 2G position with the pipe sections vertical and stationary. Both SMAW and GTAW root welds were used for these specimens, as described in Section 3.3.5 and Appendix A. Specimens 17 through 22, 3S, and 6S failed in welds having 2G GTAW root passes. Of these, only results from test Specimens 18 through 22 and 3S were included in the analysis of test results. These specimens all failed from weld root cracks and were determined to have weld geometry representative of expected in-service conditions.

Specimen 17 failed from a fatigue crack initiating between two weld passes on the outside of the pipe. Since this failure mode can be prevented by grinding the outside reinforcement flat, results from this test were not included in the analysis.

Specimen 6S failed from a weld toe crack. This failure mode also can be prevented by grinding the outside weld reinforcement so results were not included in the analysis.

4.3.2.4 2G SMAW Root Welds. Test Specimens 1S, 1SA, 2S, 2SA, 4S, 5S, and 7S all failed in welds having 2G SMAW root passes. All specimens failed from weld root cracks and were determined to have geometry representative of expected in-service conditions. The analysis of test results thus included all specimens listed above.

4.3.2.5 5G Pulsed Tig Root Specimens. Specimen PT1 was the only test specimen fabricated using the 5G Pulsed-Tig process for the root pass. After the first failure, the specimen was repaired and fatigue testing was continued as Specimen PT1A. Not enough data was generated from these two tests for a meaningful analysis of the Pulsed-Tig procedure, so results from these specimens are simply included on the 5G GTAW S-N plot for reference.

4.4 Analysis of Fatigue Test Data

4.4.1 Overview. The results of fatigue tests are presented in the form S-N fatigue curves fit to the test data, one curve for each of the three welding procedures used. The S-N curves are based on a linear regression analysis performed using the logarithm of the nominal test stress range as the independent variable and the logarithm of the number of stress cycles to failure as the dependent variable. Linear regression was performed using a Microsoft Excel 4.0 spreadsheet. The linear regression equation fit to the test data is expressed in the following form:

$$\log(N) = C + n * \log(S_r) \quad (4-1)$$

Where: N = Number of stress cycles to failure

C = Constant from regression analysis

n = Inverse slope of log-log S-N plot

S_r = Nominal test stress range

The nominal stress range was based on the pipe cross sectional area calculated using the nominal pipe outside diameter of 12.75 inches and the nominal pipe wall thickness of 0.562 inches. It is important to note that specimen failure was defined as the first through-wall crack in one of six welds on the test specimen. The S-N curves presented in Sections 4.4.2 through 4.4.4 thus reflect a 1/6 or 16.7 percent weld failure level.

Included for reference on each S-N plot are three fatigue design curves: the AASHTO Category C curve¹ and the API-X and API-X' curves². The API-X and API-X' curves are presented in the API Recommended Practice 2A document, but are intended for use with hot spot stresses in the design of tubular joints. API RP 2A states that design of pipe butt welds

should follow the fatigue provisions of the AWS D1.1 specification³. The AWS fatigue design curve C1 for "butt splices, complete joint penetration groove welds, as welded" is the same as the API-X curve, however. The AASHTO Category C curve shown on the S-N plots is that for redundant load path structures. This curve is intended for fatigue design of "base metal and weld metal in or adjacent to full penetration groove weld splices, with or without transitions having slopes no greater than 1 to 2-1/2, when the reinforcement is not removed and weld soundness is established by nondestructive inspection." It is important to note that the API and AASHTO design curves shown on the S-N plots do not represent mean fatigue lives, but rather have been adjusted to represent lower bounds of expected fatigue life.

4.4.2 S-N Curve for 5G GTAW Root Welds. The log-log linear regression analysis as described in Section 4.4.1 performed for the 5G GTAW root specimens resulted in the following equation:

$$\log(N) = 10.323 - 3.412 * \log(S_r) \quad (4-2)$$

Where: N = Number of cycles to failure

S_r = Nominal stress range

Figure 4-10 shows the fatigue test results and the regression fit to the data for the 5G GTAW root welds. Regression analysis included only the results of tests represented by diamond-shaped symbols on the plot. Test results not included in the regression analysis and non-through-wall cracks are shown on the plot for reference.

From Figure 4-10 it is apparent that the API and AASHTO fatigue design curves are generally conservative for the specimens having good geometry and included in the regression

Results of Fatigue Tests
5G GTAW Root Weld Specimens

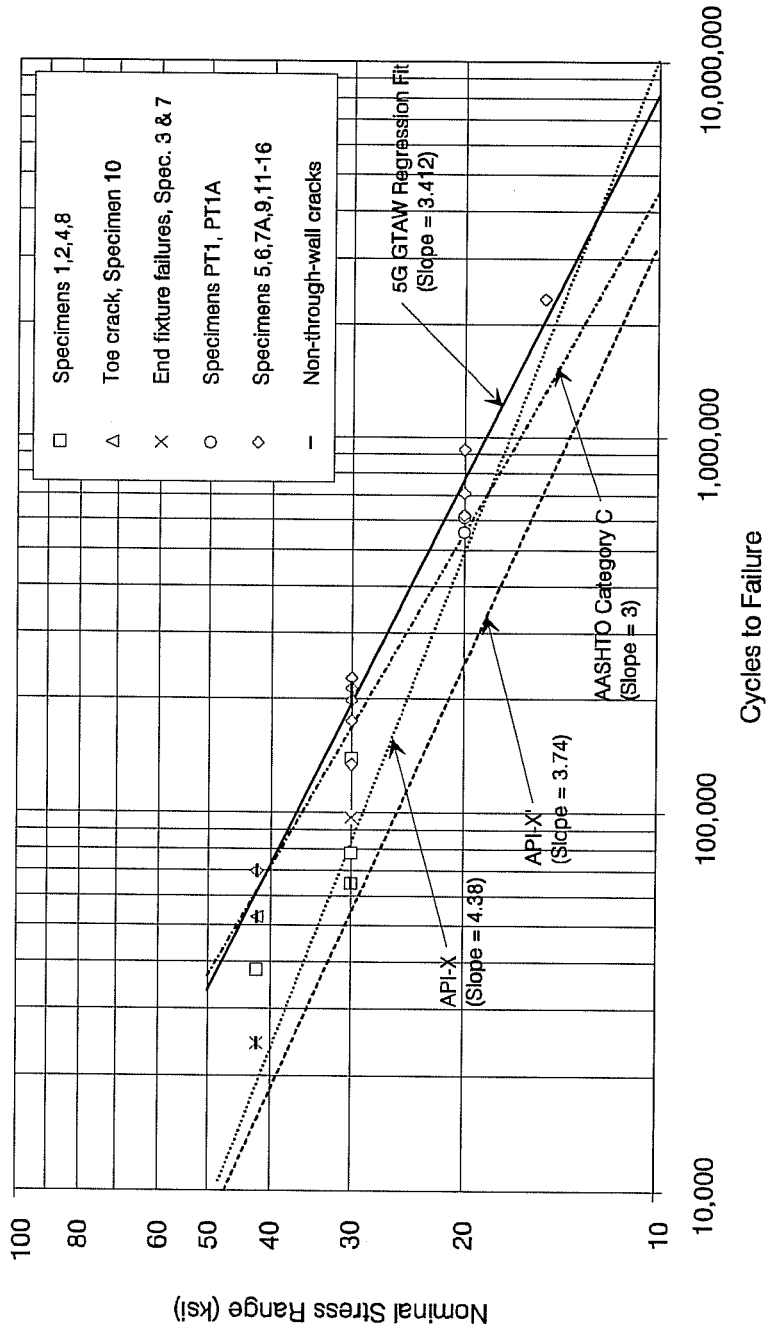


Figure 4-10 S-N Plot for 5G GTAW Root Welds

analysis. The slope of the regression curve seems to be closest to the API-X' curve, but the API-X' curve is very conservative in the sense that even data points from Specimens 1 and 2 with intentional large offsets and Specimen 8 with a serious weld flaw lie to the right of the curve. The API-X' curve appears to be most conservative at lower stress ranges.

Shown on Figure 4-10 are data from the pulsed tig root specimens PT1 and PT1A. The fatigue lives of these specimens appear to be similar to that of the 5G GTAW specimens.

4.4.3 S-N Curve for 2G GTAW Root Welds. The log-log linear regression for the 2G GTAW root specimens resulted in the following equation:

$$\log(N) = 11.052 - 3.838 * \log(S_r)$$

Where: N = Number of cycles to failure

S_r = Nominal stress range

Figure 4-11 shows the S-N plot for the 2G GTAW root specimens. From the figure, it is apparent that all fatigue design curves conservatively predicted fatigue lives for these specimens. As with the 5G GTAW root welds, the slope of the API-X' curve most closely follows that of the regression line fit to the test data. The API-X' curve appears to be quite conservative for these specimens, particularly at lower stress ranges.

Figure 4-11 shows data points for the toe crack in Specimen 6S and the crack originating between outside weld passes in Specimen 17. These data were not included in the regression analysis, but observed fatigue lives do fit well with the regression line.

Results of Fatigue Tests
2G GTAW Root Weld Specimens

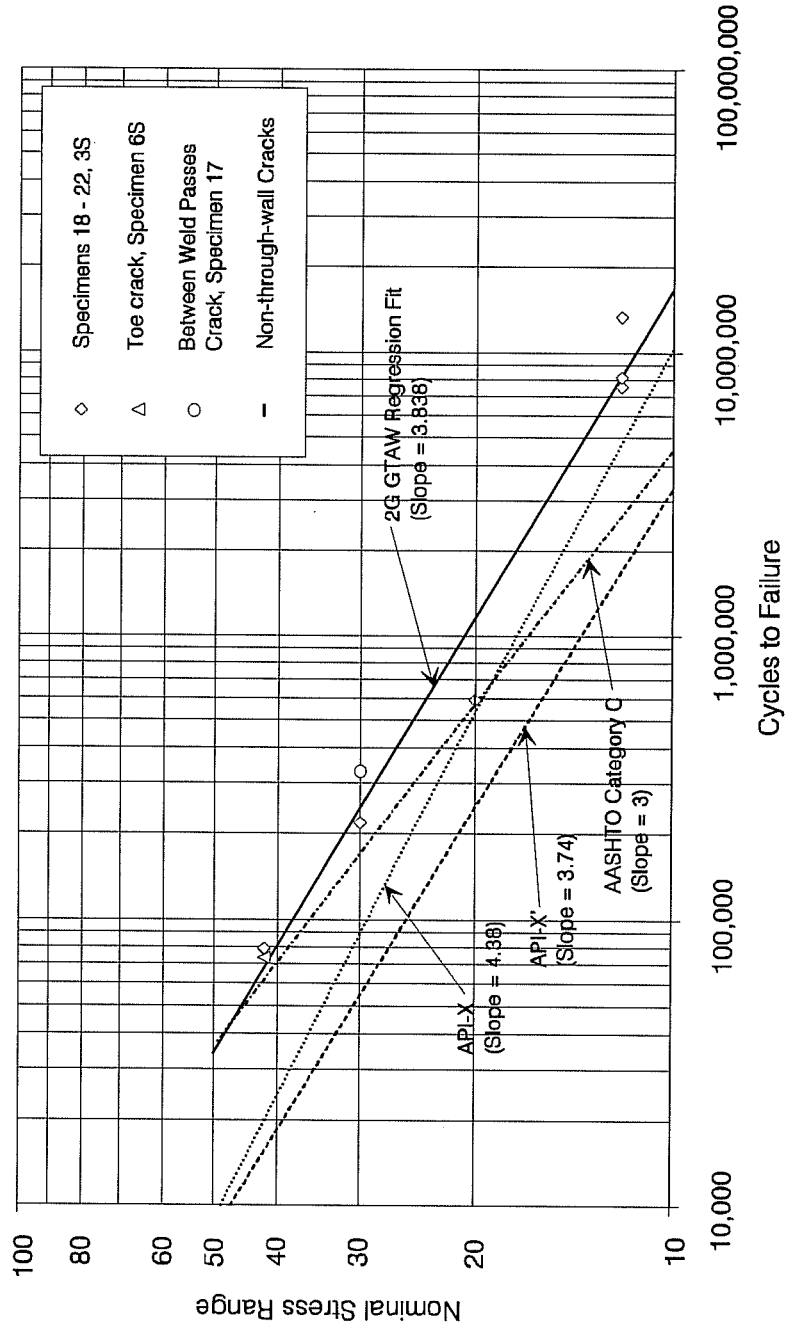


Figure 4-11 S-N Plot for 2G GTAW Root Welds

4.4.4 S-N Curve for 2G SMAW Root Welds. The log-log linear regression fit to the test data for the 2G SMAW root specimens was as follows:

$$\log(N) = 10.513 - 3.634 * \log(S_r) \quad (4-4)$$

Where: N = Number of load cycles to failure

S_r = Nominal stress range

Figure 4-12 shows a plot of the test data for the 2G SMAW root weld specimens and the regression fit to these data. The API-X and API-X' fatigue design curves shown on Figure 4-12 are generally conservative. The AASHTO-C curve appears to roughly fit the test data, being slightly unconservative at higher stress ranges but appropriately conservative at the lower stress ranges for which it is usually applied in design. As with the other welding procedures, the slope of the API-X' curve most closely matches that of the regression fit to the test data but seems highly conservative at low stress ranges.

4.5 Factors Influencing Fatigue Strength

4.5.1 Overview. An investigation of the fatigue test data was completed to identify the influence on fatigue strength of welding position, weld root process, and inside pipe offset. Fatigue behavior can be expressed by an equation of the following form:

$$N = A * (S_r)^{-n} \quad (4-5)$$

Where: N = Number of stress cycles to failure

A = A constant fit to test data

S_r = Applied nominal stress range

n = Inverse slope of log-log S-N plot

Results of Fatigue Tests
2G SMAW Root Weld Specimens

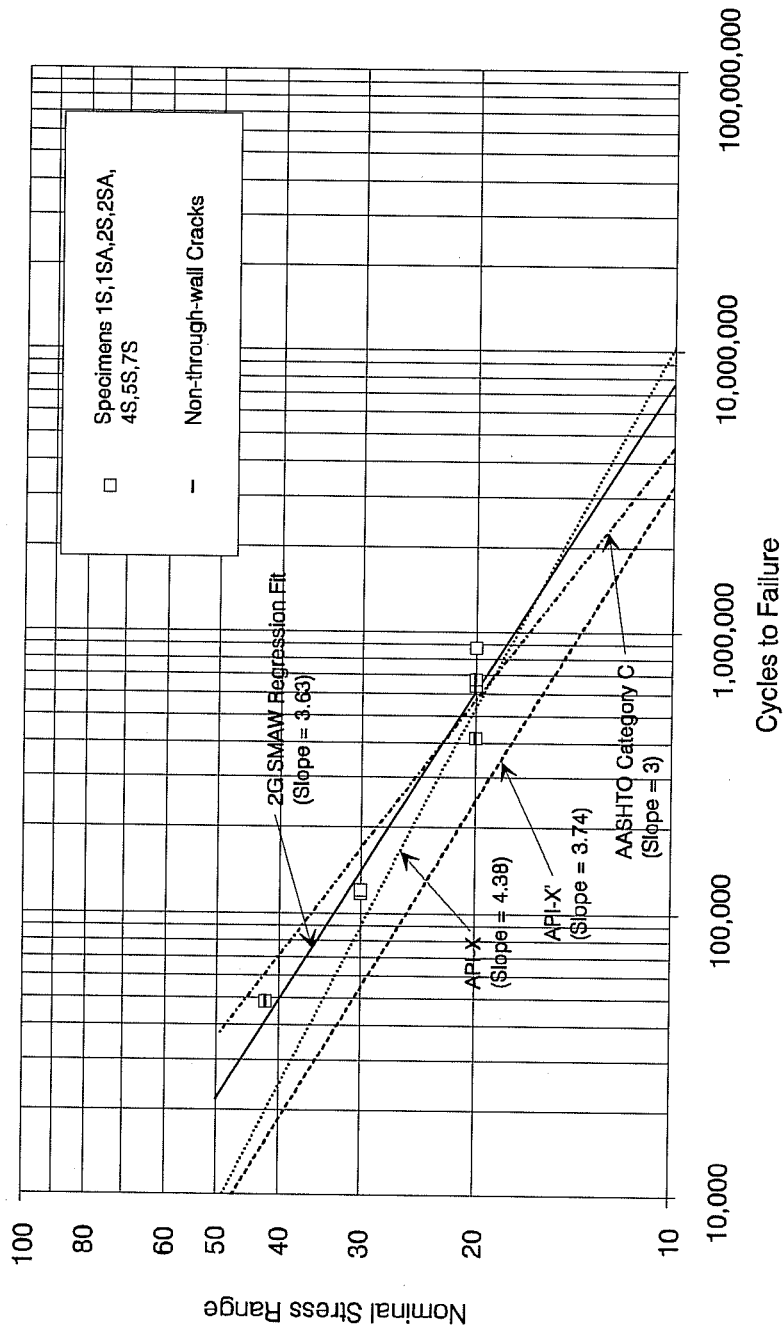


Figure 4-12 S-N Plot for 2G SMAW Root Welds

Rearranging equation 4-5 and solving for A one finds that:

$$A = N * (S_r)^n \quad (4-6)$$

Multiplying N times $(S_r)^n$ removes the influence of stress range from the analysis and any factor influencing fatigue strength is reflected by a change in the value of A. The influence of welding position, welding process, and inside pipe offset were studied by noting trends in the value of the parameter A. Analyses were completed using several values for exponent n ranging from n = 3.0 to n = 4.0. Similar trends were observed at all values of exponent n, so results are presented for the n = 3.5 case only. Where applicable, trends in the value of the parameter "A" are compared with observations from the regression lines fit to the S-N data.

4.5.2 Influence of Welding Position on Fatigue Behavior. A comparison was made between 2G GTAW test results and 5G GTAW results to investigate the influence of welding position on fatigue behavior. Somewhat unexpectedly, the 2G welds showed slightly better fatigue performance than the 5G welds. Figure 4-13 shows the S-N plot of the test data and the three regression lines fit to the data. The 2G GTAW regression curve and the 5G GTAW regression curves have slightly different slopes, but the 2G curve clearly lies to the right of the 5G curve, suggesting longer fatigue life for the 2G specimens at any given stress range. This trend also appears in an analysis of the parameter A. Tables 4-5, 4-6, and 4-7 show the values of A calculated for each test specimen included in the log-log regression analyses. Table 4-8 summarizes the data in Tables 4-5, 4-6, and 4-7 by showing average values of A for each weld type. Both the mean and median values of A are higher for the 2G GTAW welds than for the 5G GTAW welds, again suggesting longer fatigue life for the 2G GTAW specimens.

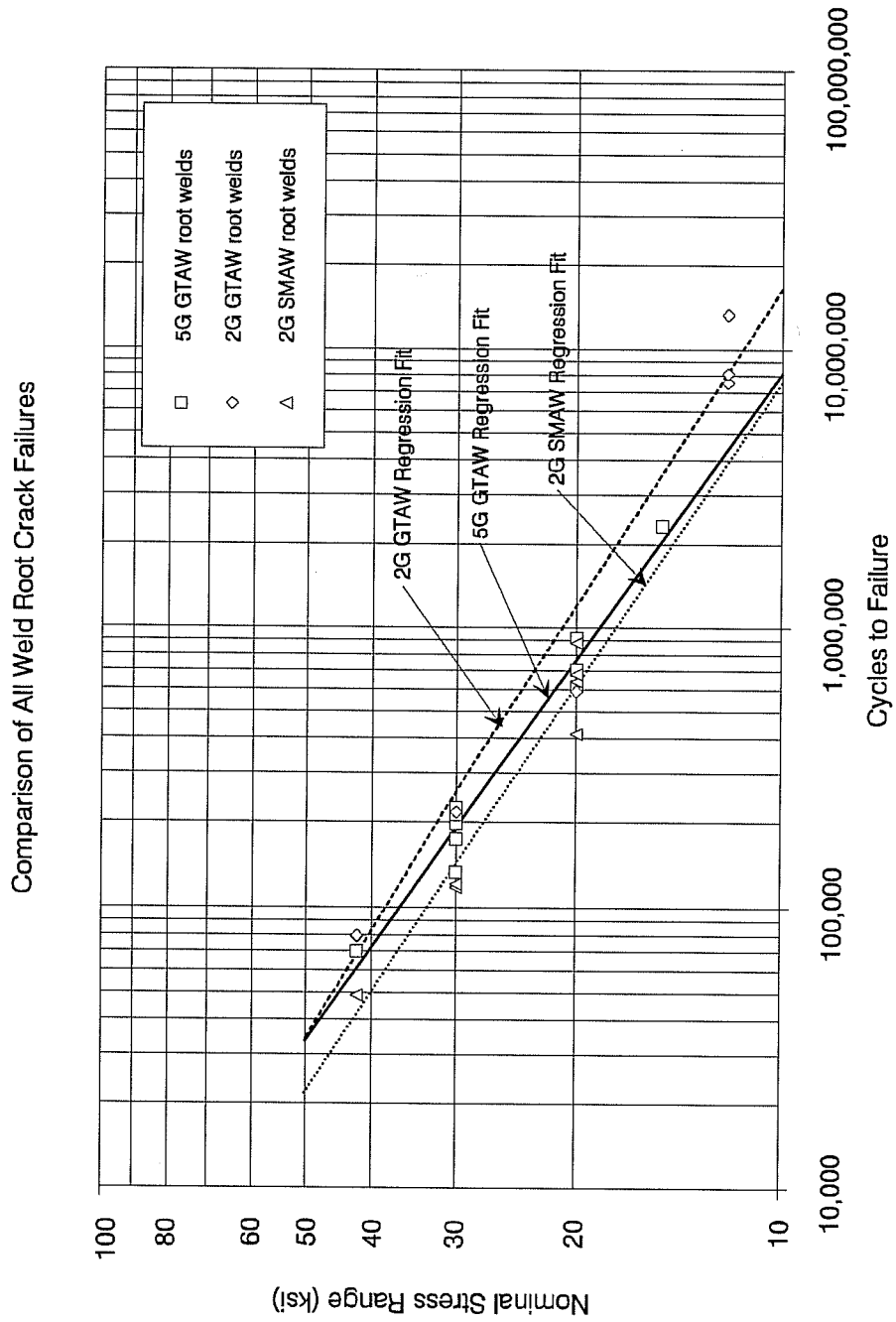


Figure 4-13 Comparison of S-N Plots

Table 4-5 Parameter "A" for 5G GTAW Root Specimens

Parameter "A" for 5G GTAW Root Specimens Failing From Root Cracks				
Specimen Number	Weld Root Procedure	Nominal Stress Range (ksi)	Pipe Inside Offset (inches)	Parameter "A" / 1×10^9 (Exponent $n=3.5$)
5	5G GTAW	30	0.015	19.762
6	5G GTAW	30	0.001	25.849
7A	5G GTAW	30	0.004	29.188
9	5G GTAW	42	0.019	33.533
11	5G GTAW	30	0.037	31.560
12	5G GTAW	20	0.026	25.318
13	5G GTAW	30	0.024	33.503
14	5G GTAW	20	0.015	22.043
15	5G GTAW	15	0.016	30.410
16	5G GTAW	20	0.017	33.070

Several explanations can be offered to account for the difference in fatigue strength. First, the 2G position could indeed result in better geometry at the weld root and thus increased fatigue strength, but no data collected during this test series seemed to suggest that this was true. The observed difference in fatigue strength could also be simply experimental error. The apparent increase in strength could be attributed to the fact that the 2G specimens were fabricated later and by that time the pipe fitters and welders were more experienced at controlling pipe offsets and the geometry of the GTAW root pass. Measured values of pipe offset do not suggest that this was true, however. The apparent increase in strength could also be attributed to the comparatively long fatigue lives of the 12 ksi 2G GTAW specimens. The

Table 4-6 Parameter "A" for 2G GTAW Root Specimens

Parameter "A" for 2G GTAW Specimens Failing From Root Cracks				
Specimen Number	Weld Root Procedure	Nominal Stress Range (ksi)	Pipe Inside Offset (inches)	Parameter "A" / 1×10^9 (Exponent $n=3.5$)
18	2G GTAW	30	0.036	32.205
19	2G GTAW	42	0.008	37.844
20	2G GTAW	42	0.019	37.992
21	2G GTAW	12	0.029	45.397
21A	2G GTAW	12	0.029	48.674
22	2G GTAW	12	0.045	79.535
3S	2G GTAW	20	0.037	21.158

three 12 ksi specimens tend to pull the 2G GTAW regression curve to the right on Figure 4-13. Perhaps testing more 5G GTAW specimens at lower stress ranges would have resulted in closer agreement between the 2G and 5G regression curves.

4.5.3 Influence of Weld Root Process on Fatigue Behavior. To investigate the influence of the welding process used to make the root weld, a comparison was made between test results from the 2G GTAW and the 2G SMAW root welds. The 2G GTAW root welds clearly had longer fatigue lives at any given stress range. The analysis of the parameter A summarized in Table 4-8 shows that both the mean and median values of A are clearly higher for the 2G GTAW root welds than for the 2G SMAW root welds. This difference in fatigue strength is also apparent in the S-N plots shown in Figure 4-13. The 2G GTAW and 2G

Table 4-7 Parameter "A" for 2G SMAW Root Specimens

Parameter "A" for 2G SMAW Specimens Failing From Root Cracks				
Specimen Number	Weld Root Procedure	Nominal Stress Range (ksi)	Pipe Inside Offset (inches)	Parameter "A" / 1×10^9 (Exponent $n=3.5$)
1S	2G SMAW	20	0.001	14.864
1SA	2G SMAW	20	0.019	22.899
2S	2G SMAW	20	0.017	24.266
2SA	2G SMAW	20	0.000	31.406
4S	2G SMAW	30	0.061	17.496
5S	2G SMAW	30	0.079	17.890
7S	2G SMAW	42	0.050	23.341

SMAW regression curves have approximately the same slope, but the 2G GTAW curve clearly lies to the right of the 2G SMAW curve, suggesting longer fatigue life for the 2G GTAW root welds at any given stress range.

This difference in fatigue strength between GTAW root and SMAW root welds was expected. At the start of the project, the GTAW root procedure was chosen as a substitute for the more commonly used SMAW root procedure as a possible means of improving fatigue strength. It was thought that the geometry and integrity of the GTAW root pass could be more closely controlled than that of the SMAW procedure. The improved root geometry and decreased incidence of weld flaws in the GTAW root appear to have been effective at improving the fatigue strength of the weld.

Table 4-8 Average Values of Parameter "A"

Average Values of Parameter "A"		
Specimen Group	Statistic	Parameter "A" / 1×10^9 (Exponent n = 3.5)
All Specimens	Mean	30.800
	Median	29.799
5G GTAW Only	Mean	28.424
	Median	29.799
2G GTAW Only	Mean	43.258
	Median	37.992
2G SMAW Only	Mean	21.738
	Median	22.899

4.5.4 Influence of Inside Pipe Offset on Fatigue Behavior. The parameter A as described in Section 4.5.1 accounts for all factors affecting weld fatigue strength, including weld flaws, overall joint geometry, and weld reinforcement shape. An attempt was made to correlate increases in inside pipe offset with decreases in A and thus decreased fatigue life. Results of this investigation were somewhat inconclusive.

Figure 4-14 shows a plot of inside pipe offset versus the parameter A for all test specimens included in the S-N regression analyses. The regression line shown on the plot shows the expected trend that as inside offset increases, the parameter A and thus fatigue life decreases. The regression fit, however, was calculated neglecting the three largest values of A. These data points represent the three 2G GTAW specimens tested at 12 ksi. Including these data points resulted in a meaningless regression line. It should also be noted that Specimens

1 and 2 which were fabricated using intentionally large offsets are not shown on the plot. Pipe offset measurements were not taken for these specimens.

Separate regression analyses were performed between inside offset and the parameter A for the 5G GTAW root welds, the 2G GTAW root welds, and the 2G SMAW root welds. Only the 2G GTAW welds showed the expected trend of A decreasing with increasing offset. Both the 5G GTAW and 2G SMAW regression lines showed increasing fatigue life with increasing inside pipe offset, which is counter-intuitive.

Although no conclusive correlation was found between fatigue life and inside pipe offset when considering all specimens, strong correlation was found between inside pipe offset and the failure location within a particular test specimen. Included in the data in Appendix A

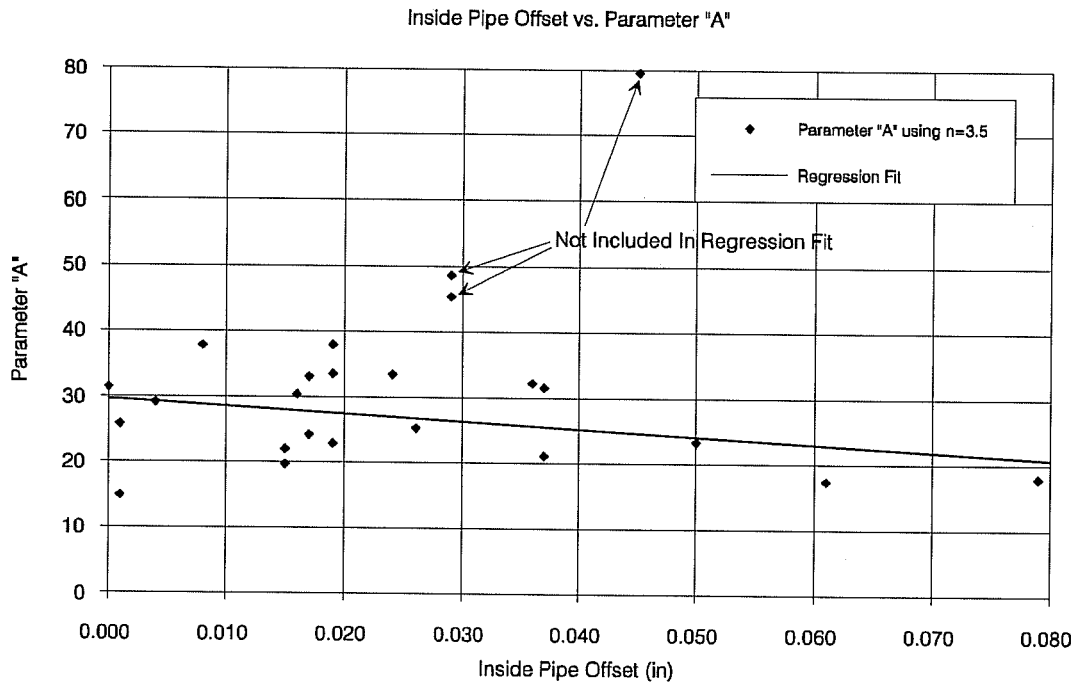


Figure 4-14 Inside Offset vs. Parameter "A"

is a comparison of the measured inside pipe offset at the failure location with measured inside offsets on the rest of the specimen. When fatigue failure did not initiate at a weld flaw, the inside offset at the failure location was generally found to rank among the largest values of inside offset measured on the specimen. Figure 4-15 shows a histogram of the inside offset rank for each specimen failure location. An inside offset rank of 1 means that the failure occurred at the location of the largest value of inside offset for that specimen, a rank of 2 means that the failure occurred at the second largest inside offset location, etc. From the histogram, the skewness to the left suggests that the magnitude of the inside offset had an influence on failure location within each test specimen.

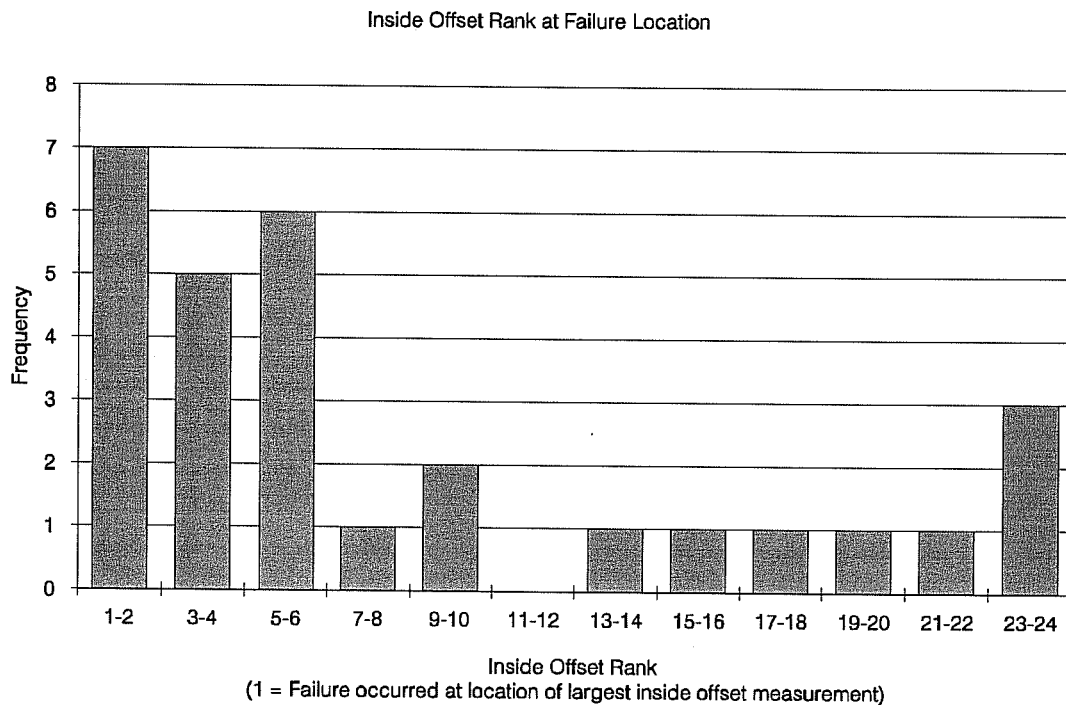


Figure 4-15 Histogram of Inside Offset Ranks

In this series of tests, the influence of inside offset on fatigue performance was not sufficiently isolated from other failure-producing variables such as inside reinforcement height or toe angle at the weld root to support conclusive evidence of the influence of inside pipe offset on fatigue performance. Other studies, however, have shown clear correlation between increased offset and decreased fatigue strength^{6,7}.

4.6 Summary of Results

It was observed that the most prevalent mode of fatigue failure for the welds tested was a weld root crack. Since this mode of failure is the most difficult to control, the analysis of fatigue test results focused on welds failing from root cracks only.

It was observed from the fatigue test results that the GTAW root welds clearly had a longer fatigue life at any given stress range than similar welds having a SMAW root pass. It was concluded that weld root process did have an effect on fatigue life and the GTAW root process resulted in longer fatigue lives at any given stress range.

In examining the effects of welding position on fatigue life, it was observed that GTAW root specimens welded in the AWS 2G position had slightly longer fatigue lives at any given stress range than GTAW root specimens welded in the AWS 5G position. It was concluded that no strong evidence suggested a correlation between fatigue life and welding position and that the observed trend could be due to experimental error.

The examination of the effect of overall weld joint geometry on fatigue life showed correlation between inside pipe offset and failure location within each specimen. It was concluded, however, that inside pipe offset was not sufficiently isolated from other failure causing parameters in this test series to show direct correlation between inside offset and

fatigue life among specimens. It was noted, however, that previous research has shown correlation between increased offset and decreased fatigue life.

CHAPTER 5

PROPOSED STRESS SHADOWING GROOVES

5.1 Overview

It has been well documented that the overall geometry of a butt welded joint has a tremendous effect on its fatigue strength. As detailed in Chapter 2, early experimental work showed that the fatigue strength of butt welds in flat plates could be increased to the fatigue strength of the parent plate if the weld root pass was back-gouged and rewelded and if the weld reinforcement was ground flush with the base metal. Back-gouging of the root pass and grinding or machining has proven quite effective in reducing fatigue problems for butt welds in flat plates and I-shaped sections, particularly in steel bridge applications. For butt welds in pipe, however, the inside of the weld is generally inaccessible and back-gouging or grinding of the root reinforcement to improve fatigue strength is not an available option. If the profile of the outside weld reinforcement is controlled by careful welding procedures or by grinding or machining, the butt welded joint in pipe will invariably fail from a fatigue crack initiating at the edge of the weld root pass.

As detailed in Chapters 2 and 4, the presence of weld root pass reinforcement leads to a stress concentration at the edge of the root pass. The magnitude of this stress concentration is increased by any offset in the parent plates at the weld^{6,7}. Offset in flat plates can generally be controlled through rigorous fit-up procedures prior to welding. For welds in pipes, however, this offset is due not only to slight misalignments in fit-up but also to variability in pipe wall thickness around the pipe and any out-of-roundness that might exist in the pipe

section. The stress concentrations at the weld root due to the presence of weld reinforcement, aggravated by unavoidable offsets due to pipe section geometry, are thus unavoidable.

As a method of reducing the effects of the unavoidable sources of stress concentration at the weld root, it is proposed that grooves be machined on the inside of the pipe sections prior to welding. It is the intention that these groove would cause stresses to "flow around" the changes in geometry at the weld root rather than causing a stress concentration in this region. The reduced stress at the weld root would thus increase fatigue life by prolonging fatigue crack initiation time and slowing crack growth.

A preliminary finite element analysis into the feasibility of the stress shadowing grooves has been completed and is detailed in the following sections. Figure 5-1 shows a cross section through the pipe and weld for the part modelled in the finite element analysis. Shown schematically on the figure are the proposed stress shadowing grooves and the overall dimensions of the finite element model. Figure 5-2 shows a cross section through the pipe weld with all geometric parameters defined. Extensive reference will be made to the parameters shown schematically in Figure 5-2.

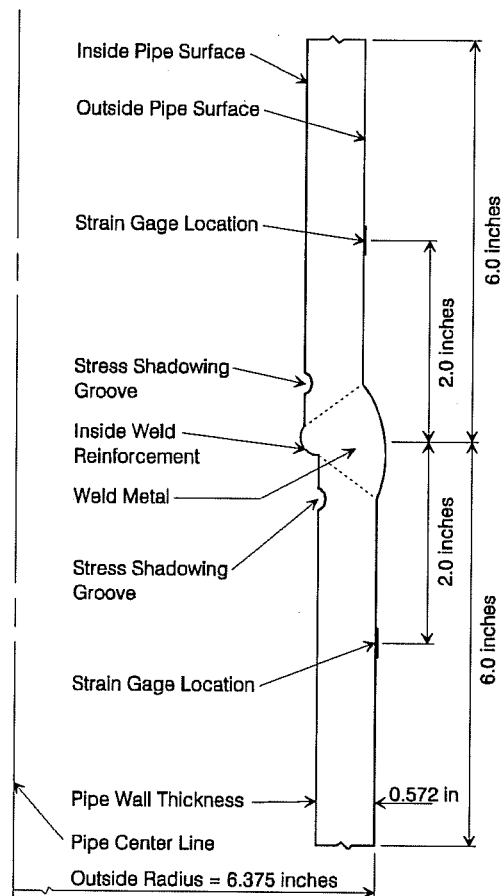


Figure 5-1 Weld Section Modelled Using Finite Elements

5.2 Critical Parameters

Based on results of previous research⁷ and some preliminary finite element analyses, several parameters were identified as critical to the magnitude of the stress concentration at the weld root. In terms of weld geometry, critical parameters included the inside reinforcement height, inside reinforcement width, and the magnitude of the inside pipe offset at the weld. Each of these parameters is defined in Figure 5-2. It is important to note that the definition of inside and outside reinforcement width and height were slightly different than that which is

commonly used. Three parameters were chosen to represent the proposed stress shadowing grooves--the groove depth, the groove radius, and the groove location with respect to the weld.

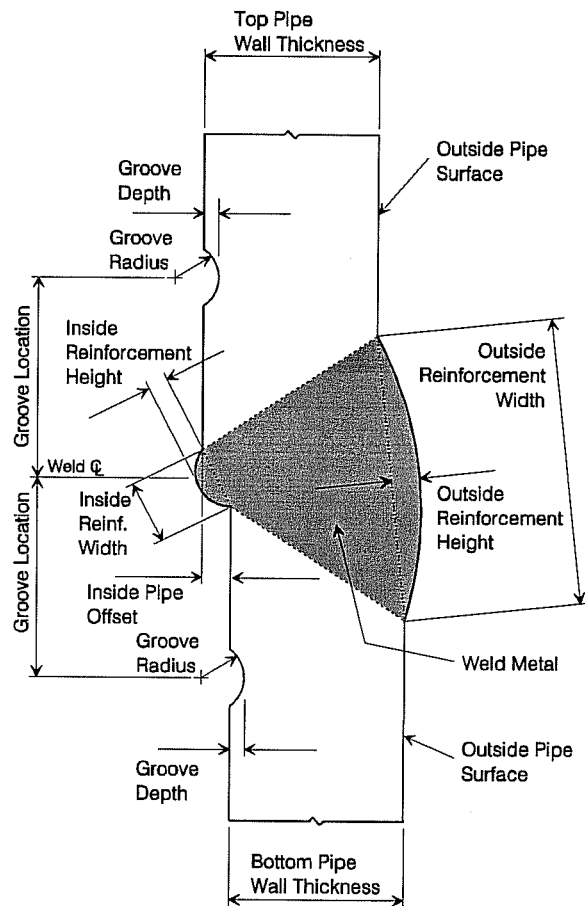


Figure 5-2 Weld Geometry Defined

5.3 Finite Element Model

The welded joint was modelled axisymmetrically using the finite element analysis program ANSYS, Revision 4.4A. The elements used in the analysis were two dimensional solid isoparametric elements with each element having four nodes and two degrees of freedom at

each node. Elastic material properties were used in the analysis. To simplify analysis and reduce the amount of computer time for each analysis run, substructuring was used for portions of the model where it was not desired to obtain magnitudes or distributions of stresses. Figure 5-1 shows a cross section through the pipe and weld and the dimensions of the finite element model. Figure 5-3 shows the model used in the analysis, including boundary conditions and the locations of substructures. A progressively finer element mesh was used in moving from the top and bottom toward the center of the model.

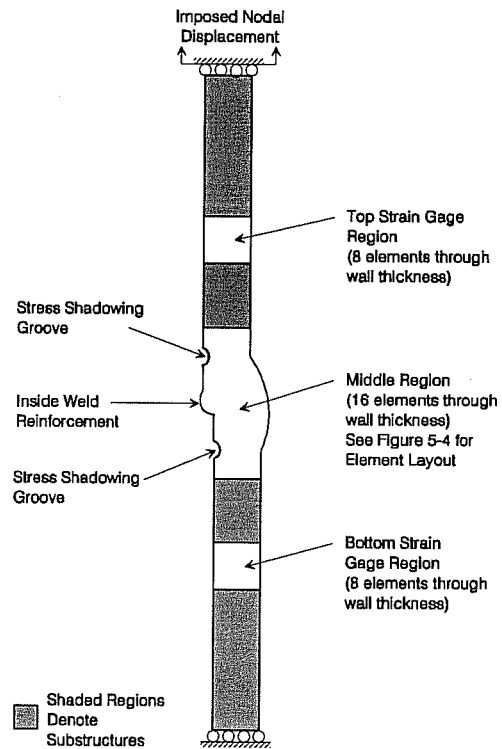


Figure 5-3 Axisymmetric Finite Element Model

Figure 5-4 shows the layout of elements in the middle region of the model. For reference, the element plot shown in Figure 5-4 is for a groove location of 0.500 inches, a groove depth of 0.050 inches, a groove radius of 0.150 inches, and an inside offset of 0.050 inches.

Loads were applied to the finite element model using imposed nodal displacements. The vertical displacement was fixed for the nodes at the bottom of the model and a vertical displacement was imposed on the nodes at the top of the model. The magnitude of this displacement was that necessary to produce a nominal axial tensile stress of 100 ksi in the pipe.

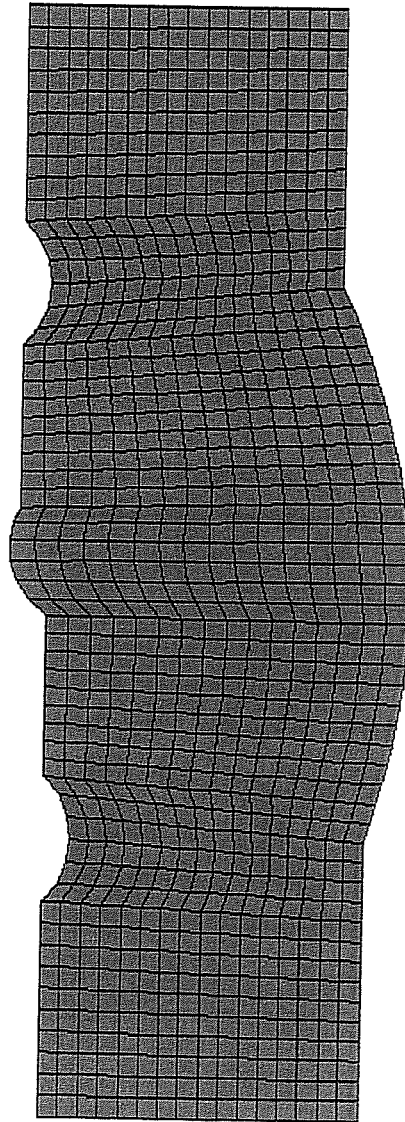


Figure 5-4 Layout of Elements in Middle Region of Finite Element Model

The cross sectional profile of both the inside and outside weld reinforcements were assumed to follow a circular arc. The cross sectional profile of the proposed stress shadowing grooves also was modelled as a circular arc.

Since the finite element analyses performed were intended only to be a preliminary investigation into the feasibility of the proposed stress shadowing grooves, representative dimensions for several parameters were chosen and held constant. The dimensions chosen were based on measurements scaled from 26 photomicrographs of weld cross sections at failure locations.

Stress concentrations due to the geometry of the outside weld reinforcement can be controlled relatively easily by machining or grinding, so for this preliminary analysis the outside reinforcement width and height were held constant at 1 inch and 0.100 inches, respectively. For reference, outside reinforcement widths scaled from the photographs ranged from 0.845 inches to 1.107 inches with an average value of 0.950 inches. Outside reinforcement heights varied from 0.029 inches to 0.103 inches with an average value of 0.067 inches.

The magnitude of the stress concentration at the inside weld reinforcement is known to vary with the height-to-width ratio of the reinforcement⁷, but the shape was held constant in this series of analyses in order to evaluate different groove configurations. The width and height of the inside weld reinforcement were held constant at 0.200 inches and 0.040 inches, respectively. For reference, the inside reinforcement widths scaled from the photomicrographs varied from 0.144 inches to 0.255 inches with a mean value of 0.196 inches. Inside reinforcement height varied from 0.012 inches to 0.068 inches with a mean value of 0.038 inches.

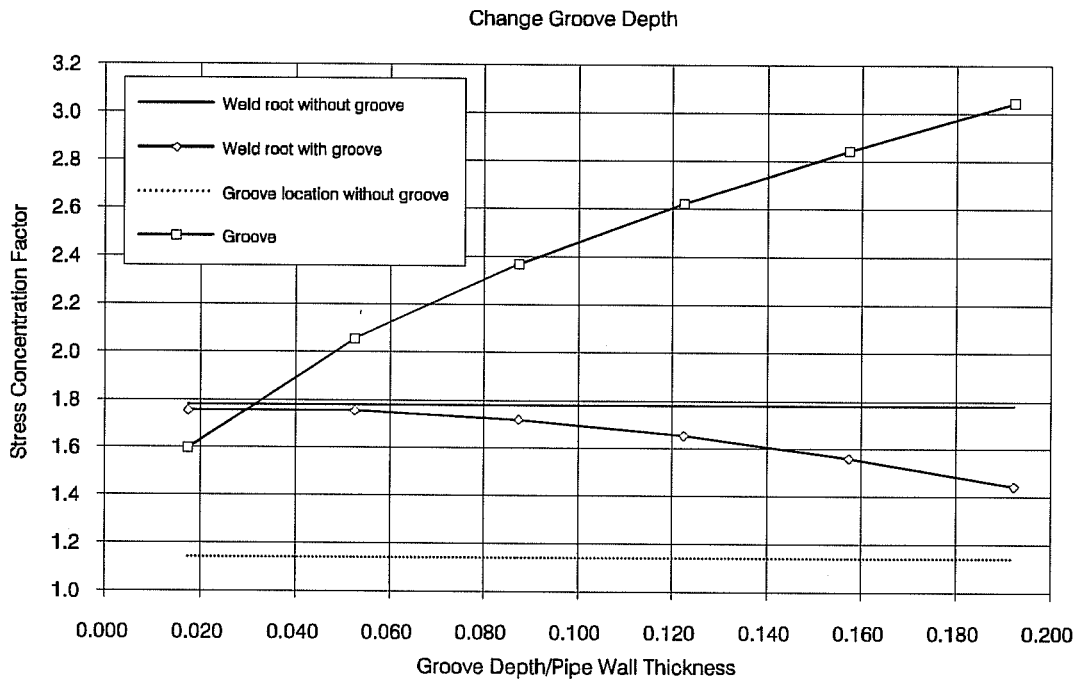


Figure 5-6 Stress Concentration Factor vs. Groove Depth

Figure 5-7 shows the relationship between stress concentration factor and normalized groove location for stresses at the weld root and at the groove location. From the figure, it is observed that as the groove is moved closer to the weld, the groove becomes more effective at reducing the stress concentration at the weld root. This reduction in weld root stress is accompanied by a slight increase in stress at the groove location, however.

5.4.5 Groove Radius. The radius of the stress shadowing groove was varied in a series of finite element analyses. The groove radius was varied from 0.050 inches to 0.500 inches, or from 8.7 percent to 87 percent of the pipe wall thickness. For this series of analyses inside pipe offset remained constant at 0.050 inches, groove depth constant at 0.050 inches, and groove

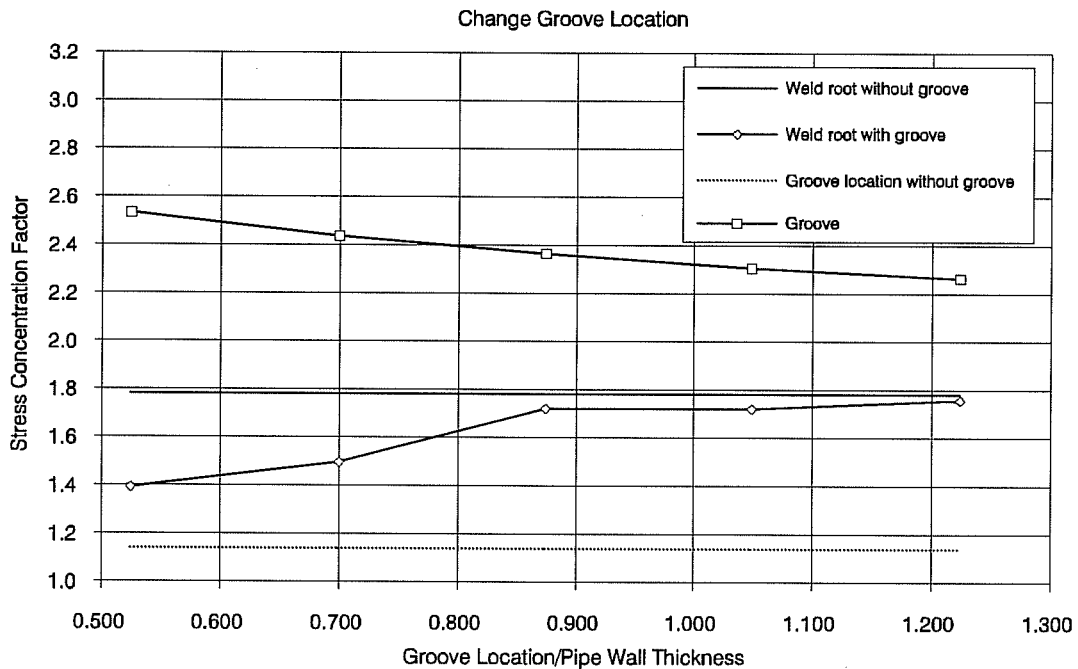


Figure 5-7 Stress Concentration Factor vs. Groove Location

location constant at 0.500 inches.

Figure 5-8 shows the results of this analysis series as a plot of stress concentration versus normalized groove radius. From the plot, it is apparent that the reduction in stress at the weld root is virtually constant as the groove radius is changed. The magnitude of stress concentration at the groove, however, is observed to decrease substantially as the groove radius increases.

5.4.6 Pipe Wall Thickness Mismatch. The final series of finite element analyses investigated the effect of wall thickness mismatches on the magnitude of stress concentrations at the weld root and the groove location. During this series of analyses, the value of top pipe wall thickness was varied from 0.520 inches to 0.620 inches while holding the bottom wall

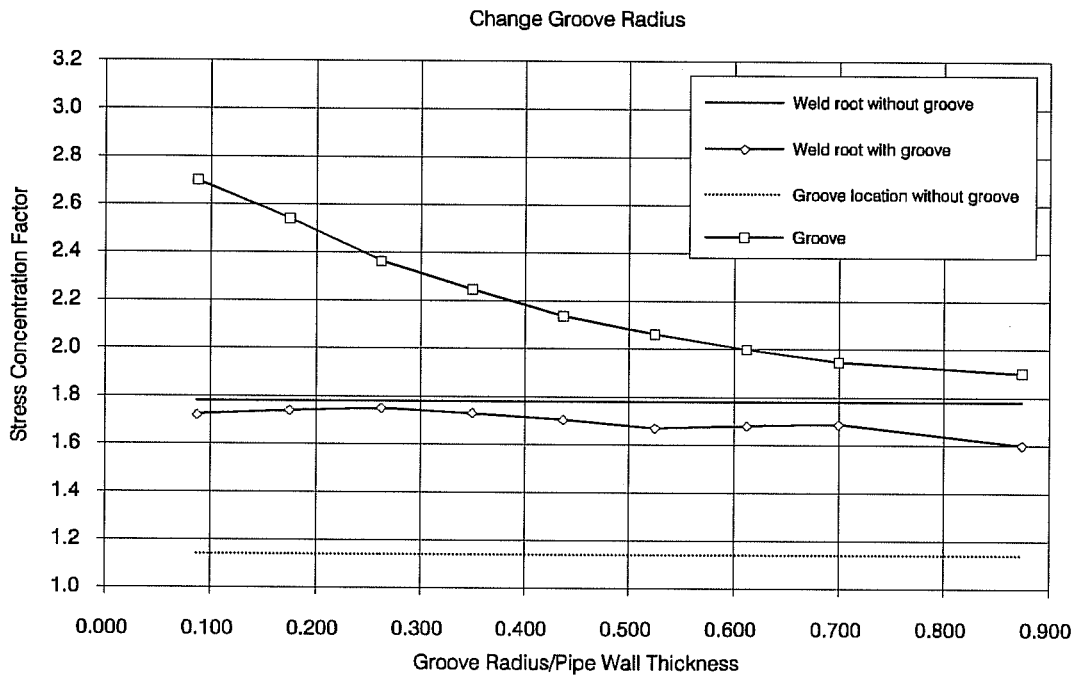


Figure 5-8 Stress Concentration Factor vs. Groove Radius

thickness constant at 0.572 inches. Also held constant were the inside pipe offset at 0.050 inches, the groove radius at 0.150 inches, the groove depth at 0.050 inches, and groove location at 0.500 inches.

Figure 5-9 shows that changes in pipe wall thickness across the weld joint had relatively little effect on the stress concentration at the weld root or at the groove location. For the cases when the top wall thickness was significantly less than the bottom wall thickness, it was observed that the maximum stress in the finite element model occurred at the top toe of the outside weld reinforcement rather than at the edge of the inside weld reinforcement as in all other analysis runs.

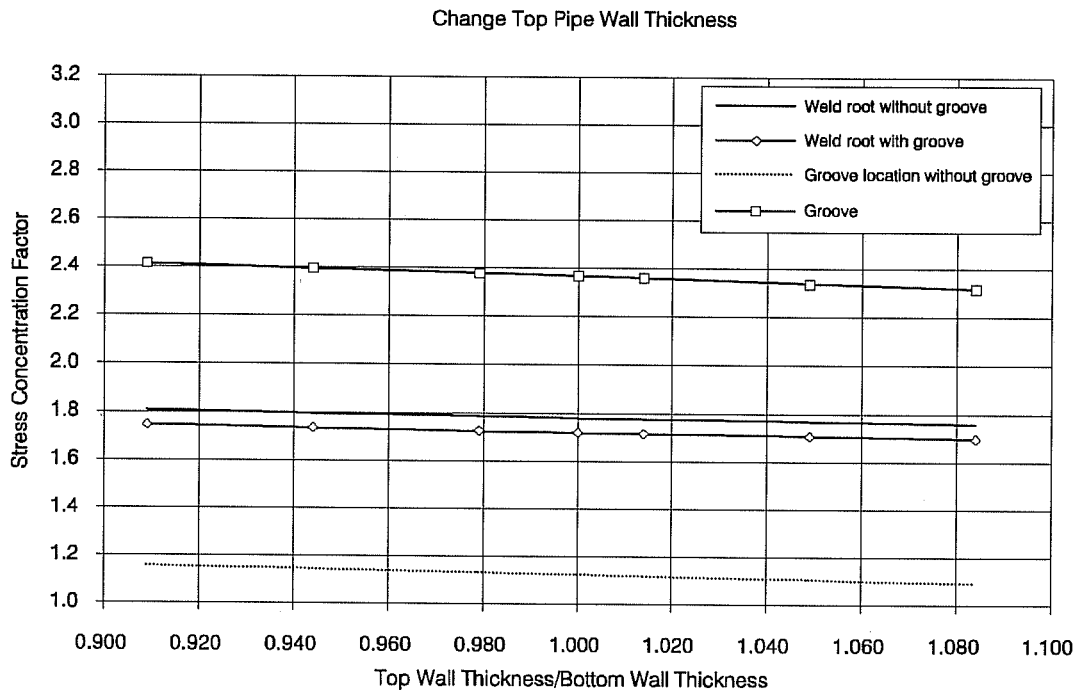


Figure 5-9 Stress Concentration Factor vs. Pipe Wall Thickness

5.5 Discussion of Results

In all cases analyzed using the finite element model of the welded joint, stress shadowing grooves were observed to reduce the stress concentration at the weld root. As outlined in Chapter 2 and Equations 2-1 through 2-3, fatigue crack propagation life is proportional to stress range raised to a negative power, typically -3. Thus even small reductions in stress result in large increases in fatigue life. In light of this, the observed reductions in stress at the weld root due to the proposed stress shadowing grooves could result in significant increases in fatigue life.

There are some detrimental effects, however, of machining stress shadowing grooves into the pipe sections prior to welding. Most importantly, the reduction in cross sectional area due to the groove itself leads to a stress concentration at the groove location. The finite

element analysis results as shown in Figures 5-5 through 5-9 show that the stress concentration at the groove location can be fairly significant.

Based on the results of the finite element analyses summarized in Section 5.4, it appears that the best balance between effectiveness at reducing weld root stress and increasing groove location stress can be obtained by using a large radius, relatively shallow groove located close to the weld reinforcement. Figures 5-10 and 5-11 show the results of an analysis run in which a 0.250 inch radius groove 0.020 inches in depth was located at a distance 0.250 inches from the center of the weld. The inside pipe offset for this analysis was 0.050 inches. Figure 5.10 shows a contour plot of axial stresses for the welded joint without stress shadowing grooves. The maximum stress at the weld root for this configuration was 177.9 ksi, or a stress concentration factor of 1.779. Figure 5.11 shows a similar contour plot for the same weld configuration with the stress shadowing grooves present. The axial stress at the weld root was decreased to 149.4 ksi, or a stress concentration factor of 1.494. This represents a reduction in stress at the weld root of 16 percent. For this model, however, the stress at the groove location increased from 123.6 ksi to 191.5 ksi with the introduction of the groove. This is an increase in stress of 55 percent. It is important to note, however, that the resulting stress concentration at the groove is only 7.6 percent higher than the original stress concentration at the weld root.

Even though the reduction in stress at the weld root invariably comes at the expense of increased stress at the groove location, it is possible that an increase in overall fatigue life of the joint could result. Most importantly, weld fatigue cracks readily initiate from minute flaws at the weld root¹² and the crack initiation life is generally negligible^{7,12}. Since these flaws would not exist at the groove location, a significant portion of the groove location fatigue life

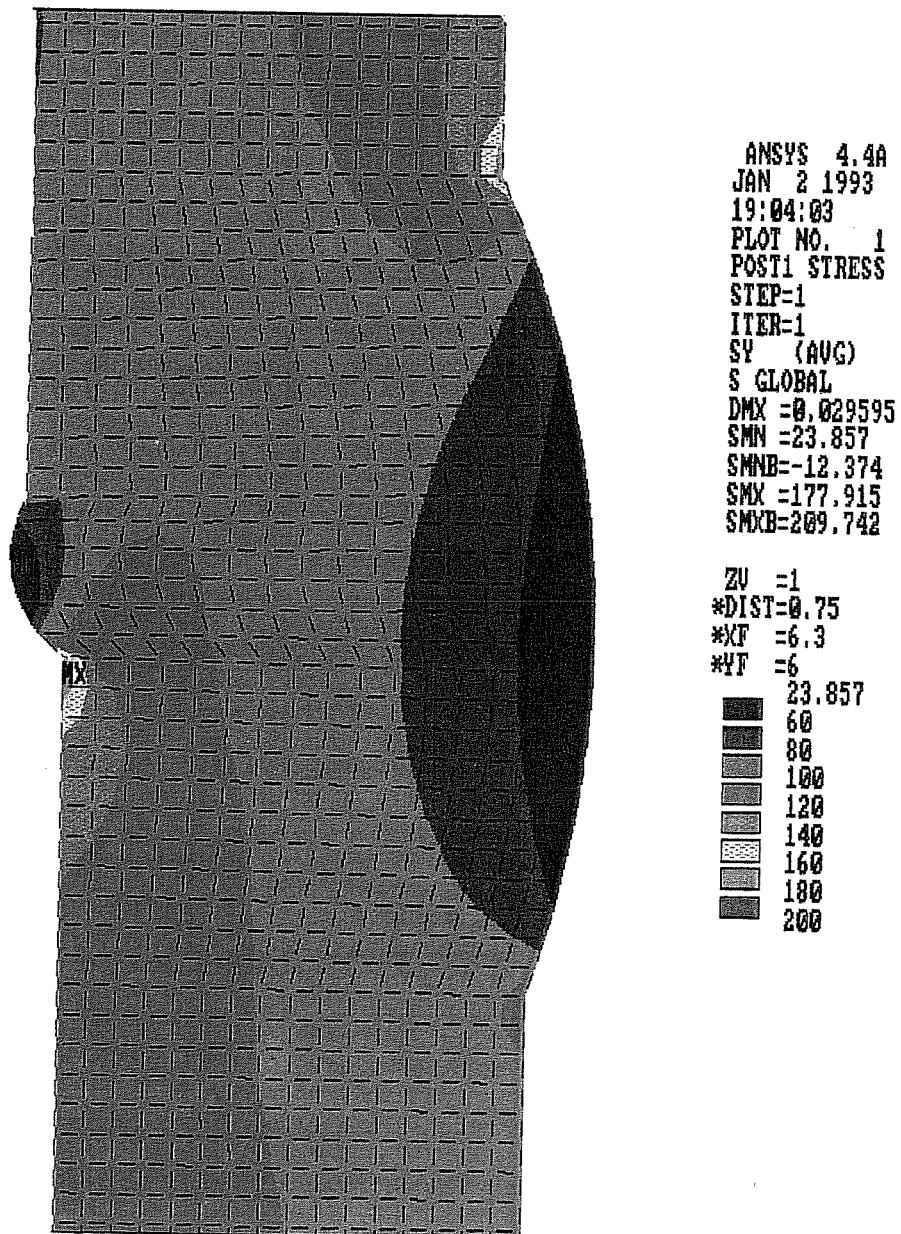


Figure 5-10 Axial Stress Distribution Without Stress Shadowing Grooves

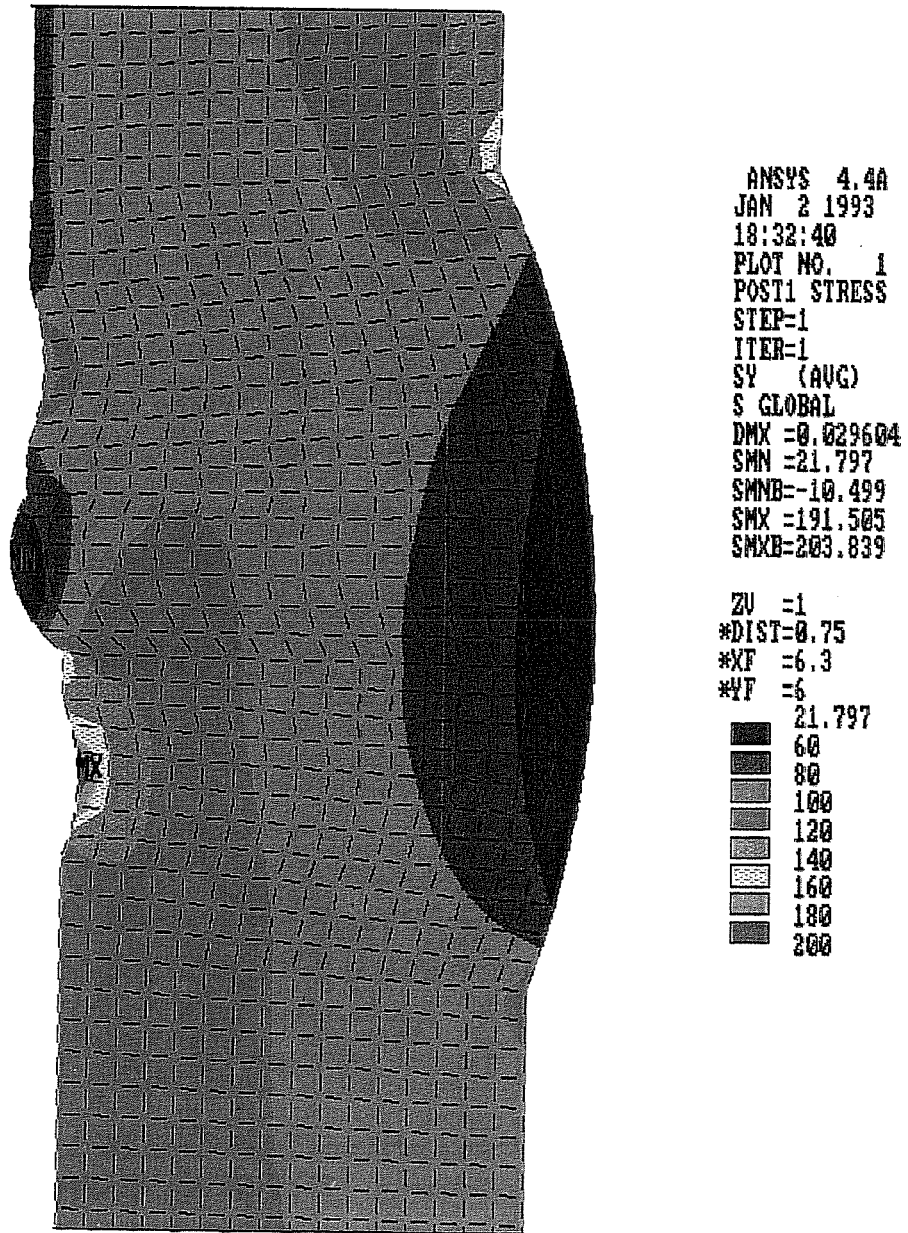


Figure 5-11 Axial Stress Distribution With Stress Shadowing Grooves

would likely be spent initiating a sharp, well-defined fatigue crack. Also, the shape and depth of the groove can be controlled quite easily by careful machining and thus the magnitude of the stress concentration in this region should be more predictable than the stress concentration at the weld root which has a highly variable geometry. Lastly, since the grooves would be machined into the pipe sections prior to welding, these grooves could be inspected for ridges or scratches or other irregular shapes which might act as initiation points for fatigue cracks. More reliable estimates of groove location stress concentration and an assurance that sharp notches do not exist at the groove would likely result in more reliable groove location fatigue life predictions.

Since other complicating factors including residual stresses and weld flaws introduced by the welding process must be considered when evaluating the true fatigue behavior of a welded joint, it is suggested that the only true test of the feasibility of the proposed stress shadowing grooves would be actual fatigue tests. These tests should include systematic investigations into the effects on fatigue life of such parameters as groove location, groove shape, and groove depth.

CHAPTER 6

SPATE SCANS AND DYNAMIC STRAIN READINGS FOR SPECIMEN 7S

6.1 Overview

As this testing program progressed, more of the specimens seemed to be failing in the pipe-to-end fixture welds on the ends of the specimens than in the interior pipe-to-pipe welds. A SPATE (Stress Pattern Analysis by Thermal Emission) was used to examine the stress distribution near an end fixture weld on Specimen 7S to assure that irregular stress patterns due to either end fixture geometry or the testing apparatus were not present. Section 6.2 details the results of the SPATE scans.

Before initiating dynamic fatigue loading, each test specimen in this series was cycled statically through the test load range four times during which strain gage readings were recorded. It was the assumption that the strains measured during the fourth static loading cycle were representative of the strains experienced by the specimen during subsequent dynamic fatigue loading. Strain gage readings were taken during fatigue loading of Specimen 7S in order to verify this assumption. Section 6.3 details the results of these dynamic strain gage readings.

6.2 SPATE Scans

6.2.1 Testing Equipment. The SPATE is essentially an ultra-sensitive infrared temperature sensing device. Its operation is based on the principles of the Kelvin effect which states that an adiabatic change in stress in a homogeneous, isotropic, elastic material is directly related to a change in material temperature²¹. By using a rapid cyclic loading pattern during

a SPATE scan, heat transfer at the surface of the specimen is diminished and adiabatic loading is approximated. The SPATE measures the change in temperature at a point on the surface of the test specimen and correlates this temperature change with a change in stress. By scanning points on a grid, the SPATE is able to obtain a complete picture of the stress pattern on the test specimen.

6.2.2 Testing Procedure. A 10 ksi stress range cycling at 2.5 hertz was applied to Specimen 7S. The SPATE equipment was set up and two scans were taken of the area near weld number 7SW1, the bottom pipe-to-end fixture weld on the specimen as shown in Figure 6-1. The first scan was a vertical strip roughly 3 inches wide by 10 inches high running from just above the weld down toward the end fixture. This is Scan Area 1 as shown schematically in Figure 6-2 and in the photograph in Figure 6-4. This scan was intended to detect any nonuniformities in the stress distribution in the end fixture. The second scan, Scan Area 2 in Figures 6-3 and 6-4, was of a horizontal strip roughly 10 inches wide by 3 inches high centered about weld number 7SW1. This

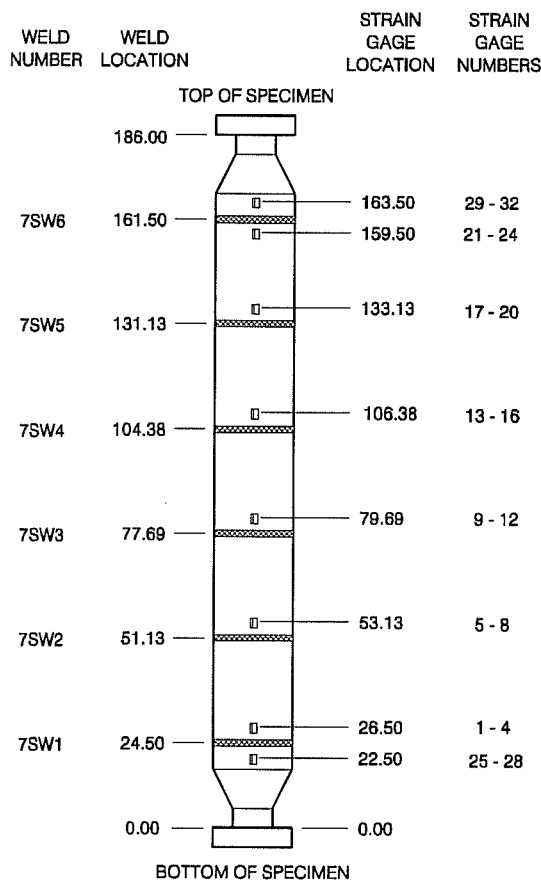


Figure 6-1 Strain Gage Layout Specimen 7S

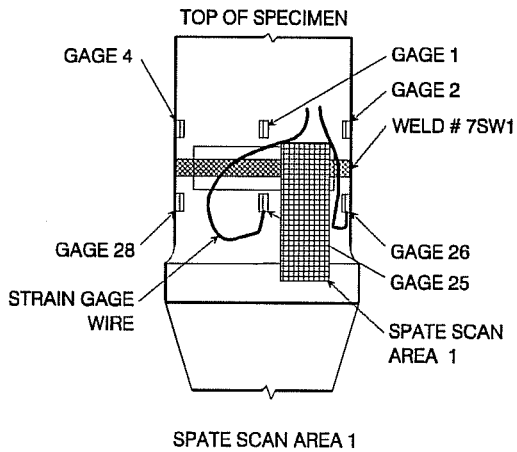


Figure 6-2 SPATE Scan Area 1

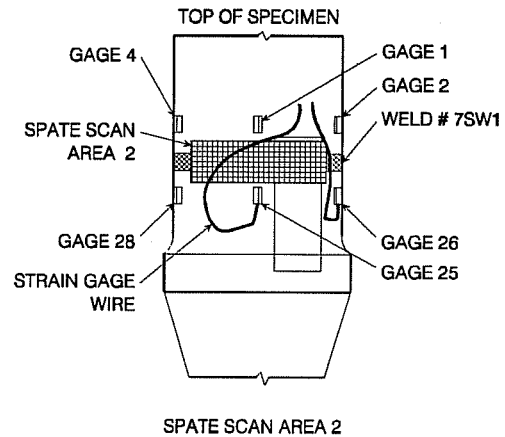


Figure 6-3 SPATE Scan Area 2

scan was intended to detect any nonuniformity in the stress pattern circumferentially along the weld.

For reference, 51,907 stress cycles were required at the 10 ksi stress range to complete the SPATE scans. The nominal test stress range during subsequent fatigue testing of this specimen was 42 ksi. Since the 10 ksi cycles were at a significantly lower stress range, these stress cycles were assumed to be non-damaging.

6.2.3 Results. Figures 6-5 and 6-6 show contour plots of the stress distributions obtained using the SPATE for Scan Areas 1 and 2, respectively. The color scale in each figure has units of stress, but results should be interpreted qualitatively only since the SPATE was not calibrated for either scan. In Figure 6-5, it is observed that the stress distribution is constant in the specimen end fixture away from the weld. Abrupt changes in the stress pattern are observed near the weld toes, as is expected due to the change in geometry in this region.

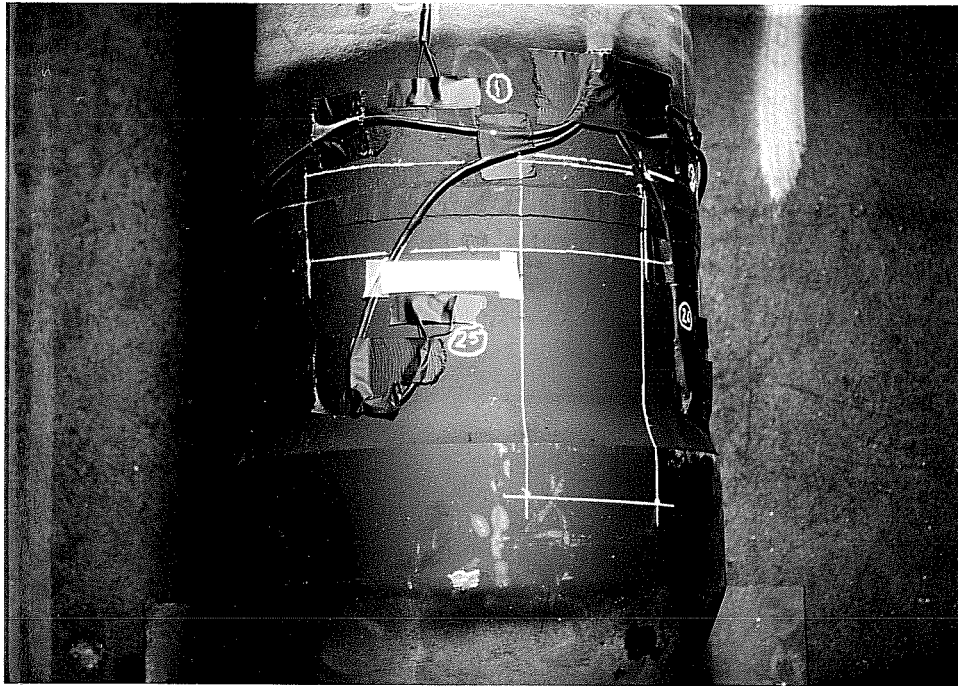


Figure 6-4 SPATE Scan Areas

Figure 6-6 shows the results for Scan Area 2 as a contour plot of stresses. This figure shows that the stress distribution is relatively constant along the circumference of the weld. Stresses are observed to change significantly at the weld toes, again due to the change in geometry in this region. Stresses away from the weld are observed to be fairly constant around the circumference of the pipe, however, suggesting that loads are applied uniformly by the testing apparatus.

Labelled in Figures 6-5 and 6-6 and shown in the photographs in Figures 6-7 and 6-8 is a spot within the both scan areas in which the weld reinforcement was ground nearly flush with the base metal. The SPATE scans of this area show a higher stress in the weld due to the

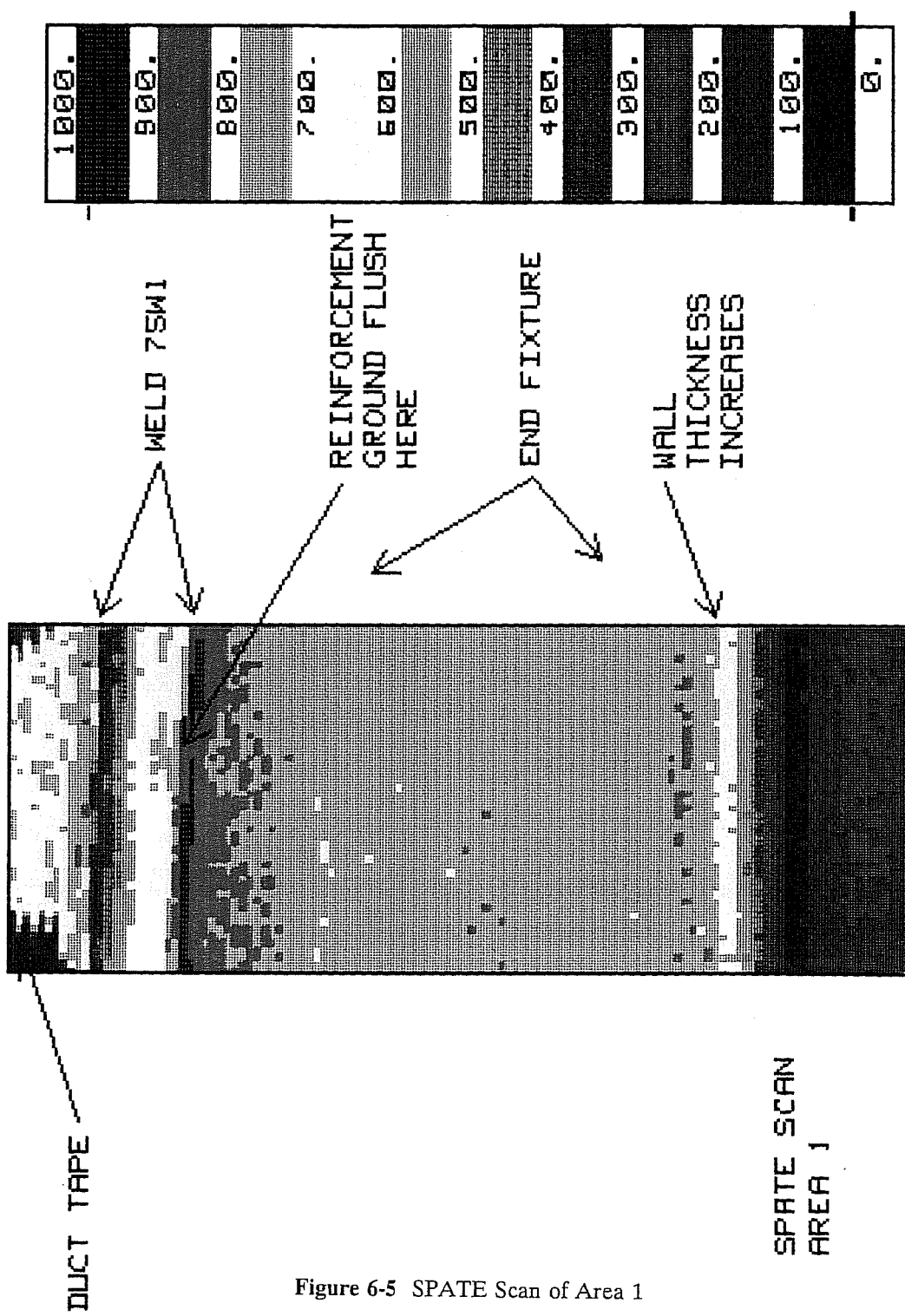


Figure 6-5 SPATE Scan of Area 1

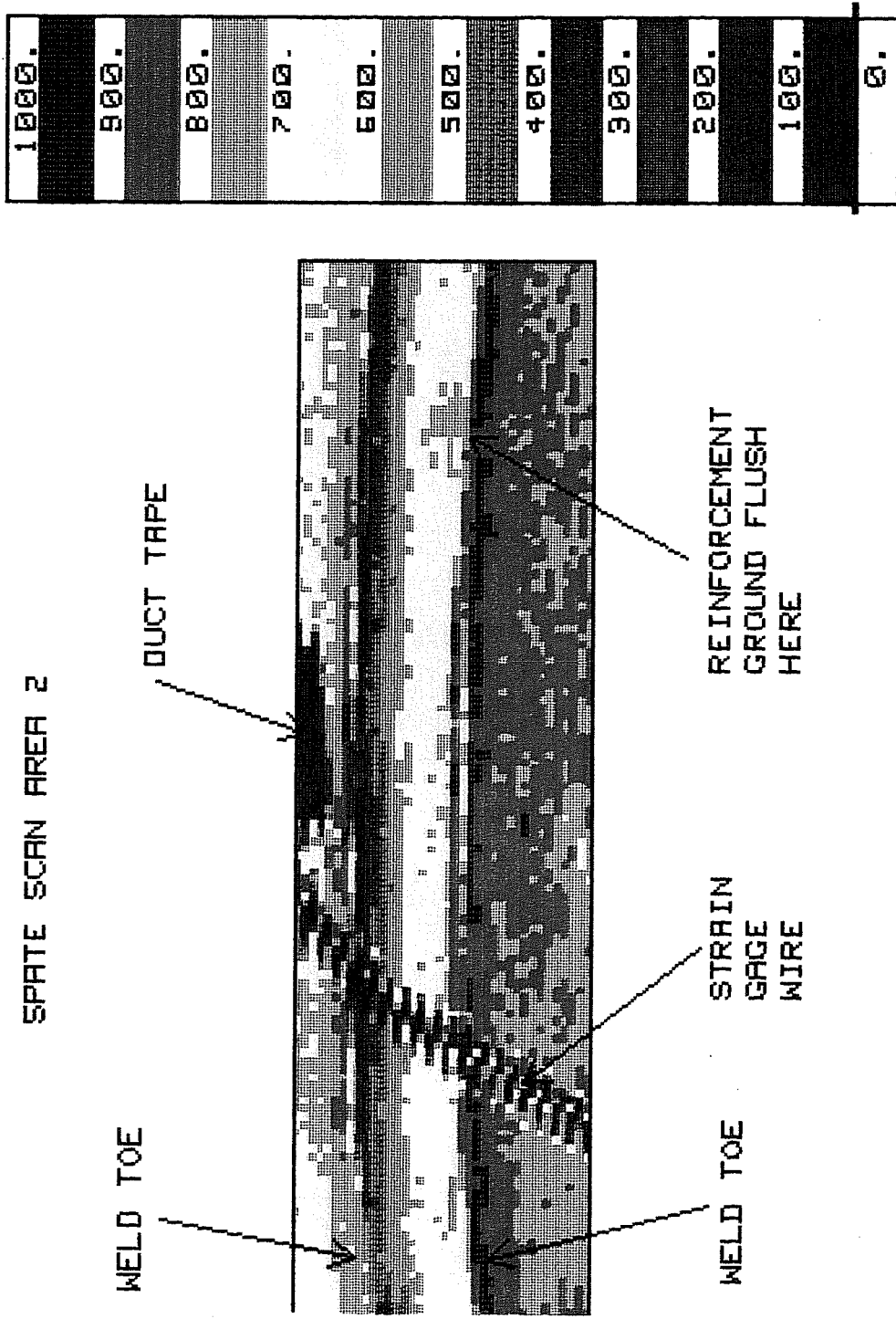


Figure 6-6 SPATE Scan of Area 2

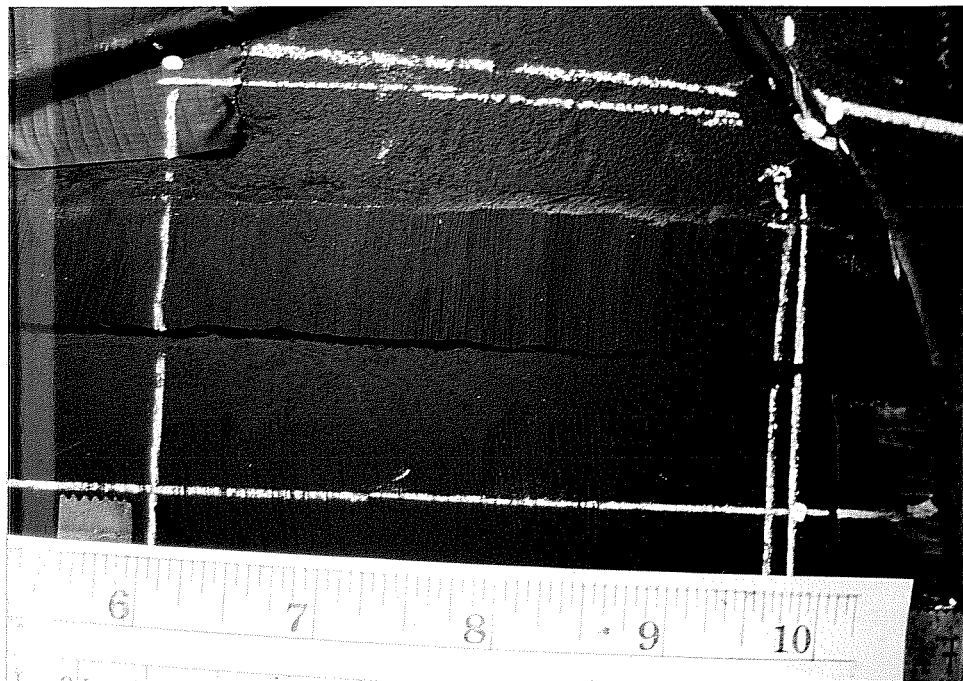


Figure 6-7 Area Common To SPATE Scans 1 and 2

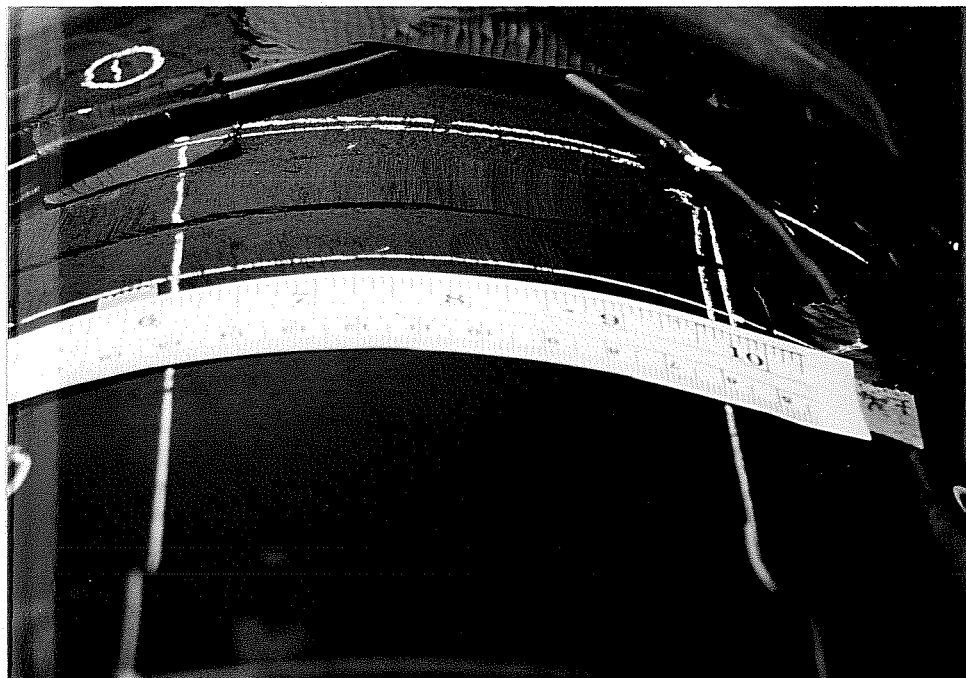


Figure 6-8 Profile of Area Common to SPATE Scan Areas 1 and 2

absence of weld reinforcement. This behavior is as expected since the smaller weld cross section should result in higher weld stresses and lower stress concentration at the weld toe. The fact that this stress distribution appeared in both spate scans of the same area verifies both the accuracy and resolution of the SPATE scans.

6.3 Dynamic Strain Gage Readings

6.3.1 Testing Equipment. Dynamic strain gage readings were recorded for 12 strain gages: gages 25 through 28 on the specimen end fixture below weld number 7SW1, gages 1 through 4 on the pipe section above weld number 7SW1, and gages 13 through 16 near weld number 7SW4 just above the middle of the specimen. Figure 6-1 shows the location and numbering of strain gages on this test specimen. Strain gage wires for these gages were connected four at a time to four separate amplifier circuits, which in turn were connected to a digital data display unit. Strain gage readings were recorded manually from the data display unit.

6.3.2 Testing Procedure. The test specimen was cycled statically through four 10 ksi stress ranges during which strain gage readings were taken at 50 kip load intervals using the data acquisition system as described in Section 3.4.5. The specimen was then cycled statically through four 42 ksi stress ranges during which strain gage readings were recorded at 100 kip load intervals. The static loading and data acquisition followed the same procedures as were used for all specimens in this testing program, as described in Section 3.5.2.

Strain gages wires were then disconnected from the data acquisition system and four gages were connected to the amplifier circuits. Static loading cycles corresponding to a 10 ksi

stress range were then applied and strain gage readings were recorded manually from the data display. This process was repeated three times until readings were recorded for all 12 gages. A 10 ksi dynamic fatigue loading pattern was introduced to the test specimen. Strain gages were again wired four at a time through the amplifier circuits and dynamic strain gage readings were recorded using a Peak/Valley function of the digital data display unit.

After all dynamic gage readings and SPATE scans were completed at the 10 ksi stress range, the test specimen was cycled statically through the 42 ksi load range. Strain gages were connected four at a time to the amplifier circuits and static strain gage readings were recorded from the data display unit. This process was repeated three times to obtain static readings for all 12 strain gages.

Fatigue loading at a 42 ksi stress range was applied to the specimen and dynamic strain gage readings were recorded for all 12 strain gages, again using the Peak/Valley function of the data display unit. Fatigue loading at the 42 ksi stress range was continued until the first through-wall crack was detected at 48,613 stress cycles.

6.3.3 Results. Table 6-1 shows the strain ranges measured using the data acquisition system and static loading, using the amplifier circuits and static loading, and using the amplifier circuits and dynamic loading for the 10 ksi nominal stress range. The static strain readings measured using the amplifier circuits agree well with similar readings taken using the data acquisition system. This agreement verifies the accuracy of the results obtained using the amplifier circuits. The last column in Table 6-1 shows the ratio of measured dynamic strain range to average static strain range from the data acquisition system measurements. For the 10 ksi stress range, dynamic strain measurements were generally found to be within 2 percent

Table 6-1 Static and Dynamic Strain Gage Readings for 10 ksi Stress Range

Static and Dynamic Strain Ranges 10 ksi Stress Range					
Strain Gage Number	Average Static** Using Data Acq'sition (μ strain)	Static Using Amplifier Load Increasing (μ strain)	Static Using Amplifier Load Decreasing (μ strain)	Dynamic Using Amplifier (μ strain)	Dynamic ----- Average Static Data Acq.
1	324	325	326	325	1.003
2	319	316	316	314	0.984
3	333	331	331	330	0.990
4	328	328	328	327	0.997
13	316	315	315	313	0.992
14	321	320	319	316	0.985
15	324	322	322	322	0.996
16	332	329	330	331	0.997
25	330	322	322	321	0.972
26	325	318	317	317	0.977
27	339	328	328	326	0.963
28	345	336	335	334	0.969
Average (Dynamic / Average Static)					0.985
** Average Static = 0.5 * (Strain Range with Load Increasing + Strain Range with Load Decreasing)					

of the static readings from the data acquisition system. Table 6-2 similarly shows comparisons of measured strain ranges for the 42 ksi stress range. Dynamic readings generally were within 3 percent of the static readings from the data acquisition system. The close agreement between

Table 6-2 Static and Dynamic Strain Gage Readings for 42 ksi Stress Range

Static and Dynamic Strain Ranges 42 ksi Stress Range					
Strain Gage Number	Average Static** Using Data Acq'sition (μ strain)	Static Using Amplifier Load Increasing (μ strain)	Static Using Amplifier Load Decreasing (μ strain)	Dynamic Using Amplifier (μ strain)	Dynamic ----- Average Static Data Acq.
1	1,392	1,389	1,380	1,380	0.992
2	1,389	1,377	1,374	1,373	0.989
3	1,420	1,412	1,408	1,403	0.988
4	1,375	1,366	1,362	1,355	0.986
13	1,358	1,356	1,355	1,350	0.995
14	1,377	1,380	1,378	1,375	0.999
15	1,368	1,360	1,358	1,359	0.994
16	1,403	1,388	1,387	1,384	0.987
25	1,527	1,460	1,457	1,433	0.939
26	1,531	1,476	1,472	1,444	0.943
27	1,563	1,486	1,485	1,456	0.931
28	1,564	1,476	1,476	1,451	0.928
Average (Dynamic / Average Static)					0.972
** Average Static = 0.5 * (Strain Range with Load Increasing + Strain Range with Load Decreasing)					

static and dynamic strain gage readings is remarkable considering that the test loads during dynamic fatigue loading are known to drift slightly and that two totally different systems were used to record the data.

6.4 Summary and Conclusions

The purpose of completing the SPATE scans was to detect any abnormalities in the stress distribution near the end fixture which might contribute to a bias toward pipe-to-end fixture weld failure. The SPATE scans did not reveal any unexpected trends in the stress distribution near the specimen end fixture weld, verifying that loads were being applied uniformly by the testing apparatus and end fixture. No evidence was found in the observed stress distributions which might suggest a bias toward pipe-to-end fixture weld failure.

The purpose of measuring strain ranges during dynamic fatigue loading was to verify the assumption that strain ranges measured during the fourth static loading cycle were representative of strain ranges experienced during subsequent dynamic fatigue loading. Static and dynamic strain gage readings agreed remarkably well, verifying this assumption.

CHAPTER 7

SUMMARY AND CONCLUSIONS

7.1 Summary

Tensile fatigue tests were completed on full-sized pipe butt welds to investigate primarily the effects of root pass welding process and position on fatigue life. Thirty test specimens with six welds each were fabricated and tested until the first through-wall fatigue crack developed in the specimen. Five of these specimens were repaired and retested until the second through-wall fatigue crack was detected.

The effect on fatigue life of welding process was investigated by testing welds having Gas Tungsten Arc Welding (GTAW) and Shielded Metal Arc Welding (SMAW) root passes. The effect of welding position on fatigue life was examined by testing specimens welded in the American Welding Society (AWS) 5G position with the pipe sections horizontal and in the AWS 2G position with the pipe sections vertical.

The results of the fatigue tests and the observed failure patterns were studied and compared with results of similar tests. A method was proposed for using stress shadowing grooves to improve the fatigue life of pipe butt welds by reducing stress concentrations at the weld root. A preliminary finite element analysis was completed to test the feasibility of the proposed stress shadowing grooves.

7.2 Conclusions

7.2.1 Fatigue Tests. The following conclusions were drawn from the fatigue tests completed on pipe butt welds:

1. Root pass welding process does influence weld fatigue life. Welds having a GTAW root pass were observed to have longer fatigue lives at any given stress range than similar welds having a SMAW root pass.
2. Welding position may or may not have an influence on weld fatigue life. GTAW root welds fabricated in the AWS 2G position showed slightly longer fatigue life than similar welds fabricated in the AWS 5G position. No conclusive evidence was found to suggest that this slight difference was not due to scatter in the data.

7.2.2 Analysis of Fatigue Test Results. After studying the results of the fatigue tests and correlating this data with trends observed in previous investigations of transverse butt welds, the following conclusions were drawn:

1. If reasonable care is taken to remove or reduce sources of stress concentration from the outside weld reinforcement, butt welds in pipe will invariably fail from fatigue cracks initiating at the edge of the weld root pass.
2. Fatigue cracks initiate at the weld root of pipe welds due to geometric stress concentrations at the edge of the weld root pass reinforcement and due to slight weld flaws resulting from the root pass being welded with no backing.
3. Since the weld root pass is inaccessible after welding, grinding of the inside weld reinforcement to remove sources of stress concentration or back gouging and rewelding of the root pass is not possible. Methods of improving fatigue life must thus focus on

reducing the detrimental effects on fatigue life of these unavoidable weld flaws and sources of stress concentration.

4. Since the welder has more control over the deposition of weld metal when using the GTAW root process than the SMAW process, improved fatigue life of the GTAW welds likely resulted from reduced stress concentrations due to smoother transitions between weld metal and base metal at the weld root and from reduced incidence of weld flaws in the GTAW weld root.

7.2.3 Proposed Stress Shadowing Grooves. Study of the results of the finite element analysis into the feasibility of the proposed stress shadowing grooves led to the following conclusions:

1. The proposed grooves significantly reduced the stress concentration at the weld root. This reduction in weld root stress came at the expense of increased stress at the groove location, however, due to the reduction in cross sectional area from the machined groove.
2. The reduction in stress concentration at the weld root was influenced by groove depth and groove location. The increase in stress at the groove was influenced by groove radius and groove depth. The best balance between reduction in stress at the weld root and increase in stress at the groove location appears to result from using a relatively shallow, large radius groove located close to the weld root.
3. The only true test of the proposed stress shadowing grooves would be actual fatigue tests in which the effect on fatigue life of such parameters as groove shape, groove location, and groove depth are systematically investigated. The preliminary finite

element analysis did not include such complications as variations in weld root reinforcement profile, weld flaws, and residual stresses which are known to influence weld fatigue behavior.

APPENDIX A

DETAILED SPECIMEN FAILURE DESCRIPTIONS

A1 Overview

After the first through-wall fatigue crack was detected in a specimen, the specimen was returned to the fabricator for a complete post-fatigue radiographic inspection. Sections of weld were removed at locations where inspection revealed a fatigue crack and these sections were sent to a testing lab for further analysis. The fatigue cracks were broken open and closely examined for evidence of weld flaws at the crack initiation sites. Photographs were taken of the fracture surface and the weld profile in the location of the crack. This Appendix details the results of fatigue tests on a specimen by specimen basis with specific attention to the results of post-fatigue analysis of the cracks.

Test specimens are grouped in this appendix by the welding process used for the root pass of the failed weld. Listed for each test specimen is the nominal test stress range, the number of stress cycles to failure, the failed weld number, the calculated inside pipe offset at the failure location, and any non-through-wall cracks detected during post-fatigue analysis. Welds were numbered from weld number 1 at one end fixture consecutively to weld number 6 at the other end fixture. For most specimens, weld number 1 corresponded with the bottom weld on the specimen when the specimen was in its vertical testing position. Listed are calculated inside pipe offsets. Since the inside of the weld was inaccessible, this parameter was calculated using measured wall thicknesses and the measured outside pipe offset. Section 3.3.8 presents the inside offset parameter more in depth.

A2 5G GTAW Root Specimens***A2.1 Specimen 1***

Stress Range:	42 ksi
Cycles to Failure:	38,113
Failed Weld:	Weld Number P4A
Failure Type:	Root Crack
Calculated Pipe Inside Offset:	Not Available
Non-through-wall Cracks:	None

Comments: This specimen was fabricated using intentional inside pipe offsets of roughly 1/16 inch. The failure initiated in an area of large inside pipe offset. Pipe offsets and wall thicknesses were not recorded for this specimen, so no data is available to calculate the magnitude of the inside pipe offset.

A2.2 Specimen 2

Stress Range:	30 ksi
Cycles to Failure:	138,793
Failed Weld:	Weld Number P9
Failure Type:	Root Crack
Calculated Pipe Inside Offset:	Not Available
Non-through-wall Cracks:	None

Comments: This specimen also was fabricated using intentional pipe offsets of roughly 1/16 inch. The failure initiated in a region of very large inside pipe offset. As with Specimen 1, pipe offsets and wall thickness measurements were not recorded

and calculation of the inside pipe offset was not possible. No weld flaws were noted in the area of crack initiation.

A2.3 Specimen 3

Stress Range:	42 ksi
Cycles to Failure:	24,391
Failed Weld:	None
Failure Type:	End Fixture Failure
Calculated Pipe Inside Offset:	Not Applicable
Non-through-wall cracks:	Weld Number 3W6

Comments: This specimen failed in the machined end fixture away from the weld. Post-fatigue analysis of the failure location showed a sharp groove left in the surface during machining and the notch effect of this groove led to crack initiation. The non-through-wall crack initiated at a section having a large inside offset and a slight amount of undercut at the edge of the root pass. The non-through-wall crack propagated approximately 1/2 way through the weld metal.

A2.4 Specimen 4

Stress Range:	30 ksi
Cycles to Failure:	78,011
Failed Weld:	Weld Number 4W6
Failure Type:	Root Crack
Calculated Pipe Inside Offset:	0.023 inches

(9th largest of 24, largest = 0.036 inches)

Non-through-wall Cracks: None

Comments: Post-fatigue analysis showed evidence of a slight cold lap at the fatigue crack initiation site. The failure was in a pipe to end fixture weld in which the end fixture weld preparation might have had poor geometry. Several early machined end fixtures were delivered with an improperly large root face on the single V weld preparation. This condition was remedied by manual grinding which likely resulted in an irregular weld preparation angle and a highly variable weld root gap. The poor geometry of the weld preparation likely contributed to this failure.

A2.5 Specimen 5

Stress Range: 30 ksi

Cycles to Failure: 133,629

Failed Weld: Weld Number 5W6

Failure Type: Root Crack

Calculated Pipe Inside Offset: 0.015 inches

(4th largest of 24, largest = 0.028 inches)

Non-through-wall Cracks: None

Comments: Two distinct crack initiation sites roughly 2 inches apart were apparent in the photograph of the fracture surface of the weld. A very slight roll-over of weld metal was apparent in a photomicrograph of the cross section through the weld at the crack location.

A2.6 Specimen 6

Stress Range: 30 ksi
Cycles to Failure: 174,789
Failed Weld: Weld Number 6W1
Failure Type: Root Crack

Calculated Pipe Inside Offset: 0.001 inches
(23rd largest of 24, largest = 0.047 inches)

Non-through-wall Cracks: None

Comments: The photograph of the fracture surface showed some porosity and lack of fusion defects in the GTAW fill passes, but these did not contribute to crack initiation.

A2.7 Specimen 7

Stress Range: 30 ksi
Cycles to Failure: 96,708
Failed Weld: None
Failure Type: End Fixture Failure

Calculated Pipe Inside Offset: Not Applicable

Non-through-wall Cracks: Weld Number 7W1

Comments: This specimen failed in the machined end fixture away from the weld. Post-failure analysis revealed a sharp machining groove left on the inside surface of the end fixture at a radiused transition in cross section. The end fixture failures in Specimens 3 and 7 prompted a slight end fixture design change as detailed in Section 3.2.3.

The non-through-wall crack in weld number 7W1 was a root crack extending 1/4 inch into the weld metal from a very tight lack of fusion flaw. This specimen was repaired by cutting out and replacing both pipe to end fixture welds and was retested as Specimen 7A.

A2.8 Specimen 7A (Retest of Specimen 7)

Stress Range:	30 ksi
Cycles to Failure:	96,708 + 100,664 = 197,372
Failed Weld:	Weld Number 7W3
Failure Type:	Root Crack
Calculated Pipe Inside Offset:	0.004 inches (19th largest of 24, largest = 0.029 inches)
Non-through-wall Cracks:	None

Comments: The root crack in this weld originated at either a start/stop in the weld root pass or at a tack weld. Some porosity was evident in the first fill pass, but this did not contribute to crack initiation. This specimen was a continuation of the test on Specimen 7 which failed in the specimen end fixture.

A2.9 Specimen 8

Stress Range:	30 ksi
Cycles to Failure:	64,906
Failed Weld:	Weld Number 8W1
Failure Type:	Root Crack
Calculated Pipe Inside Offset:	0.003 inches

(18th largest of 24, largest = 0.028 inches)

Non-through-wall Cracks: Weld Number 8W1

Comments: Post-fatigue analysis revealed a large lack of fusion defect in the first fill pass of this weld. The fatigue crack appears to have initiated at the weld root, propagated through the lack of fusion area and then through the thickness of the remaining weld metal. The non-through-wall root crack in weld number 8W1 initiated at a lack of fusion defect in a tack weld. This crack propagated through approximately 3/4 of the thickness of the weld metal.

A2.10 Specimen 9

Stress Range: 42 ksi

Cycles to Failure: 69,839

Failed Weld: Weld Number 9W2

Failure Type: Root Crack

Calculated Pipe Inside Offset: 0.019 inches

(6th largest of 24, largest = 0.030 inches)

Non-through-wall Cracks: Weld Number 9W6 (Two cracks)

Comments: The fatigue crack in this specimen initiated at the edge of the weld root pass, but did not propagate directly through the weld metal. The crack propagation followed the pipe edge preparation, suggesting a lack of fusion in the weld fill passes. Both non-through-wall weld cracks were weld root cracks. One crack initiated at a shallow undercut in the root pass and was 1/4 inch in depth. The second crack was 0.025 inches in depth and initiated in a region having no visible weld flaws.

A2.11 Specimen 10

Stress Range:	42 ksi
Cycles to Failure:	52,602
Failed Weld:	Weld Number 10W6
Failure Type:	Toe Crack
Calculated Pipe Inside Offset:	0.035 inches (2nd largest of 24, largest = 0.045 inches)
Non-through-wall Cracks:	Weld Number 10W1 (Two cracks)

Comments: The toe crack in this specimen initiated at the edge

of the weld reinforcement on the outside surface of the pipe and propagated through the base metal. The outside weld reinforcement was quite high in the area of the crack and the angle quite steep between weld metal and base metal. No weld flaws were apparent at the weld toe.

The two non-through-wall cracks were both weld root cracks. One crack propagated 1/2 way through the weld metal and the other 7/8 of the way through the thickness. No weld flaws were apparent at either non-through-wall crack location. Figures 4.5 and 4.6 show photographs of the cross section through the weld at the through-wall failure location and the fracture surface of the crack.

A2.12 Specimen 11

Stress Range:	30 ksi
Cycles to Failure:	213,411
Failed Weld:	Weld Number 11W6
Failure Type:	Root Crack

Calculated Pipe Inside Offset: 0.037 inches
(2nd largest of 24, largest = 0.057 inches)

Non-through-wall Cracks: Weld Number 11W6 (Two cracks)

Comments: No weld flaws were apparent in the location of the through-wall root crack or either of the non-through wall weld cracks. Both non-through-wall cracks were root cracks. One crack propagated 7/8 of the way through the wall thickness and the other propagated 0.030 inches into the weld metal. Figures 4.2 and 4.3 show photographs of a cross section through the weld at the through-wall failure location and the fracture surface of the crack.

A2.13 Specimen 12

Stress Range: 20 ksi

Cycles to Failure: 707,673

Failed Weld: Weld Number 12W1

Failure Type: Root Crack

Calculated Pipe Inside Offset: 0.026 inches
(Largest of 24 measurements)

Non-through-wall Cracks: None

Comments: No weld flaws were noted during post-fatigue analysis.

A2.14 Specimen 13

Stress Range: 30 ksi

Cycles to Failure: 226,548

Failed Weld: Weld Number 13W1

Failure Type: Root Crack

Calculated Pipe Inside Offset: 0.024 inches
(4th largest of 24, largest = 0.043 inches)

Non-through-wall Cracks: None

Comments: No weld flaws were apparent in the photograph of the fracture surface. This root crack was somewhat unusual in that the crack extended for over 10 inches along the inside of the pipe before propagating through the entire pipe wall thickness.

A2.15 Specimen 14

Stress Range: 20 ksi

Cycles to Failure: 616,112

Failed Weld: Weld Number 14W2

Failure Type: Root Crack

Calculated Pipe Inside Offset: 0.015 inches
(6th largest of 24, largest = 0.054 inches)

Non-through-wall Cracks: None

Comments: No weld flaws were noted during post-fatigue analysis.

A2.16 Specimen 15

Stress Range: 15 ksi

Cycles to Failure: 2,326,481
Failed Weld: Weld Number 15W1
Failure Type: Root Crack
Calculated Pipe Inside Offset: 0.016 inches
(10th largest of 24, largest = 0.045 inches)
Non-through-wall Cracks: None
Comments: This specimen was tested at the lowest stress range

of any of the 5G GTAW root weld specimens. No weld flaws were noted at the failure location.

A2.17 Specimen 16

Stress Range: 20 ksi
Cycles to Failure: 924,337
Failed Weld: Weld Number 16W5
Failure Type: Root Crack
Calculated Pipe Inside Offset: 0.017 inches
(8th largest of 24, largest = 0.045 inches)
Non-through-wall Cracks: None
Comments: No weld flaws were noted during post-fatigue failure

analysis.

A3 2G GTAW Root Specimens***A3.1 Specimen 17***

Stress Range: 30 ksi
 Cycles to Failure: 329,728
 Failed Weld: Weld Number 17W6
 Failure Type: Outside-in crack from between two weld passes
 Calculated Pipe Inside Offset: 0.003 inches

(23rd largest of 24, largest = 0.030 inches)

Non-through-wall Cracks: None

Comments: Two adjacent fatigue cracks propagated through the

wall thickness of this specimen. Both cracks initiated in a deep valley between two weld passes on the outside of the specimen. Crack propagation was from the outside toward the inside of the pipe. Figures 4.8 and 4.9 show photographs of the weld profile at the crack location and the fracture surface of the cracks.

A3.2 Specimen 18

Stress Range: 30 ksi
 Cycles to Failure: 217,770
 Failed Weld: Weld Number 18W6
 Failure Type: Root Crack
 Calculated Pipe Inside Offset: 0.036 inches
 (Largest of 24 measurements)
 Non-through-wall Cracks: None

Comments: Post-fatigue analysis of the crack location revealed no weld flaws.

A3.3 Specimen 19

Stress Range: 42 ksi
 Cycles to Failure: 78,818
 Failed Weld: Weld Number 19W1
 Failure Type: Root Crack
 Calculated Pipe Inside Offset: 0.008 inches
 (13th largest of 24, largest = 0.040 inches)
 Non-through-wall Cracks: Weld Number 19W1

Comments: No weld flaws were apparent during post-fatigue analysis of the crack. The non-through-wall crack was located approximately 90 degrees from the through-wall crack. The non-through-wall root crack propagated 3/4 of the way through the wall thickness.

A3.4 Specimen 20

Stress Range: 42 ksi
 Cycles to Failure: 79,126
 Failed Weld: Weld Number 20W1
 Failure Type: Root Crack
 Calculated Pipe Inside Offset: 0.019 inches
 (6th largest of 24, largest = 0.029 inches)

Non-through-wall Cracks: Weld Number 20W1

Comments: No weld flaws were apparent at the location of the through-wall fatigue crack. The non-through-wall crack initiated at the outside surface of the weld between two weld passes. This crack propagated 1/2 way through the wall thickness.

A3.5 Specimen 21

Stress Range: 12 ksi

Cycles to Failure: 7,583,900

Failed Weld: Weld Number 22W6

Failure Type: Root Crack

Calculated Pipe Inside Offset: 0.029 inches

(6th largest of 24, largest = 0.046 inches)

Non-through-wall Cracks: Not Available

Comments: Post-fatigue analysis of this specimen is not yet available. This specimen was repaired by removing and replacing weld number 22W6. The specimen was retested as Specimen 21A.

A3.6 Specimen 21A (Retest of Specimen 21)

Stress Range: 12 ksi

Cycles to Failure: $7,583,900 + 547,510 = 8,131,410$

Failed Weld: Weld Number 22W1

Failure Type: Root Crack

Calculated Pipe Inside Offset: 0.029 inches

(6th largest of 24, largest = 0.046 inches)

Non-through-wall Cracks: Not Available

Comments: Post-fatigue analysis is not yet available. This specimen was a continuation of the test on Specimen 21. The short life during the retest suggests that a complete radiographic inspection was not completed during repairs to the specimen and that a fairly large non-through-wall crack was present at the failure location at the start of the retest.

A3.7 Specimen 22

Stress Range: 12 ksi

Cycles to Failure: 13,286,940

Failed Weld: Weld Number 32W6

Failure Type: Root Crack

Calculated Pipe Inside Offset: 0.045 inches

(Largest of 24 measurements)

Non-through-wall Cracks: Not Available

Comments: Post-fatigue analysis is not yet available.

A3.8 Specimen 3S

Stress Range: 20 ksi

Cycles to Failure: 591,385

Failed Weld: Weld Number 3SW6

Failure Type: Root Crack

Calculated Pipe Inside Offset: 0.059 inches
(Largest of 24 measurements)

Non-through-wall Cracks: Weld Number 3SW6

Comments: No weld flaws were apparent at either the location of the through-wall crack or the non-through-wall crack. The non-through-wall crack was a root crack 1/8 inch deep.

A3.9 Specimen 6S

Stress Range: 42 ksi

Cycles to Failure: 73,463

Failed Weld: Weld Number 6SW6

Failure Type: Toe Crack

Calculated Pipe Inside Offset: 0.035 inches
(4th largest of 24, largest = 0.063 inches)

Non-through-wall Cracks: Weld Number 6SW6

Comments: The through-wall toe crack was somewhat unusual in that it initiated in an area in which the weld reinforcement was ground flat. The reinforcement was not ground flush with the base metal, but the transition between base metal and weld metal was relatively smooth. In the same region as the through-wall crack, a non-through-wall root crack was present. The root crack was roughly 1/8 inch deep.

A4 2G SMAW Root Specimens***A4.1 Specimen 1S***

Stress Range:	20 ksi
Cycles to Failure:	415,455
Failed Weld:	Weld Number S1W1
Failure Type:	Root Crack
Calculated Pipe Inside Offset:	0.001 inches (22nd largest of 24, largest = 0.071 inches)
Non-through-wall Cracks:	Weld Number S1W1

Comments: The through-wall root crack initiated at an area of slight undercut. The non-through-wall root crack extended 0.16 inches into the weld metal and also initiated at an area of root pass undercut. Specimen 1S was repaired by cutting out and replacing weld number S1W1. Testing was continued on this specimen as Specimen 1SA.

A4.2 Specimen 1SA (Retest of Specimen 1S)

Stress Range:	12 ksi
Cycles to Failure:	415,455 + 224,602 = 640,057
Failed Weld:	Weld Number S1W4
Failure Type:	Root Crack
Calculated Pipe Inside Offset:	0.019 inches (6th largest of 22, largest = 0.071 inches)
Non-through-wall Cracks:	Weld Number S1W3 (Two cracks)

Comments: This test was a continuation of the test on Specimen 21. No weld flaws were evident near the crack initiation site in weld number S1W4. One non-through-wall root crack in weld number S1W3 propagated 3/4 of the way through the weld metal. No weld flaws were noted for this crack. The other non-through-wall root crack propagated 3/16 inch into the weld thickness and initiated at and undercut or lack of fusion flaw at the edge of the root pass.

A4.3 Specimen 2S

Stress Range: 20 ksi
 Cycles to Failure: 678,261
 Failed Weld: Weld Number S2W1
 Failure Type: Root Crack
 Calculated Pipe Inside Offset: 0.017 inches
 (16th largest of 24, largest = 0.053 inches)
 Non-through-wall Cracks: Weld Number S2W1

Comments: No weld flaws were noted at the location of the through-wall root crack, but the inside weld reinforcement height was large compared with typical weld cross sections. The non-through-wall crack initiated at a slight undercut at the edge of the root pass and propagated 0.040 inches into the weld metal. This specimen was repaired by replacing both pipe to end fixture welds and was retested as Specimen 2SA.

A4.4 Specimen 2SA (Retest of Specimen 2S)

Stress Range: 20 ksi

Cycles to Failure: 678,261 + 199571 = 877,832

Failed Weld: Weld Number S2W2

Failure Type: Root Crack

Calculated Pipe Inside Offset: 0.000 inches
(24th largest of 24, largest = 0.053 inches)

Non-through-wall Cracks: None

Comments: This specimen was a continuation of the test on Specimen 2S. Post-fatigue crack analysis showed that the crack initiated at a slight undercut at the edge of the root pass.

A4.5 Specimen 4S

Stress Range: 30 ksi

Cycles to Failure: 118,311

Failed Weld: Weld Number 4SW2-C

Failure Type: Root Crack

Calculated Pipe Inside Offset: 0.061 inches
(3rd largest of 24, largest = 0.064 inches)

Non-through-wall Cracks: None

Comments: Post-fatigue analysis revealed no weld flaws at the failure location, other than the large amount of inside pipe offset.

A4.6 Specimen 5S

Stress Range: 30 ksi

Cycles to Failure: 120,975
 Failed Weld: Weld Number 5SW4
 Failure Type: Root Crack
 Calculated Pipe Inside Offset: 0.079 inches
 (Largest of 24 measurements)
 Non-through-wall Cracks: None
 Comments: No weld flaws were noted during post-fatigue

analysis, other than the large amount of inside pipe offset.

A4.7 Specimen 7S

Stress Range: 42 ksi
 Cycles to Failure: 48,613
 Failed Weld: Weld Number 7SW4
 Failure Type: Root Crack
 Calculated Pipe Inside Offset: 0.050 inches
 (3rd largest of 24, largest = 0.076 inches)
 Non-through-wall Cracks: Weld Numbers 7SW4 and 7SW5
 Comments: No weld flaws were noted in the area of the through-

wall root crack. The non-through-wall crack in weld number 7SW4 propagated 1/2 way through the wall thickness and appears to have initiated from a slight undercut at the weld root. The non-through-wall crack in weld number 7SW5 was a toe crack propagating 1/2 way through the pipe wall thickness. The outside reinforcement was ground flat in the failure

region, but not flush with the pipe surface. The angle between the weld metal and base metal at the weld toe was quite sharp.

A5 Pulsed Tig Root Specimen

A5.1 Specimen PT1

Stress Range:	20 ksi
Cycles to Failure:	556,901
Failed Weld:	Weld Number 352E
Failure Type:	Root Crack
Calculated Pipe Inside Offset:	Not Available
Non-through-wall Cracks:	Not Available

Comments: Specimen PT1 was fabricated using a pulsed tig procedure. Pipe wall thicknesses were not recorded during fabrication and thus calculation of inside offsets was impossible. The post-fatigue analysis of this specimen is not yet available. The specimen was repaired by removing and replacing weld number 352E. Fatigue testing was continued as Specimen PT1A.

A5.2 Specimen PT1A (Retest of Specimen PT1)

Stress Range:	20 ksi
Cycles to Failure:	$556,901 + 54,495 = 611,396$
Failed Weld:	Weld Number 352D
Failure Type:	Root Crack
Calculated Pipe Inside Offset:	Not Available

Non-through-wall Cracks: Not Available

Comments: This specimen was a retest of Specimen PT1. Pipe wall thicknesses were not measured and thus inside offset calculations were not possible. The post-fatigue analysis of this specimen is not yet available.

BIBLIOGRAPHY

1. American Association of State Highway and Transportation Officials. Standard Specifications for Highway Bridges. 14th ed. Washington, DC, 1989.
2. American Petroleum Institute. Recommended Practice for Planning, Designing, and Constructing Fixed Offshore Platforms: API Recommended Practice 2A. 17th ed. Washington, DC, 1987.
3. American Welding Society. Structural Welding Code: Steel. 11th ed. Miami, FL, 1988.
4. Boulton, C.F. "Acceptance Levels of Weld Defects for Fatigue Service." *Welding Journal: Welding Research Supplement*. January 1977, pp. 13s-22s.
5. Broek, David. Elementary Engineering Fracture Mechanics. 4th revised ed. Kluwer Academic Publishers, Norwell, MA, 1991.
6. Gunn, K.W. and McLester, R. "Effect of Mean Stress on Fatigue Properties of Aluminium Alloy Butt-Welded Joints." *British Welding Journal*, Vol 7 No 3, 1960, pp 201-7.
7. Gurney, T.R. Fatigue of Welded Structures. 2nd ed. Cambridge University Press, Cambridge, 1979.
8. Iida, Kunihiro and Yazaki, Youichi. "Bending Strength of Welded Steel Pipe with Uniform Mismatch." *Transactions of the Japan Welding Society*, Vol 5 No 2, September 1974.

9. Lawrence, F.V., Jr., Mattos, R.J., Higashida, Y., and Burk, J.D. "Estimating the Fatigue Crack Initiation Life of Welds." Fatigue Testing of Weldments: ASTM STP 648. D.W. Hoepfner, ed. American Society for Testing and Materials, 1978, pp 134-158.
10. Lawrence, F.V. "Estimation of Fatigue-Crack Propagation Life in Butt Welds." Welding Journal: Welding Research Supplement. May 1973, pp 212s-220s.
11. Lawrence, F.V. and Munse, W.H. "Fatigue Crack Propagation in Butt Welds Containing Joint Penetration Defects." Welding Journal: Welding Research Supplement. May 1973, pp 221s-225s, 232s.
12. Maddox, S.J. "Fatigue Behavior of Welded Joints." Advances in Fatigue Science and Technology. Branco, C.M. and Rosa, L.G., ed. Kluwer Academic Publishers, Dordrecht, Netherlands, 1989, pp 539-550.
13. Maddox, S.J. "Fatigue Design Optimisation in Welded Joints." Advances in Fatigue Science and Technology. Branco, C.M. and Rosa, L.G., ed. Kluwer Academic Publishers, Dordrecht, Netherlands, 1989, pp 551-568.
14. Munse, W.H. "Fatigue of Weldments--Tests, Design, and Service." Fatigue Testing of Weldments: ASTM STP 648. Hoepfner, D.W., ed. American Society for Testing and Materials, 1978, pp 89-112.
15. Newman, R.P. and Dawes, M.G. "Exploratory Fatigue Tests on Transverse Butt Welds Containing Lack of Penetration." British Welding Journal, Vol 12 No 3, 1965, pp 117-20.
16. Reemsnyder, H.S. "Development and Application of Fatigue Data for Structural Steel Weldments." Fatigue Testing of Weldments: ASTM STP 648. Hoepfner, D.W., ed. American Society for Testing and Materials, 1978, pp 3-21.

17. Sanders, W.W., Jr., Derecho, A.T., and Munse, W.H. "Effect of External Geometry on Fatigue Behavior of Welded Joints." *Welding Journal: Welding Research Supplement*. February 1965, pp 49s-55s.
18. Scholte, H.G. and Buisman, B.C. "Investigation of the Fatigue Behaviour of Butt Welded Tubular Connections with Root Defects." Delft University, Ship Structures Laboratory, Netherlands.
19. Wilson, W.M., Bruckner, W.H., Coombe, J.V., and Wilde, R.A. "Fatigue Tests of Welded Steel Joints in Structural Steel Plates." *University of Illinois Engineering Experiment Station Bulletin Series No. 327*. Urbana, IL, February 25, 1941.
20. Wilson, W.M., Bruckner, W.H., McCrackin, T.H., Jr., and Beede, H.C. "Fatigue Tests of Commercial Butt Welds in Structural Steel Plates." *University of Illinois Engineering Experiment Station Bulletin Series No. 344*. Urbana, IL, October 12, 1943.
21. SPATE Series 9000 User's Manual. Ometron, Inc. Sterling, VA.

VITA

James Matthew Light was born in East China Township, Michigan, on May 26, 1969, the son of James Howard Light and Catherine Janet (Becker) Light. A lifelong resident of East China Township, James graduated from nearby St. Clair High School in 1987. In the fall of that same year, he enrolled in the College of Engineering at Michigan Technological University in Houghton, Michigan. James received the degree of Bachelor of Science in Civil Engineering from Michigan Technological University in the spring of 1991 and enrolled in the Graduate School at the University of Texas at Austin in the fall of 1991.

Permanent Address: 3350 South River Road
East China, Michigan 48054

This thesis was typed by the author.

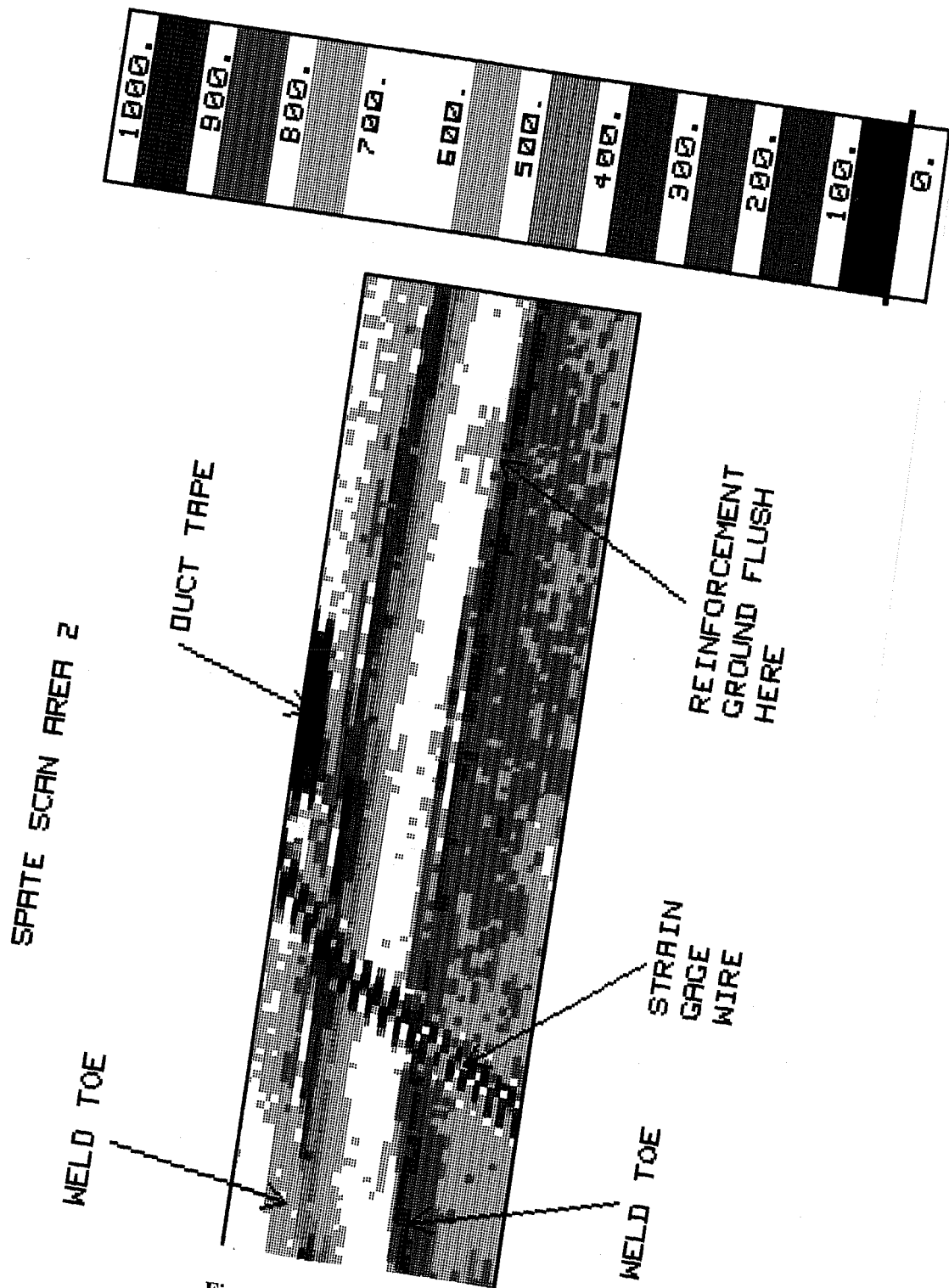


Figure 6-6 SPATE Scan of Area 2

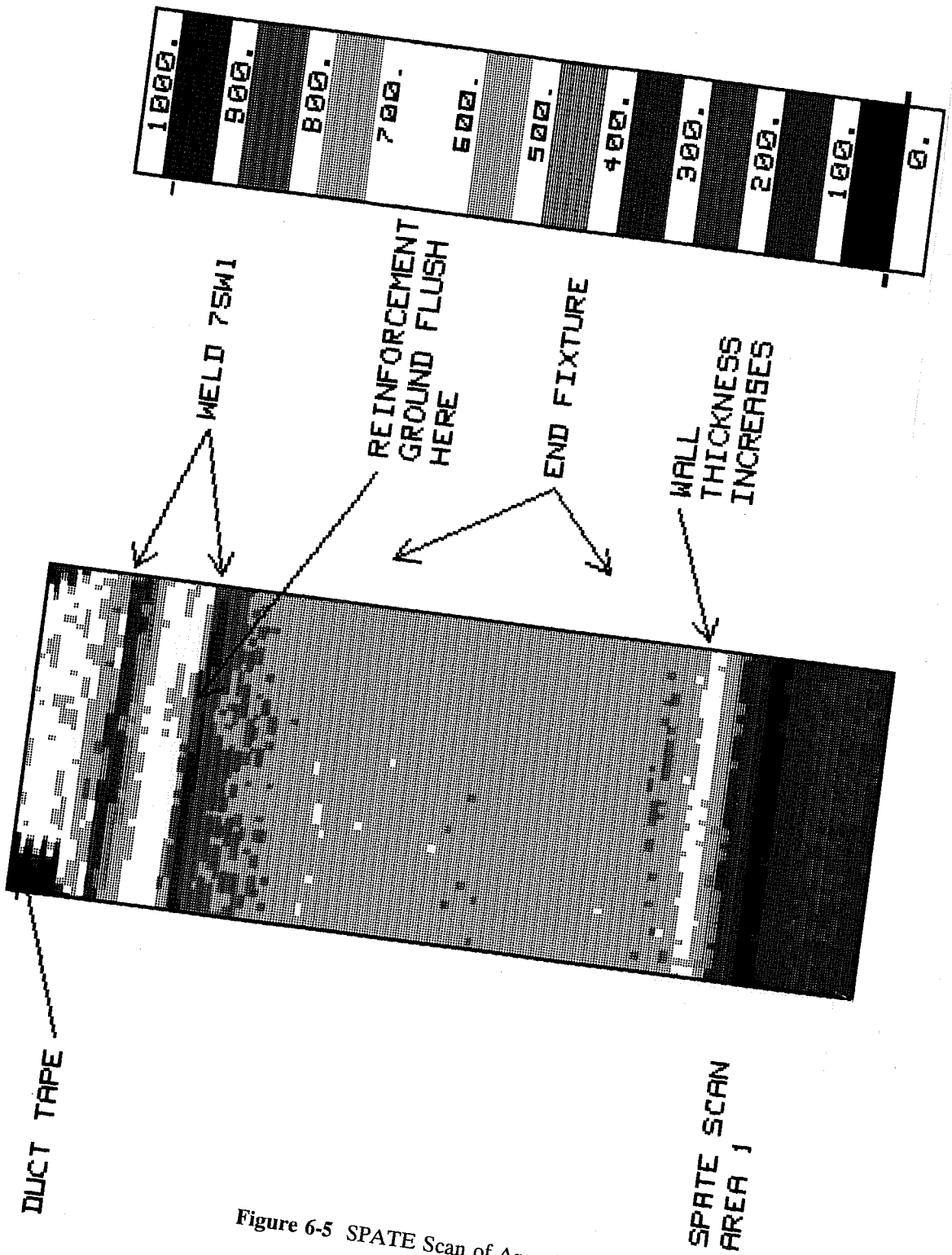


Figure 6-5 SPATE Scan of Area 1

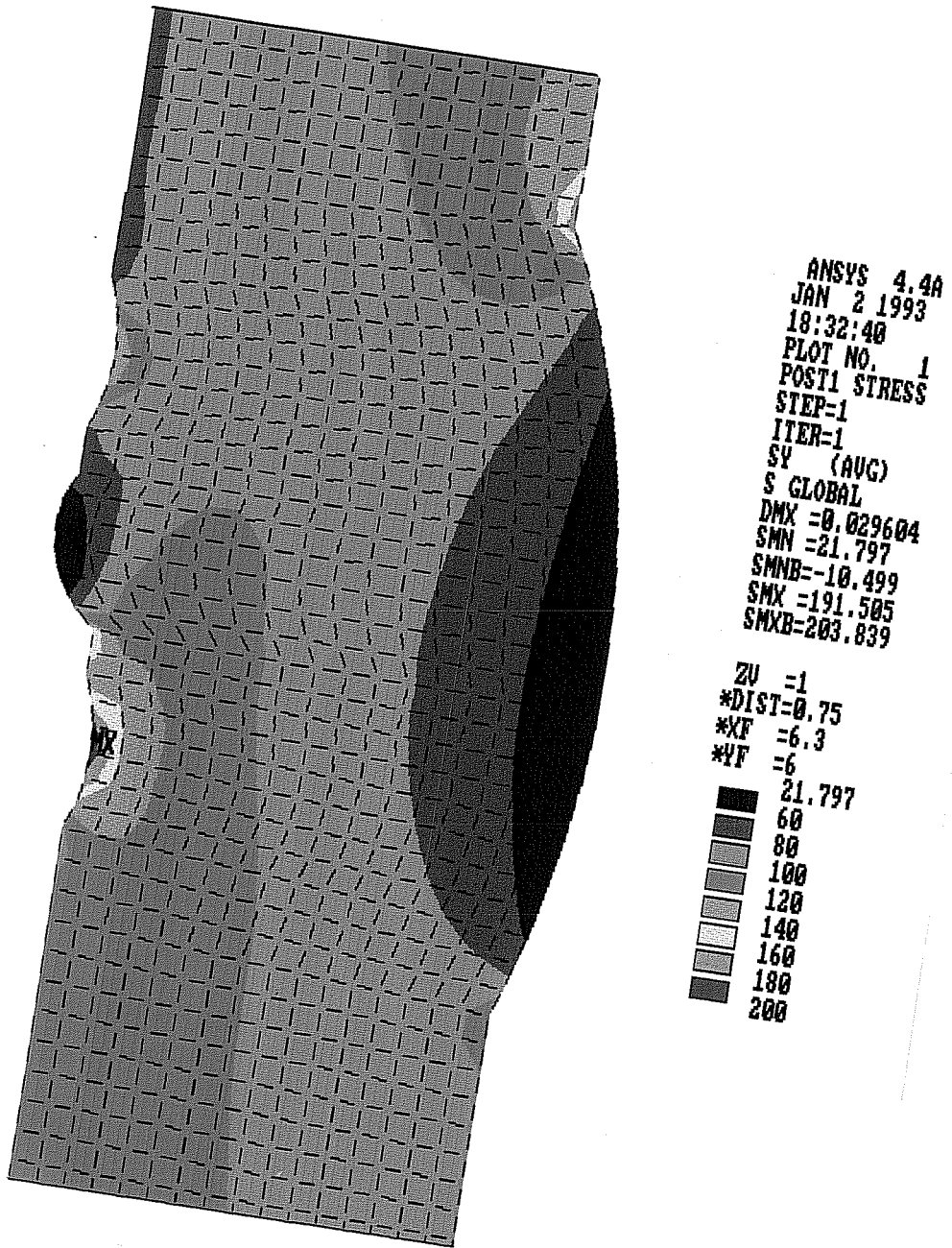


Figure 5-11 Axial Stress Distribution With Stress Shadowing Grooves

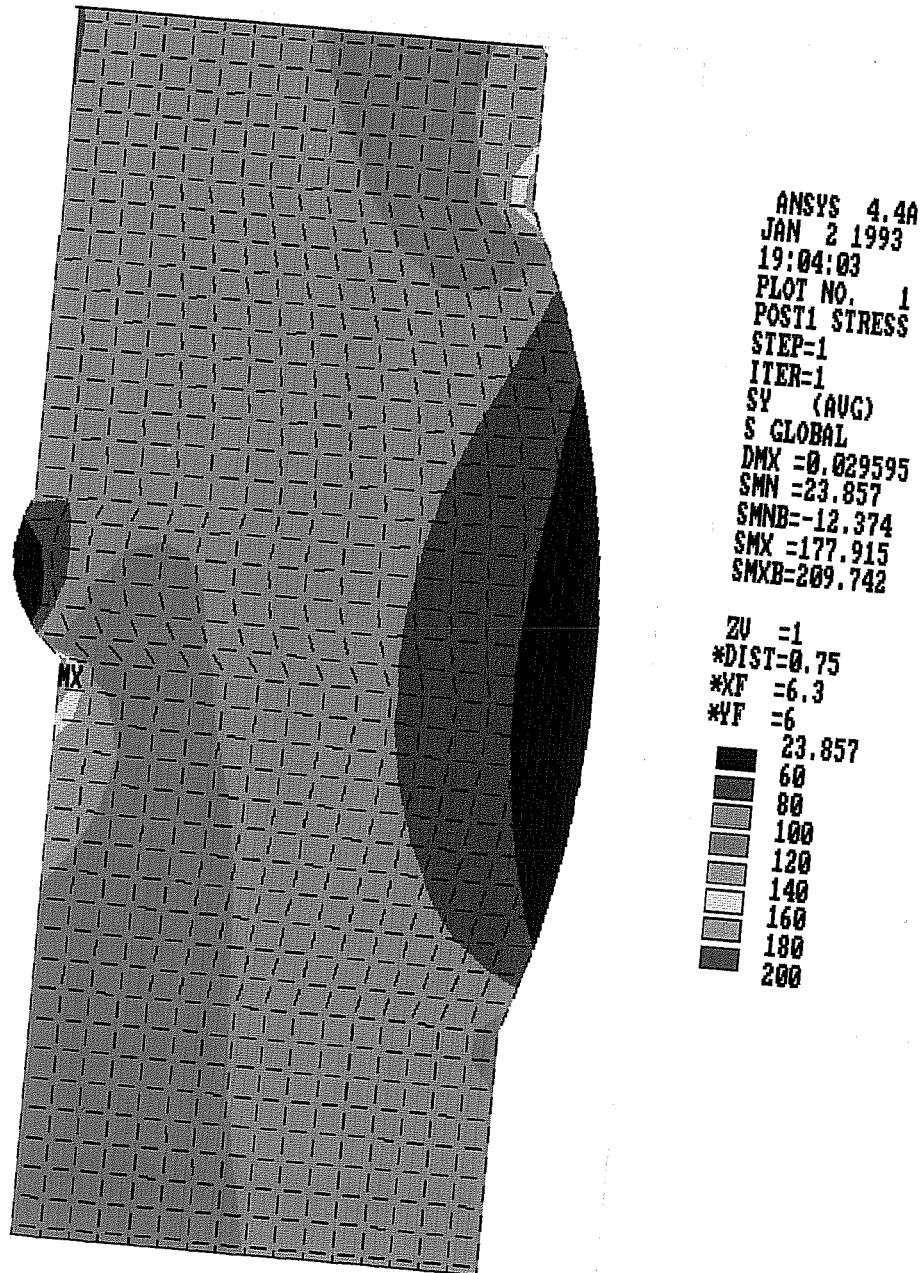


Figure 5-10 Axial Stress Distribution Without Stress Shadowing Grooves

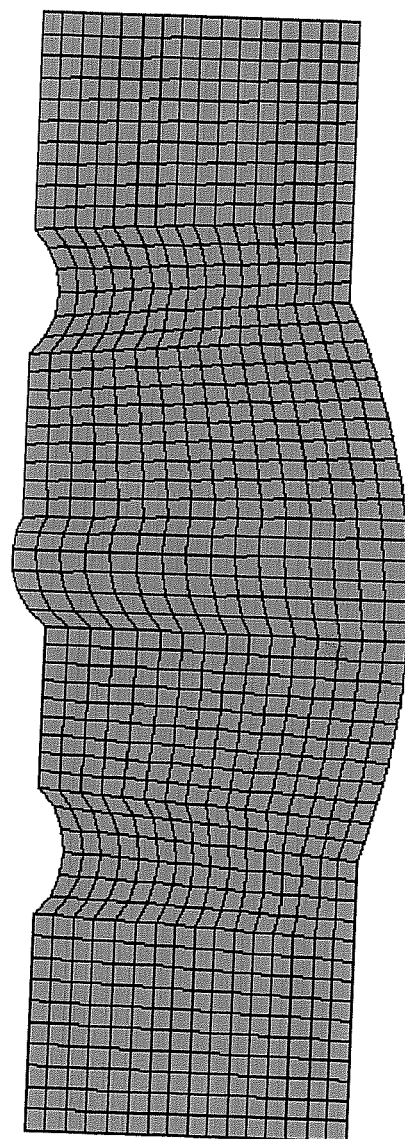


Figure 5-4 Layout of Elements in Middle Region of Finite Element